

INFORMATION TO USERS

This manuscript has been reproduced from the microfilm master. UMI films the text directly from the original or copy submitted. Thus, some thesis and dissertation copies are in typewriter face, while others may be from any type of computer printer.

The quality of this reproduction is dependent upon the quality of the copy submitted. Broken or indistinct print, colored or poor quality illustrations and photographs, print bleedthrough, substandard margins, and improper alignment can adversely affect reproduction.

In the unlikely event that the author did not send UMI a complete manuscript and there are missing pages, these will be noted. Also, if unauthorized copyright material had to be removed, a note will indicate the deletion.

Oversize materials (e.g., maps, drawings, charts) are reproduced by sectioning the original, beginning at the upper left-hand corner and continuing from left to right in equal sections with small overlaps.

Photographs included in the original manuscript have been reproduced xerographically in this copy. Higher quality 6" x 9" black and white photographic prints are available for any photographs or illustrations appearing in this copy for an additional charge. Contact UMI directly to order.

**ProQuest Information and Learning
300 North Zeeb Road, Ann Arbor, MI 48106-1346 USA
800-521-0600**

UMI[®]

University of Alberta

**A Method for Calculating Transient Temperature and Pressure Profiles for Crude
Oil and Water Flowing in a Buried Pipeline**

by

Paul Skoczylas



**A thesis submitted to the Faculty of Graduate Studies and Research in partial
fulfillment of the requirements for the degree of **Master of Science****

Department of Mechanical Engineering

Edmonton, Alberta

Fall, 2001



**National Library
of Canada**

**Acquisitions and
Bibliographic Services**

**395 Wellington Street
Ottawa ON K1A 0N4
Canada**

**Bibliothèque nationale
du Canada**

**Acquisitions et
services bibliographiques**

**395, rue Wellington
Ottawa ON K1A 0N4
Canada**

Your file Votre référence

Our file Notre référence

The author has granted a non-exclusive licence allowing the National Library of Canada to reproduce, loan, distribute or sell copies of this thesis in microform, paper or electronic formats.

The author retains ownership of the copyright in this thesis. Neither the thesis nor substantial extracts from it may be printed or otherwise reproduced without the author's permission.

L'auteur a accordé une licence non exclusive permettant à la Bibliothèque nationale du Canada de reproduire, prêter, distribuer ou vendre des copies de cette thèse sous la forme de microfiche/film, de reproduction sur papier ou sur format électronique.

L'auteur conserve la propriété du droit d'auteur qui protège cette thèse. Ni la thèse ni des extraits substantiels de celle-ci ne doivent être imprimés ou autrement reproduits sans son autorisation.

0-612-69814-9

Canada

University of Alberta

Library Release Form

Name of Author: Paul Skoczylas

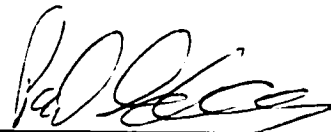
Title of Thesis: A Method for Calculating Transient Temperature and Pressure Profiles for Crude Oil and Water Flowing in a Buried Pipeline

Degree: Master of Science

Year this Degree Granted: 2001

Permission is hereby granted to the University of Alberta Library to reproduce single copies of this thesis and to lend or sell such copies for private, scholarly or scientific research purposes only.

The author reserves all other publication and other rights in association with the copyright in the thesis, and except as herein before provided, neither the thesis nor any substantial portion thereof may be printed or otherwise reproduced in any material form whatever without the author's prior written permission.



3903-38th Street
Edmonton, Alberta
T6L 6S9

Date: October 1, 2001

University of Alberta

Faculty of Graduate Studies and Research

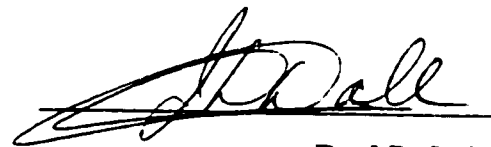
The undersigned certify that they have read, and recommend to the Faculty of Graduate Studies and Research for acceptance, a thesis entitled **A Method for Calculating Transient Temperature and Pressure Profiles for Crude Oil and Water Flowing in a Buried Pipeline** submitted by **Paul Skoczylas** in partial fulfillment of the requirements for the degree of **Master of Science**.



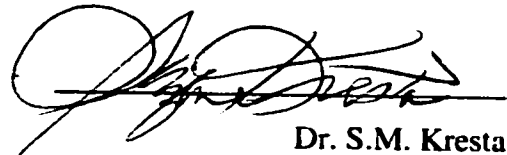
Dr. K.R. Fyfe (Co-supervisor)



M.Y. Ackerman (Co-supervisor)



Dr. J.D. Dale



Dr. S.M. Kresta

Date: September 25, 2001

Abstract

Heavy oil produced from a well must be transported from the well to a processing facility. In Eastern Alberta and Western Saskatchewan, the primary method of transport is by tanker truck. Oil producers are concerned about using pipelines because of the potential for extreme pressure loss due to the high viscosity of heavy oil. Viscosity of heavy oil is highly dependent upon temperature; therefore, any calculation of pressure losses must consider the temperature of the oil throughout the length of the pipeline. A steady-state calculation is easily done, but this does not allow consideration of seasonal temperature changes and the effects of changes in flow rate, and start ups and shutdowns. The present work is the construction of a model for calculating temperature (and therefore viscosity and pressure loss) in a heavy oil pipeline in transient conditions.

Acknowledgements

The research described in this document was done as part of a joint industry project administered by C-FER Technologies of Edmonton. The participants in the project are Alberta Energy Research Institute, Anadarko Canada Petroleum, Canadian Natural Resources Ltd., Husky Oil Operations Ltd., Nexen Inc., and YPF-Repsol. The support of these companies is gratefully appreciated.

I would like to thank my employer, C-FER Technologies, for its generous support in this project and in my graduate studies. In particular, I would like to thank Dr. Francisco Alhanati, Bob Nichol and Brian Wagg for their input and support. I would also like to thank my supervisors at the University of Alberta, Dr. Ken Fyfe and Mark Ackerman, for their assistance and support.

Table of Contents

1. Introduction	1
1.1 Background	1
1.2 HOGS Joint Industry Project, Phase I (HOGS I)	6
1.2.1 Scope	6
1.2.2 Results	7
1.3 HOGS Joint Industry Project, Phase II (HOGS II)	8
1.3.1 Scope	8
1.4 Outline of Thesis	9
2. Fluid Flow and Heat Transfer Considerations	11
2.1 Pressure Loss in Single Phase Flow	11
2.1.1 Laminar Flow	12
2.1.2 Turbulent Flow	13
2.1.3 Emulsion	14
2.1.4 Diluent	16
2.1.5 Core-Annular Flow	17
2.1.6 Other Flow Regimes	19
2.2 Heat Transfer from Fluid	20
2.3 Combined Heat Transfer and Pressure Loss	29
2.3.1 Effect of Temperature on Viscosity	29
2.3.2 Pressure Loss, Considering Effect of Temperature	34
2.3.3 Effects of Viscous Heating	36
2.3.4 Analysis of Steady State Results	38
2.3.5 Transient Effects	43
3. Ground Temperature Effects	45
3.1 One-Dimensional Heat Conduction Equation	46
3.1.1 Analytical Solutions	47
3.1.2 Numerical Solutions	50
3.2 Effects of Different Boundary Conditions	52
3.2.1 Convection at the Surface	52
3.2.2 Insulating Layer at Surface	53
3.2.3 Radiation	56
3.2.4 Moisture in the Ground	56
4. Transient Heat Loss Calculations	61
4.1 Transient Heat Conduction Equation	61
4.2 Finite Difference Method	61
4.2.1 Derivation of Radial Coordinate System Equations	65
4.2.1.1 Method Using Assumption of Small Discretization	66
4.2.1.2 Method Without Using Assumption of Small Discretization	68
4.2.1.3 Comparison	69
4.2.1.4 Symmetry Boundary Condition	70
4.2.1.5 Connection of Two Radial Systems	71
4.2.1.6 Convective Boundary Conditions	75

4.2.2	Derivation of Ground Coordinate System Equations.....	83
4.2.2.1	Transformation of Variables	83
4.2.2.2	Transformation of Conduction Equation.....	85
4.2.2.3	Finite Difference Model	86
4.2.3	Connection of Ground System to Radial System.....	88
5.	Calculation Algorithm.....	91
5.1	Construction of Model	91
5.2	Coefficient Matrix	96
5.3	Matrix Solutions.....	98
5.3.1	Gaussian Elimination	98
5.3.2	Iterative Methods.....	99
5.3.3	LU Decomposition	99
5.3.4	Banded Solution Methods	100
5.3.5	Sparse Solution Methods.....	100
6.	Results	102
6.1	Parametric Studies in Constant Flow	102
6.1.1	Flow Rate	104
6.1.2	Pipe Size.....	111
6.1.3	Pipeline Length	114
6.1.4	Burial Depth	118
6.1.5	Insulation Thickness.....	121
6.1.6	Flow Start Date.....	124
6.1.7	Inlet Temperature	126
6.1.8	Fluid Properties	129
6.1.9	Preheat Time	132
6.1.10	Effect of Ground Conductivity.....	134
6.2	Parametric Studies in Shutdowns.....	136
6.2.1	Shutdown Date	137
6.2.2	Shutdown Length	139
6.3	Parametric Studies in Varying Flow Rates	141
6.3.1	Increasing Oil Flow, No Water	141
6.3.2	Decreasing Oil Flow, No Water.....	142
6.3.3	Constant Flow Rate, Increasing Water Fraction	143
6.3.4	Constant Flow Rate, Decreasing Water Fraction	145
7.	Discretization in Finite Difference Model	147
7.1	Effects of Varying Spatial Discretization.....	150
7.2	Effects of Varying Time Step.....	154
7.3	Effect of Time Step in a Transient Calculation.....	155
8.	Finite Element Modelling of Transient Heat Transfer in Two Dimensions ..	157
8.1	Description of Finite Element Method for Calculating Heat Conduction	157
8.1.1	Steady State Conduction with only Fixed Temperature or Adiabatic Boundaries.....	160
8.1.2	Steady State Conduction with Fixed Temperature, Adiabatic or Convective Boundaries	160

8.1.3 Transient Conduction with only Fixed Temperature or Adiabatic Boundaries.....	161
8.1.4 Transient Conduction with Fixed Temperature, Adiabatic or Convective Boundaries	161
8.2 Verifying Validity of Finite Element Model.....	162
8.2.1 Steady State, Constant Properties, Constant Temperature Boundaries	163
8.2.2 Steady State, Constant Properties, Constant Temperature and Convective Boundaries	167
8.2.3 Steady State, Different Properties	169
8.2.4 Transient, Constant Properties, Constant Temperature Boundaries .	169
8.2.5 Transient, Constant Properties, Convective and Constant Temperature Boundaries.....	172
8.2.6 Discussion of Test Cases.....	172
8.3 Finite Element Method Applied To Buried, Insulated Pipe.....	173
8.3.1 Grid Construction.....	173
8.3.1.1 Grid Type #1	173
8.3.1.2 Grid Type #2.	175
8.3.2 Steady State Case with Constant Temperature Boundaries	176
8.3.3 Transient Comparison to Finite Difference Results.....	176
8.4 Other Issues with FEM.....	179
8.4.1 Phase Changes.....	179
8.4.2 Revised Convective Coefficients	179
9. Summary and Conclusions.....	181
10. Future Work	184
References	185
Appendix A. Transformation of Variables for Bicylindrical Coordinate System	188
Appendix B. Derivation of Laplacian for the Bicylindrical Coordinate System	191

List of Figures

Figure 1.1 A typical heavy oil lease	2
Figure 2.1 Regions through which heat must flow	21
Figure 2.2 A fluid element in the pipe	23
Figure 2.3 Viscosity vs. temperature relationship of Western Canadian heavy oils	30
Figure 2.4. Linearized relationship between viscosity and temperature	31
Figure 2.5 Parity plot for viscosity correlation	33
Figure 2.6 Relationship of pressure loss to flow rate	39
Figure 2.7 Tornado chart for base flow rate of 200 m ³ /d	41
Figure 2.8 Tornado chart for base flow rate of 20 m ³ /d	43
Figure 3.1 Mean Daily Temperature at Elk Point	45
Figure 3.2 Surface and ground temperatures through one year.	48
Figure 3.3 Comparison of analytical and numerical solutions.....	51
Figure 3.4 Finite difference model on boundary of two regions.....	54
Figure 3.5 Effect of convective coefficient and insulating surface layer.....	56
Figure 3.6 Seasonal ground temperature variation for dry and moist ground.....	59
Figure 4.1 Node numbering	64
Figure 4.2 Nodal geometry in radial system	67
Figure 4.3 Error in radial finite differences.....	70
Figure 4.4 A node at the intersection of two cylindrical regions	72
Figure 4.5 Nodes used in convective boundary with finite difference method....	79
Figure 4.6 Coordinate system used in the ground.....	85
Figure 4.7 Convergence of finite difference calculation.....	87
Figure 4.8 Connection of radial and bicylindrical coordinate systems	88
Figure 6.1 Effect of flow rate on pressure loss	105
Figure 6.2(a) Pressure loss with varying flow rate.....	107
Figure 6.2(b) Temperature with varying flow rate.....	107
Figure 6.3(a) Pressure loss with varying flow rate.....	108
Figure 6.3(b) Temperature with varying flow rate.....	108
Figure 6.4 Start-up pressures.....	109
Figure 6.5 Operating pressures.....	110
Figure 6.6. Effect of pipe size on pressure loss.....	112
Figure 6.7(a) Pressure loss with varying pipe size.....	113
Figure 6.7(b) Temperature with varying pipe size	113
Figure 6.8 Effect of pipeline length on maximum pressure	115
Figure 6.9(a) Pressure loss with varying pipeline length	116
Figure 6.9(b) Temperature with varying pipeline length	116
Figure 6.10 Effect of length on pressure	117
Figure 6.11 Effect of depth on start-up pressure.	118
Figure 6.12(a) Pressure loss with varying pipeline depth	119
Figure 6.12(b) Temperature with varying pipeline depth	120
Figure 6.13 Effect of insulation thickness on start-up pressure	121

Figure 6.14(a) Pressure loss with varying insulation thickness	122
Figure 6.14(b) Temperature with varying insulation thickness	123
Figure 6.15 Pressure with varying insulation thickness	124
Figure 6.16(a) Effect of start date on pressure loss.....	125
Figure 6.16(b) Effect of start date on temperature	126
Figure 6.17 Effect of inlet temperature on start-up pressure.....	127
Figure 6.18(a) Effect of inlet temperature on pressure loss	128
Figure 6.18(b) Effect of inlet temperature on outlet temperature	128
Figure 6.19(a) Effect of API gravity on pressure.....	131
Figure 6.19(b) Effect of API gravity on temperature.....	131
Figure 6.20(a) Effect of preheat length on pressure loss.....	133
Figure 6.20(b) Effect of preheat length on temperature	133
Figure 6.21(a) Effect of ground thermal conductivity on pressure loss.....	135
Figure 6.21(b) Effect of ground thermal conductivity on temperature	136
Figure 6.22(a) Effect of shutdown date on pressure	138
Figure 6.22(b) Effect of shutdown date on temperature	138
Figure 6.23(a) Effect of shutdown length on pressure	140
Figure 6.23(b) Effect of shutdown length on outlet temperature	140
Figure 6.24. Pressure and temperature response to increasing oil rate	142
Figure 6.25 Pressure and temperature response to decreasing oil rate.....	143
Figure 6.26. Response of pressure loss and temperature to changing water fraction	144
Figure 6.27 Response of pressure loss and temperature to changing water fraction	145
Figure 7.1 Error over time.....	149
Figure 7.2 Effect of varying the number of layers of nodes in the pipe wall....	150
Figure 7.3 Effect of varying the number of layers of nodes in the insulation....	151
Figure 7.4 Effect of varying the number of layers of nodes in the ground	152
Figure 7.5 Effect of varying the number of nodes in each layer	153
Figure 7.6 Effect of varying the time step.....	154
Figure 7.7(a) Effect of time step (in days) in transient calculation.....	155
Figure 7.7(b) Effect of time step (in days) in transient calculation.....	156
Figure 8.1(a) Sample grid on rectangular bar	162
Figure 8.1(b) Sample grid on hollow cylinder	163
Figure 8.2. Effect of varying number of nodes on steady state calculation of steady state temperature in a bar	164
Figure 8.3 Effect of varying number of nodes on steady state calculation of steady state temperature in a hollow cylinder	165
Figure 8.4 Effect of element aspect ratio	166
Figure 8.5 Effect of varying number of nodes on steady state calculation of steady state temperature in a bar	167
Figure 8.6 Effect of varying number of nodes on steady state calculation of steady state temperature in a hollow cylinder	168
Figure 8.7 Accuracy of transient temperature calculation in bar	170

Figure 8.8 Accuracy of transient temperature calculation in hollow cylinder ...	171
Figure 8.9 Accuracy of transient temperature calculation in bar with convection	172
Figure 8.10 First grid type.....	174
Figure 8.11 Second grid type	175
Figure 8.12 Results of transient comparison	178

List of Tables

Table 2.1 Base case values.....	38
Table 6.1 Base case parameters.....	103
Table 6.2 Flow rates and pressures	104
Table 6.3 Pressure losses with varying pipe sizes.....	111
Table 6.4 Pressure losses with varying pipeline lengths.....	114
Table 6.5 Pressure losses with varying burial depths	118
Table 6.6 Pressure losses with varying insulation thicknesses	121
Table 6.7. Effect of start date on pressure loss.....	125
Table 6.8 Effect of inlet temperature on pressure loss.....	127
Table 6.9 Fluid properties	130
Table 6.10 Effect of API gravity on pressure.....	130
Table 6.11 Effect of preheat length on pressure.....	132
Table 6.12 Effect of ground thermal conductivity on pressure.....	135
Table 6.13 Effect of shutdown date on maximum restart pressure	137
Table 6.14 Effect of shutdown length on restart pressure.....	139
Table 7.1 Properties used in steady state comparison	148

Nomenclature

A	coefficient matrix	R	thermal resistance, K/W
A	area, m ²	\hat{R}	Thermal Resistance over unit length, K·m/W
API	API gravity	Re	Reynolds number
Bi	Biot number	Re_l	core flow effective Reynolds number
c	specific heat, J/kg·K	t	time, s
D	diameter (normally pipe inside diameter), m	T	temperature, °C
DF	diluent fraction (by volume)	v	velocity, m/s
f	friction factor	V	volume, m ³
F	flux vector	\dot{W}	power, W
Fo	Fourier number	WF	water fraction (by volume)
h	convective coefficient (W/m ² ·K)	x	depth, m
H	enthalpy, kJ/kg	x	distance, m
i	$\sqrt{-1}$	y	distance, m
k	thermal conductivity, W/m·K	Z	pipe burial depth (at centreline), m
K, K'	conductivity matrices	C, k	arbitrary constants
L	length, m	$A, B, c, C, D, E, F, X, \alpha_o$	coefficients
L	latent heat of fusion, J/kg	$i, j, r, \theta, \alpha, \beta$	node references
m	viscosity ratio (for core flow)	α, β	bicylindrical coordinates
m	mass, kg	x, y	cartesian coordinates
\dot{m}	mass flow rate, kg/s	ϵ	pipe surface roughness, m
M	number of layers of nodes	ϕ	volume fraction of dispersed phase
M	heat capacity matrix	ϕ	ratio of depth to radius
N	number of nodes	μ	viscosity, Pa·s (or cp in some instances)
Nri	number of layers of nodes in insulation	θ	angle, rad
Nrp	number of layers of nodes in pipe	ρ	density, kg/m ³
$Nalf$	number of layers of nodes in ground	ρ_c	core flow effective density, kg/m ³
$Nang$	number of nodes in each layer	κ	thermal diffusivity, m ² /s
Nu	Nusselt Number	ω	angular frequency, rad/s
ΔP	pressure loss, Pa		
Pr	Prandtl Number		
q	heat flow, J		
\dot{q}	heat flow rate, W		
Q	flow rate, m ³ /s		
r	radius, m		
R	adjusted water fraction (for core flow)		
		Subscripts:	
		amp	amplitude
		avg	average
		c	cylindrical (or radial) region

cont continuous phase
d diluent
eff effective
f fluid
g ground
i insulation
L length
nodal referring to one node
o oil

p pipe
s surface
t transformed region
w water

0,1,2,3,4 different layers
i,j,r,θ,α,β node references

1. Introduction

1.1 Background

In Eastern Alberta and Western Saskatchewan, particularly in the Lloydminster to Cold Lake region, there are many heavy oil reservoirs. The oil found in this area can have API gravity ranging from 8-15, and viscosity as high as 250,000 cp. (See Section 2.3.1 for a definition of API gravity.) These reservoirs are typically 400 m to 600 m below the surface. (In general, the further north, the shallower the reservoir.) A typical production well drilled into these formations has the following periods in its life:

- **Start-up.** This period is typically on the order of a few days. Production rates ramp up from zero to a stable value in this time.
- **Low water.** In this period, which can last up to five years (although in some wells it can be very short or even non-existent), the amount of produced water is low (0-10%). There can be significant sand production; in extreme cases as high as 50% of the total production earlier in this period, although it typically decreases with time to about 2-5%.
- **Water-breakthrough.** Eventually, the water layer below the oil in the reservoir breaks through to the wellbore, and the water fraction increases drastically in a short period of time (perhaps a few months). Sand production from this point on is typically quite low (0-5%).
- **High water.** For the remainder of the life of the well, far more water than oil is produced. The water fraction will typically increase slowly throughout this time.

The flow rate of oil from one of these wells can be 5-30 m³/d in the low water period, and will normally decrease after water breakthrough, although the total rate of produced fluid can increase dramatically after water breakthrough.

These heavy oil wells are usually produced with downhole progressing cavity pumps. These are rotating positive displacement pumps, which have a non-pulsating flow and a low internal shear rate. Many older wells still use the commonly seen reciprocating pumps (evidenced by the presence of a pump jack at surface), but these wells are usually producing high water fractions.

Figure 1.1 shows a typical heavy oil lease in this area. (This particular wellsite is near Cold Lake.) Visible is the wellhead, with a drivehead for rotating the rods connecting to the progressing cavity pump downhole, a hydraulic system (for powering the drivehead) driven by a propane-powered internal combustion engine, the flow line from the well to the tank, and the burner on the tank (the projection on the right side of the tank) for heating the fluids within.

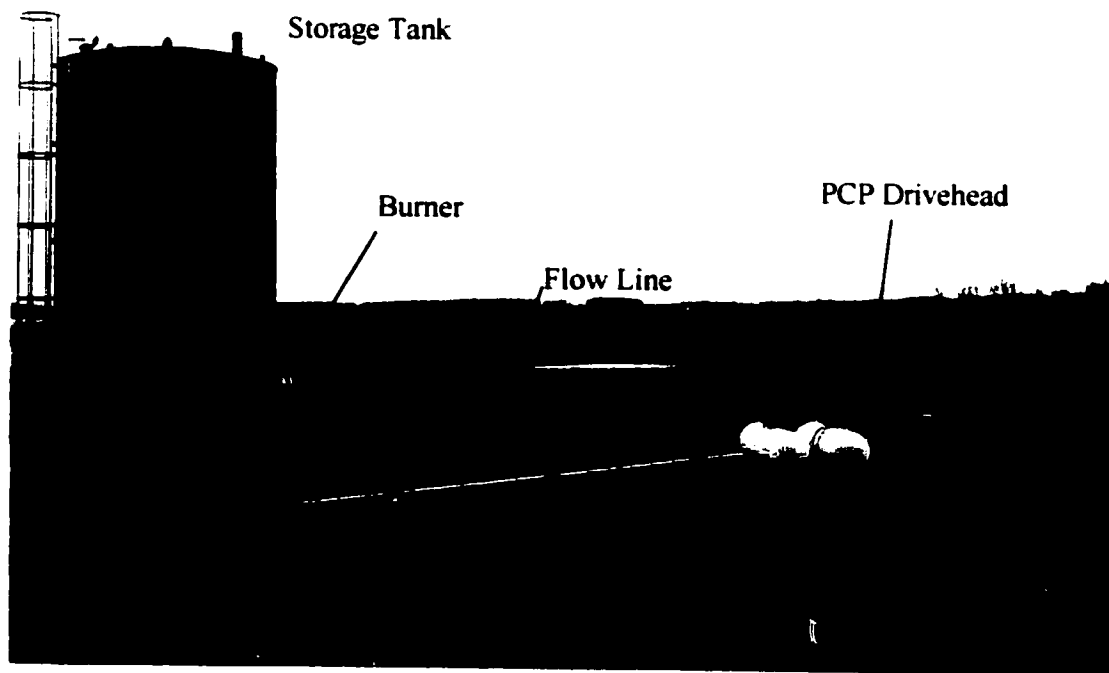


Figure 1.1 A typical heavy oil lease

The oil produced from the well is normally piped a short distance (approximately 10 m) to a tank on the lease. This tank is heated to about 70°C. At this

temperature, the oil viscosity is substantially reduced from the temperature at which it was produced (typically 15-20°C for Alberta and Saskatchewan heavy oil wells). The lower viscosity is important to facilitate the separation of the oil, water, and sand within the tank. The oil and water are drained from the tank into tank trucks and transported in the trucks to a processing facility (called a battery). The sand is emptied from the bottom of the tank using a vacuum truck and is taken to a cleaning and disposal facility, which may or may not be located at the battery.

There are several reasons why trucking the fluids from the wellsite to the battery may not be the optimal solution for transport. Expense is a major issue. There is no economy of scale for trucking fluids; the truck operators, who are independent contractors, get paid per load, regardless of the number of loads that they carry. This is especially of concern after the water breakthrough occurs. The oil producing company must transport all the fluids from the wellsite; as the amount of water increases, this clearly becomes more and more expensive, while the oil production, and therefore revenue, decreases. A typical heavy oil reservoir has less than 5-10% of the oil in place produced before it becomes either uneconomic or technically unfeasible to continue producing wells in that reservoir. If the relative cost of producing water from these reservoirs can be decreased, in many cases it may be possible to increase the overall production from the reservoir.

Secondly, the areas of Alberta and Saskatchewan where these heavy oil reservoirs are located are rich agricultural regions. The wells are located in farmland, and the roads from the wells to the batteries run through farmland. These roads therefore are also used by farmers, and many of these farmers are unhappy with the increasing numbers of large tank trucks driving around their neighbourhoods. They are concerned, justifiably, with safety. They are also unhappy about the noise produced by the large trucks, and about the dust thrown up by the trucks

driving on dirt roads. As the number of wells increases, and the flow rates from each well increase as water breaks through, the amount of truck traffic will clearly increase, and with it, the farmers' concerns.

The farmers place pressure on the regulatory bodies (in Alberta, this is the Alberta Energy and Utilities Board, or AEUB) to reduce truck traffic. The farmers also complain to the regulators about many other issues, including flaring and venting of gas, and disrespect of their land by some oil company personnel. At one level, the regulators have addressed this by requiring the oil companies to designate specific truck routes. This is only a partial solution, though. The regulators have in recent years encouraged oil companies to consider the possibility of pipelining oil from the wells to the batteries. In fact, in their approval of one heavy oil operation, the AEUB required one oil company to do a feasibility study (or participate in a joint study) of pipelining heavy oil.

In lighter oil fields in the rest of Western Canada, and in fact in onshore light and heavy oil fields around the world, it is most common for oil to be piped from the wells to the batteries in pipelines. There are reasons why this has not commonly been done in the Lloydminster-Cold Lake area:

- The viscosity of the oil in this area is among the highest found in any oilfield in the world. Highly viscous fluid is problematic to flow in pipelines of any significant length due to exceptionally high pressure losses.
- The oil flow rates are typically quite low, as mentioned earlier. This means the revenue stream is smaller than in most other oilfields in Western Canada, and around the world. In addition, heavy oil is normally worth less money per barrel than lighter oils; this further reduces potential revenue from heavy oil wells. Oil companies are less likely to be willing

to spend capital dollars installing pipelines when the payback period is quite long.

- In order to flow heavy oil through a pipeline, it would normally have to be heated in order to reduce the viscosity. Because the climate in Western Canada is so cold, especially in the winter, heat loss from a hot oil pipeline becomes a significant concern. This is especially true if an unplanned shut down occurs, for example if a power failure causes the pump to shut off. As the oil is stationary within the pipe, it cools further, possibly to the point at which it will become impossible to restart the flow without expensive intervention.
- Sand content is a concern to the operators, who are not confident in the ability of a heavy oil pipeline to carry sand.

Other heavy oil fields around the world, which do use pipelines to transport oil from the wells to the batteries, have a some significant differences as compared to Western Canadian heavy oil fields:

- They have much higher flow rates. This means that revenue is higher. The capital cost of a pipeline is then less of a concern. It also means that they can afford to import diluent from lighter oilfields to mix with the heavy oil before transporting it. (This is common practice in Venezuela, for instance.)
- In most cases, the climate is significantly warmer than in Canada. This means the heat loss issues are significantly less of a problem.
- The oil is typically less viscous than in Western Canada, even for the same density of oil at the same temperature.

Within Western Canada, there is essentially no activity in the area of pipelining heavy oil with low water fractions in a gathering system situation. A few areas do use pipelines to transport heavy oil from wells to central facilities, but these are

virtually all mixed with water in large amounts (either produced from the well in large quantities, or recirculated from the facility) to ensure the overall pressure loss is small.

1.2 HOGS Joint Industry Project, Phase I (HOGS I)

In 1998, C-FER Technologies, a research company located in Edmonton, formed a joint industry project (JIP) entitled Heavy Oil Gathering Systems Alternatives (HOGS). Several oil producing companies in Alberta and Saskatchewan, in addition to the government of Alberta, joined the project. Some time after the JIP was completed, in mid-1999, an Argentinean oil company also decided to join the project in order to obtain its results.

1.2.1 Scope

The project was intended to consider alternatives to trucking over a wide range of possible operating conditions, from both the technical and economic points of view. Factors which were considered included fluid type, pipe size, pipeline length, insulation thickness, cost of construction, price of oil, cost of water disposal, discount rate, production performance, and many others. It would then be possible to determine which conditions would be best suited to further study, and which would be best left at the status quo (i.e., trucking). It would also address which factors had the greatest effect on project economics. A technical model was developed for the project which estimated pressure drop under steady state conditions. It was not considered feasible to develop a transient model and run hundreds of possible scenarios within a reasonable time frame. More practical was to use a simpler (and much faster) model to screen the large number of cases, and if the results were promising, a more detailed model could be built at a later date.

1.2.2 Results

The first phase of HOGS indicated that it could be economically feasible to pipeline heavy oil in many cases [1]. This is particularly true if wells were drilled in a pad configuration, with several wells producing into the same lease tanks and from there, pumped into the same pipeline. An added advantage of this is that the technical and economic feasibility of the recovery of natural gas vented from the well casing and from the tanks is improved. The effects of gas entrained in the pipeline along with the produced oil and water are not considered in the present work.

If a well is produced only until the water breakthrough occurs, it may not be profitable to build a pipeline. However, if the pipeline was constructed at the start of the well's life, the pipeline would, in many cases, not only be profitable, but have an improved net discounted cash flow over the life of the well, as compared to trucking. This is because the cost of transporting the increased water from the well by pipeline is very small compared to the cost of trucking it. Reduced water handling costs lead in turn to an increased well life, since a well would be produced only so long as its revenue exceeds its operating costs.

HOGS I analyzed a set of typical well production histories over the entire lives of the wells (i.e., with varying water, oil, and sand flow rates). The flow calculations assumed various types of flow regime, described in more detail in Chapter 2. Where water needed to be added or removed from the flow to satisfy limits on some of these flow regimes, the water could be sourced or disposed through a second pipeline, a water source or disposal well, or by trucking.

The results from HOGS I of most relevance to the current work were the following:

- Heavy oil pipelines with higher flow rates are more likely to be technically feasible. This makes groups of directional wells drilled from the same site (a “pad” of wells) more attractive. (Some companies now routinely drill pads of wells for other reasons.)
- Short pipelines are more likely to be technically feasible.
- Less viscous oil is more easily pipelined.
- Flow regimes such as core-flow or water-assisted flow have the potential to greatly increase the range of application of pipelining to heavy oil transport, but have limits which must be addressed.
- When a well is in its later stages of life, producing a very high water fraction, the problems are more likely to be economic than technical (although it must be assured that the produced water has a high enough salt content to prevent freezing in longer pipelines, or if the flow is stopped for some reason in winter).

These points will be addressed further in Chapter 2.

1.3 HOGS Joint Industry Project, Phase II (HOGS II)

The current work was conducted as part of the HOGS II research project.

1.3.1 Scope

The sole deliverable of HOGS II is a software tool for calculating the effects of transient variations on the flow conditions in a heavy oil pipeline. Transient conditions that could have an effect could include the following:

- Seasonal temperature variations
- Starting flow of hot oil into a cold pipe
- Temporary stoppage of flow
- Preheat of pipe by flowing hot water

The software tool will also be able to consider conditions such as:

- Varying flow rates and water fractions through the life of the well

- Different flow regimes (emulsion, addition of diluent, core/annular flow, water-assisted flow)

The work described here constitutes the technical development behind this software tool.

The scope of this work does not include pressure transients caused during the start and stop of flow (often called “water hammer”). Pressure waves caused by these transients travel through the fluid at approximately the speed of sound in the fluid. The current work is concerned with pressure effects caused by *thermal* transients. The time scale of these effects is much longer. For the remainder of this work, the term “transient” is used to refer only to thermal transients.

1.4 Outline of Thesis

The remaining chapters in this thesis are described below.

Chapter 2 covers issues relating to fluid flow and heat transfer. This includes the effects of various flow regimes, and the effects of changing the temperature of the fluid on the pressure loss. Methods of calculating the temperature in steady state are discussed.

Effects of heat transfer within ground in which there is no pipeline are discussed in Chapter 3. These are one-dimensional effects. Conduction within the ground, and the effects of various boundary conditions at the surface are described.

A finite difference model for calculating the transient temperature distribution in the ground surrounding a buried, insulated pipeline is developed in Chapter 4. Included within this model is the effect of convection at the inner surface of the pipe on the heat conduction and on the temperature of the fluid flowing within the pipe.

Chapter 5 describes how the model developed in the previous chapter is built into a method of calculating the temperature and pressure loss along the full length of a pipeline. Also discussed are matrix solution methods which are used in determining the temperature profile within the ground at each step in time.

Chapter 6 describes results of the calculation, showing the effects of variations in certain parameters on the pressure loss and temperature in a pipeline.

In Chapter 7, the importance of choosing an appropriate level of discretization within the numerical model is discussed. Discretization in both time and space is covered.

A finite difference model has some limitations. For this reason, a finite element model is developed in Chapter 8. It is compared to the finite difference model previously built.

Chapter 9 summarizes the current work, and presents conclusions and recommendations. Chapter 10 briefly lists some work which must still be done in order to fully realize the potential of the current work.

2. Fluid Flow and Heat Transfer Considerations

2.1 Pressure Loss in Single Phase Flow

A primary concern when pumping fluid through a pipeline is the pressure loss. A higher pressure loss means a higher inlet pressure is required; the pipe must be capable of withstanding a greater pressure, and the pump at the start of the pipeline must be larger and cost more to operate. These factors add both capital and operating expense to the construction and operation of the pipeline. Pipelines used to transport fluids over large distances use booster pumping stations spaced along their length. It is unlikely, however, that this would be economically feasible on gathering system pipelines, remembering that these would not normally be longer than a few kilometres.

The pressure loss depends greatly on the flow regime. If the fluid flows as a single phase, the flow regime is either laminar or turbulent, and the distinction is determined by the Reynolds number (Re):

$$Re = \frac{v D \rho}{\mu} \quad (2.1)$$

Where:

v is the mean velocity

D is the pipe inside diameter

ρ is the fluid density

μ is the fluid viscosity

If the Reynolds number is less than 2000, the flow regime is normally laminar, and if it is greater than 4000, the flow regime is normally turbulent. Between Reynolds numbers of 2000 and 4000, it is not normally possible to be certain which regime the flow is in; the flow could be one or the other, or could be oscillating between them. In the current work, flow is assumed to be laminar if the Reynolds number is less than 2200, and turbulent above that. In laboratory

conditions, laminar flows have been maintained to much higher Reynolds numbers, and turbulent flows have been triggered at much lower Reynolds numbers, but these have been accomplished under carefully controlled conditions and this is extremely unlikely to occur in pipeline conditions.

The fluid can be considered to be a single phase for pressure loss calculations when any different fluids coexistent in the pipeline are miscible, or if they are very finely dispersed in one another (i.e. emulsified).

The current work does not consider flow of liquid with free gas. If any gas is present, it must be in solution, in which case the density, viscosity, and other properties of the fluid must reflect this.

2.1.1 Laminar Flow

Heavy oil flowing in a gathering system pipeline will almost always be in laminar flow. The pressure loss in laminar flow is calculated using the following equations, which are derived analytically in [2]:

$$\frac{\Delta P}{L} = \frac{\rho f v^2}{2 D} \quad (2.2)$$

$$f = \frac{64}{Re} \quad (2.3)$$

Where:

ΔP is the pressure loss

f is the friction factor

L is the pipe length

These can be combined into:

$$\frac{\Delta P}{L} = \frac{32 \mu v}{D^2} \quad (2.4)$$

Velocity can be calculated using:

$$\begin{aligned}
 v &= \frac{Q}{A} \\
 &= \frac{4Q}{\pi D^2}
 \end{aligned}
 \tag{2.5}$$

Where:

Q is the flow rate

A is the cross sectional area

So, in terms of flow rate, the pressure loss is:

$$\frac{\Delta P}{L} = \frac{128 \mu Q}{\pi D^4}
 \tag{2.6}$$

This equation is based on the assumption that the viscosity and pipe diameter are constant over the length for which the pressure loss is being calculated. The constant viscosity assumption will be violated in the case where hot oil is piped through a buried pipeline. The effects of violating this assumption will be discussed in Section 2.3.

This pressure loss is due to fluid friction only; effects of changes in elevation are not considered in the current work. Also, for a long length of pipeline, it is assumed that the effects of any bends are not significant to the pressure loss, and that there are no intermediate valves or fittings which will effect the pressure loss.

2.1.2 Turbulent Flow

When the pipelined fluid has a large water fraction, the flow is likely to be turbulent. In this case, the pressure loss is still governed by the same base equation as in laminar flow [2]:

$$\frac{\Delta P}{L} = \frac{\rho f v^2}{2D}
 \tag{2.7}$$

In turbulent flow, however, the friction factor is not so easily calculated. The widely accepted formulation for the friction factor is the Colebrook equation [2]:

$$\frac{1}{\sqrt{f}} = -2.0 \times \log \left(\frac{\epsilon/d}{3.7} + \frac{2.51}{Re \cdot \sqrt{f}} \right) \quad (2.8)$$

Where:

ϵ is the surface roughness of the pipe

This is the equation which was used in developing the commonly used Moody diagram for friction factors. The Colebrook equation is iterative. To use it, one must estimate a friction factor and use this to calculate an improved estimate. Normally only a small number of iterations are required. A non-iterative (explicit) method is often considered preferable for use in computer applications. There are large numbers of different variations on this in the literature. One such equation is by Haaland [2]:

$$f = \left[-1.8 \log \left(\left[\frac{\epsilon/d}{3.7} \right]^{1.11} + \frac{6.9}{Re} \right) \right]^{-2} \quad (2.9)$$

These equations again make the assumption that the fluid density and viscosity, and the pipe diameter and roughness do not change over the length of the pipeline.

2.1.3 Emulsion

An emulsion is essentially a dispersion of one phase within another in the form of very small droplets. In oil-water flow, emulsions can be characterized as either oil-in-water or water-in-oil, depending on which phase is dispersed within the other. When calculating the flow losses of emulsions within a pipe, they can be calculated in the same way as single phase flow, using an effective viscosity. The fluid density can be easily calculated from the water fraction and the densities of the water and oil:

$$\rho = WF \rho_w + (1 - WF) \rho_o \quad (2.10)$$

Where:

WF is the water fraction

o refers to the oil

w refers to the water

The effective viscosity (μ_{eff}) is dependent on the viscosity of the continuous phase and the concentration of the dispersed phase. There are various correlations available in the literature; the one given in the *Petroleum Engineering Handbook*[3] is:

$$\mu_{eff} = \mu_{cont} (1 + 2.5\phi + 14.1\phi^2) \quad (2.11)$$

Where:

ϕ is the volumetric fraction of the dispersed phase

$cont$ refers to the continuous phase

Knowing at what water fraction an oil-in-water will switch to water-in-oil, or vice versa, is critical. This is called the inversion point. It is not uncommon for an emulsified flow with a water fraction of 60% to have the oil as the continuous phase. In this case, it can be expected that the effective viscosity will be more than 7.5 times the viscosity of the oil. The inversion point depends greatly upon the fluid chemistry. Trace chemicals naturally present in either the produced water or oil, or added by the oil company, can cause the inversion point to change drastically.

Another critical issue is whether or not an emulsion is formed at all. An emulsion requires that the dispersed phase be present only in very small droplets. In some cases, a small amount of agitation may be all that is required to meet this condition, and when formed the emulsion will be very stable (i.e. the droplets will not tend to coalesce). In other cases, it may take a large amount of agitation to produce an emulsion, and the emulsion will be unstable when formed. Again, where in between these extremes a particular oil-water mixture will fall depends greatly on the composition of the fluids. In some cases chemicals can be added to the fluid to force an emulsion to become either more or less stable. Much research [e.g., 4] has been done on this, but the chemical nature of oil and water

produced from different reservoirs can cause large differences in the types and amounts of surfactants which must be added to create a stable emulsion.

Some companies form emulsions by adding water and surfactant specifically to decrease pressure losses in transport over long distances [5]. The drawback with this is that an emulsion which is stable for the length of time to travel 50-80 km (in some cases) may be very difficult to de-emulsify when received at the end of the pipeline. A product called Orimulsion® is available (from PDVSA, the state-owned oil company in Venezuela), which is essentially a very stable heavy oil/water emulsion with a high oil fraction but a relatively low viscosity [6,7]. PDVSA discovered it could be more economic to sell such a product for use as a coal replacement fuel than to remove the water and further refine it.

2.1.4 Diluent

In some cases, oil companies will choose to mix a diluent with the heavy oil in order to reduce its viscosity. The diluent is normally a lighter (and less viscous) crude oil, although a refined product could also be used (but likely at a greater cost). The two hydrocarbon phases (heavy oil and diluent) are normally miscible, and so become a single phase after being mixed. This single hydrocarbon phase will then flow with water in a flow regime such as emulsion (Section 2.1.3), core-annular flow (Section 2.1.5) or another regime (Section 2.1.6). The viscosity of the hydrocarbon mixture can be calculated in different ways. A weighted average (by volume) is sometimes used, but a logarithmic mixing formula has been found to match test data more accurately [8, 9, 10]. This is the Arrhenius equation:

$$\log \mu = DF \log \mu_d + (1 - DF) \log \mu_o \quad (2.12)$$

Where:

DF refers to the volumetric fraction of diluent

This formula was originally developed for oil-water mixtures, but has been found to be suitable when used to match data from heavy oil and light hydrocarbon mixtures, as published by AOSTRA [11].

Other formulations for viscosity of hydrocarbon blends are discussed in [9] and [10]. In some cases, especially if experimental data is available to determine an empirical factor used in some formulations, these may be more accurate, but the Arrhenius equation is simple, does not require an empirical correction factor, and is widely used.

Diluent is used extensively in Venezuelan heavy oil fields, and those of other countries. Diluent is either injected directly into oil wells in order to take advantage of its effects in producing as well as transporting the oil, or is injected into the gathering lines directly at the wellhead. At least one company imports diluent from producing fields in Africa [12]; the combined heavy oil and diluent mixture is often exported together, as this can be more economic than separating and recirculating the diluent. While Canada has large heavy oil reserves, the conditions are such that it is often not economic to use diluent (although it is used in some fields).

2.1.5 Core-Annular Flow

A flow regime that has been of great interest in recent years is core-annular flow. In this regime, a core of viscous oil surrounded by a thin annular layer of water can be pumped with flow losses little more than those of pure water flow, while maintaining a very small water fraction. Research into the creation and stability of this type of regime is ongoing.

Published papers in this field include: Arney et al [13], Bobok et al [14], Ooms et al [15], Nunez et al [5], Bannwart et al [16], Rivero et al [17], and Huang et al [18], among many others. (Most of these papers refer to several other papers not listed here.) Theoretical considerations, experimental work, and field observations have all been incorporated into the literature to date.

One issue which has been studied extensively is the stability of core-annular flow. Various stability criteria have been researched extensively [e.g., 5, 15, 16]. It is recognized that core-annular flow requires a core fluid of a much higher viscosity than the annular fluid, and that the core must occupy most of the pipe (i.e., a narrow range of water fraction is acceptable). Moreover, it has been observed that a minimum velocity is generally required to maintain the flow regime. One factor which has been observed is that if oil sticks to the pipe wall, the stability of the core-annular flow or the pressure gradient can be negatively effected. Experiments have been performed with cement-lined pipe [17], which is hydrophilic, in efforts to combat this problem. Other issues which have been studied include the use of special nozzles to help create the core flow at the start of the pipeline, and whether the core-annular flow will re-establish itself after a shutdown and restart of flow in a pipeline.

If core-annular flow can be created and stabilized within a heavy oil pipeline, one method of estimating the pressure loss is by using the following set of equations [13]:

$$R = \sqrt{1 - 1.35WF + 0.35WF^2} \quad (2.13)$$

$$\rho_c = (1 - R^2)\rho_w + R^2 \rho_o \quad (2.14)$$

$$m = \frac{\mu_w}{\mu_o} \quad (2.15)$$

$$Re_1 = \frac{\rho_c D v}{\mu_w} (1 + R^4 (m - 1)) \quad (2.16)$$

$$\Delta P = f \frac{L}{D} \rho_c \frac{v^2}{2} \quad (2.17)$$

Where:

R is the ratio of the core diameter to the pipe inside diameter

ρ_c is the effective density of the core and annulus together

m is the ratio of viscosities

Re_1 is an effective Reynolds number

f is the friction factor, which is a function of Reynolds number

A full derivation and discussion of these equations is given in [13]. The results using these equations give pressure losses that are significantly less than the pressure loss of the oil alone. These equations, however, do not consider the stability of the regime, and whether it can be formed at all for the given flow rates of oil and water; this must be verified separately, as discussed above.

2.1.6 Other Flow Regimes

It is not well known just how viscous, heavy crude oil and water will flow when pumped together in a pipeline. Studies by the Saskatchewan Research Council (SRC) and others have shown that in some cases the pressure loss can be only a bit higher than for water alone. This tends to occur over a reasonably small range of water fractions, and in some cases only if a minimum flow velocity is maintained [19]. These studies have not incorporated any flow visualization, so it is not known if a core-annular flow regime is naturally formed, or if some other flow regime exists. In general, flows in which the presence of low water fractions can show significant decrease in pressure loss relative to pure oil flow can be called “water-assisted flow”.

Work on the flow of heavy oil and water mixtures through horizontal pipes has been studied for some time. Charles *et al* at the Alberta Research Council performed experiments in this field over forty years ago [20]. The viscosity of the oils used in these tests (6.3 to 65.0 cp) were far below the viscosities of interest in the present work (see Section 2.3.1). Lighter oils were used, with carbon tetrachloride added to increase the density to that of water. It is noted that the viscosity of the fluids used in these tests is significantly less than the viscosity of the heavy oil of interest in the current work. Charles *et al* observed and described many different flow patterns in their experiments: water drops in oil, oil in water

concentric (core flow), oil slugs in water, oil bubbles in water, and oil drops in water. In their terminology, drops are small compared to the diameter of the pipe, bubbles can approach the diameter of the pipeline but are not significantly longer than they are wide, and slugs nearly fill the inside diameter of the pipeline and are significantly longer than they are wide. The flow patterns were dependent on the oil properties and the flow rates of both the water and oil. One of their conclusions was: “The addition of increasing amounts of water to oil...lowers the pressure gradient to a minimum, after which the addition of more water increases the pressure gradient and, with sufficient water, the pressure gradient exceeds the pressure gradient for the oil flowing alone.” It should be noted, though, that the behaviour is somewhat different for each of the oils they tested. Taking note of this, and considering that heavy oils, even of the same density and from the same area, can have significant compositional differences, it is doubtful that a general correlation can be developed for non-emulsified heavy oil/water flow.

2.2 Heat Transfer from Fluid

Heat transfer (when radiation is not a factor) is a linear process (i.e., heat transfer is proportional to the temperature difference between two points). Because of this, resistance to heat transfer through several layers can be calculated as a sum of the resistance to heat transfer through each separate layer. This is often called an electrical analogy—heat flux, thermal resistance and temperature difference are analogous to current, resistance and voltage, respectively, in an electrical circuit. Consider a steady state case with a constant fluid temperature specified inside an insulated, buried pipe, and a constant temperature specified at the surface of the ground. There are four separate thermal resistances through which the energy must pass: convection to the pipe wall, the pipe wall itself, the insulation, and the ground. The regions are shown in Figure 2.1.

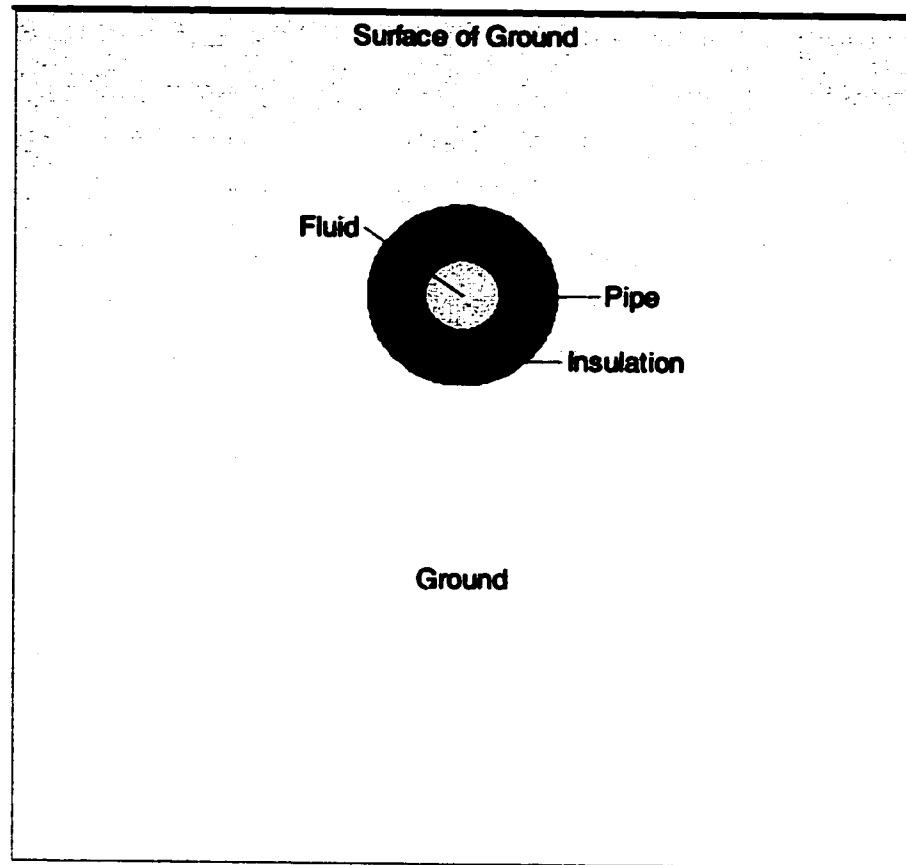


Figure 2.1 Regions through which heat must flow

These resistances can be described by the following equations [21]:

$$R_1 = \frac{1}{h 2 \pi r_0 L} \quad (2.18)$$

$$R_2 = \frac{\ln \frac{r_1}{r_0}}{2 \pi k_p L} \quad (2.19)$$

$$R_3 = \frac{\ln \frac{r_2}{r_1}}{2 \pi k_i L} \quad (2.20)$$

$$R_4 = \frac{\cosh^{-1} \left(\frac{Z}{r_2} \right)}{2 \pi k_s L} \quad (2.21)$$

Where:

R is a thermal resistance

h is the convective coefficient

r_0 is the inside radius of the pipe

r_1 is the outside radius of the pipe

r_2 is the outside radius of the insulation

k is the thermal conductivity

Z is the burial depth at the pipe centreline

p refers to the pipe

i refers to the insulation

g refers to the ground

The heat flow is then:

$$\dot{q} = \frac{\Delta T}{\sum R} \quad (2.22)$$

There is one problem with using the equations above to calculate heat loss. The temperature difference is considered to be constant over the length of the pipe. In fact, the fluid will cool as it travels through the pipe, so the temperature difference will be less at the end of the segment than it was at the beginning. The above formulation then is just an approximation which assumes that the fluid cools only a very small amount relative to the temperature difference between the fluid and the surface. When this assumption is not satisfied, there can be a large error in these equations are used to calculate the heat transfer from the fluid to its surroundings.

To determine the total heat loss from the fluid without making this assumption, it is more convenient to first consider the change in temperature of the fluid. Consider a small element of the pipeline, with a length dx , as shown in Figure 2.2.

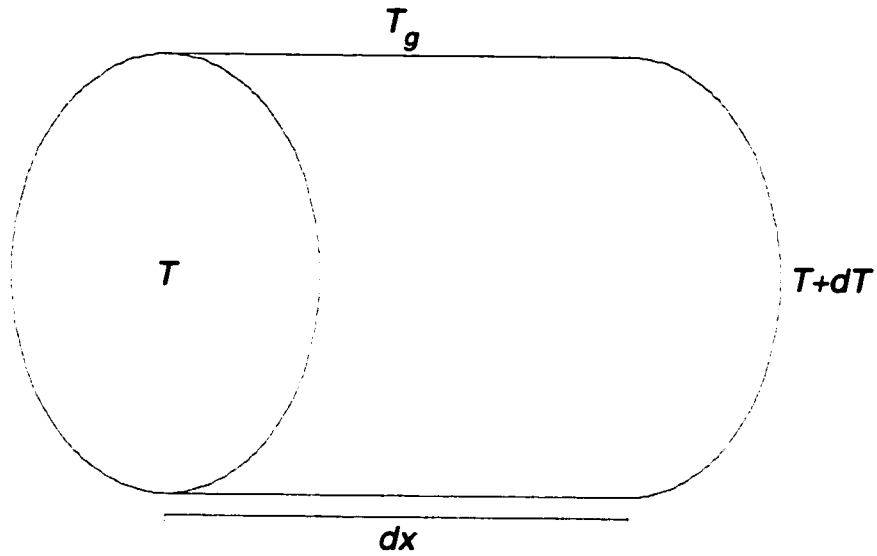


Figure 2.2 A fluid element in the pipe

The change in the fluid temperature, dT , in this element [21] is given by :

$$dT = -\frac{d\dot{q}}{\dot{m}c} \quad (2.23)$$

Where:

\dot{q} is the heat flux (J/s; the dot indicates a rate per unit time)

\dot{m} is the mass flow rate

c is the specific heat of the fluid

Note that this formulation assumes that the fluid is incompressible. More accurately, the conservation of energy principle [23] is expressed as:

$$\dot{q} = \dot{m} \Delta H \quad (2.24)$$

Where:

H is the enthalpy.

The enthalpy is:

$$H = u + \frac{P}{\rho} \quad (2.25)$$

Where:

u is the internal energy

Since the density does not change with pressure or temperature in an incompressible fluid, the change in enthalpy is equal to the change in internal energy. The specific heat of a fluid in general is expressed in one of two ways:

$$c_v = \left(\frac{\partial u}{\partial T} \right)_v \quad \text{or} \quad c_p = \left(\frac{\partial H}{\partial T} \right)_p \quad (2.26a, 2.26b)$$

For an incompressible fluid (or solid), these two terms are identical [23]. The current work uses the symbol c to refer to the specific heat for liquids and solids.

The heat transfer from the fluid to the ground in this element is given by:

$$d\dot{q} = \frac{T - T_g}{R} = \frac{T - T_g}{\hat{R}} dx \quad (2.27)$$

Where:

T_g is the temperature of the surroundings

$$\hat{R} = R dx \quad (2.28)$$

\hat{R} is the thermal resistance for a unit length of pipe

It is assumed that the thermal resistance does not change over the length of the pipe. This implies that the various properties used in calculating the resistance also do not change. The effects of this assumption are discussed below.

Combining equations 2.23 and 2.27, we get:

$$dT = -\frac{T - T_g}{\hat{R} \dot{m} c} dx \quad (2.29)$$

Rearrange this to obtain:

$$\frac{dT}{T - T_g} = -\frac{dx}{\hat{R} \dot{m} c} \quad (2.30)$$

Integrate both sides:

$$\ln(T - T_g) = -\frac{x}{\hat{R} \dot{m} c} + C \quad (2.31)$$

Take the exponential of both sides, and replace $\exp(C)$ with k :

$$T - T_g = k \cdot \exp\left(-\frac{x}{\hat{R}\dot{m}c}\right) \quad (2.32)$$

To solve for k , we need to apply a boundary condition. We know the temperature at the start of the pipeline, so we can use this:

$$\begin{aligned} x = 0 &\Rightarrow T = T_f \\ \therefore (T_f - T_g) &= k \end{aligned} \quad (2.33)$$

So:

$$T = T_g + (T_f - T_g) \exp\left(-\frac{x}{\hat{R}\dot{m}c}\right) \quad (2.34)$$

This equation can now be used to determine the temperature at any point in a buried pipeline flowing in a steady state. To determine how much heat is transferred to the ground over a given length of pipe, L , the following equation is used:

$$\dot{q} = (T_f - T_L) \dot{m}c \quad (2.35)$$

Where:

T_L is the temperature after length L .

Insert the temperature at L into the equation:

$$\begin{aligned} \dot{q} &= \left[T_f - \left(T_g + (T_f - T_g) \exp\left(-\frac{L}{\hat{R}\dot{m}c}\right) \right) \right] \dot{m}c \\ &= \left[T_f - T_g - (T_f - T_g) \exp\left(-\frac{L}{\hat{R}\dot{m}c}\right) \right] \dot{m}c \\ &= (T_f - T_g) \left(1 - \exp\left(-\frac{L}{\hat{R}\dot{m}c}\right) \right) \dot{m}c \end{aligned} \quad (2.36)$$

Clearly, as L gets longer, the *increase* in heat loss from the fluid gets smaller. The maximum energy the fluid can lose is when it has cooled to ground temperature.

There is still an assumption that the ground temperature at the point where it is specified (in this case at the surface) is not affected by the change in heat flux over the length of the pipe. This assumption should normally be much safer than the assumption (now removed) that the fluid temperature did not change over the length. As the temperature changes, there will be slight changes in the thermal conductivities of the pipe, insulation and ground, but these will normally be very small, and should not have a noticeable effect on the overall results. What is more important to be aware of is changes in the convective coefficient. If this changes by any significant amount (for example, due to a change in flow regime), the above equation will not be valid.

The convective coefficient is calculated depending on various properties. In general it is found using Eq. 2.37 [21]:

$$h = \frac{Nu k}{D} \quad (2.37)$$

This is for single phase flow (with miscible constituents). If the flow is not single phase (i.e., if it is an emulsion, core-annular flow, or some other flow regime), special consideration is required. The calculation of the Nusselt number (Nu) depends on whether the flow is laminar or turbulent. If the flow is laminar, the Nusselt number is a constant. In the case where the surface temperature is specified, this can be determined analytically to be 3.66, while in the case where the flux is specified, this is determined to be 4.36 [21]. In the present case, the fluid temperature is specified; this matches neither of the well-defined cases demonstrated in many textbooks. The value for constant temperature ($Nu = 3.66$) is used in the current work, as its conditions more closely match the given case.

In turbulent flow, there are several correlations available. One of the better ones, according to Incropera and DeWitt is by Gnielinski [21], and is:

$$Nu = \frac{\frac{f}{8}(Re - 1000)Pr}{1 + 12.7\sqrt{\frac{f}{8}}(Pr^{\frac{1}{4}} - 1)} \quad (2.38)$$

Where:

Pr is the Prandtl number

The Prandtl number is given by:

$$Pr = \frac{\mu c}{k} \quad (2.39)$$

The thermal conductivity of oil and water change slightly over the temperature range of interest, but not enough to have a significant effect on the results. Of more concern is whether the flow regime changes between laminar and turbulent in the pipe, as this will cause a drastic change in the convective coefficient. Care must be used to ensure that within a region of interest, the properties do not change significantly; otherwise the calculations described here may be invalid.

From 0°C to 70°C, the thermal conductivity of water changes from 0.569 to 0.660 W/m·K. The thermal conductivity of engine oil (which is not the same as unrefined heavy oil, but is used here as an illustration) changes from 0.147 to 0.139 W/m·K over the same range. These temperatures were chosen since 70°C is a common temperature to which heavy oil tanks are heated, and 0°C is an extreme value at the lower end of the temperature scale—it is unlikely that a heavy oil pipeline in which the temperature dropped as low as 0°C could be successfully operated.

Entrance effects may be significant in the heat transfer. In laminar flow, the hydrodynamic entry length can be approximated by Eq. 2.40 [2].

$$x_{fd,h} \approx 0.05 D Re \quad (2.40)$$

As an example, consider a heavy oil with a viscosity of 1000 cp and a density of 1000 kg/m³ flowing at 1 m/s through a pipe with an inside diameter of 5 cm. The

Reynolds number for this flow will be 50, and the entrance length will be about 12.5 cm. This is very short relative to the length of the pipeline and can be neglected in the pressure loss calculations. The thermal boundary layer development, however, is not necessarily the same as the hydrodynamic boundary layer. The length of the thermal boundary layer can be approximated by Eq. 2.41 [2]:

$$x_{fd,h} \approx 0.05 D Re Pr \quad (2.41)$$

Consider again the example above. If the oil has a specific heat of 2000 J/kg·K and a thermal conductivity of 0.1 W/m·K, then its Prandtl number is 20,000, and the thermal entrance length is about 2.5 km. This has significant implications, since the theoretical convective coefficient at the point where the thermal boundary layer has not yet started to form approaches infinity.

A correlation is available for calculating the average convection coefficient in a region with a fully developed velocity profile but developing thermal boundary layer [2]:

$$\overline{Nu} = 3.66 + \frac{0.0668(D/L)Re Pr}{1 + 0.04[(D/L)Re Pr]^{1/4}} \quad (2.42)$$

It should be noted that the region in which the thermal boundary layer has not yet begun to form is at the outlet of the heated tank. The piping at this point is above ground—it will lead from the tank to a pump and only then into the buried pipeline. It should be feasible, both technically and economically to apply heat tracing to this section of above ground piping to help prevent excessive heat losses. In a typical case, for a well-insulated, buried pipeline, the thermal resistance of the convection will be only 10-25% of the total thermal resistance; the effect of reducing the convection resistance (as would be the case in the entry region) can only reduce the overall resistance by that much, or less. Furthermore, the Prandtl number of heavy oil is highly dependent upon temperature. The effects of this in the entry region have not been investigated. It should be

expected that the oil in the boundary layer where it begins to form should cool quickly due to the high convective coefficient, giving a very different Prandtl number at the wall than in the bulk fluid. The effect of this on the validity of Eq. 2.42 has not been investigated. Entry effects are assumed to have only a small overall effect on the results, and are neglected in the current work.

2.3 Combined Heat Transfer and Pressure Loss

2.3.1 Effect of Temperature on Viscosity

The pressure loss equations in Section 2.1, are based on the assumption that the fluid density and viscosity do not change throughout the pipeline. Clearly the properties of any fluid do change with temperature. Over the temperature range of interest, the density of water and oil change by only a very small amount, and ignoring these will not introduce a significant error into the results. Similarly the viscosity of water changes by less than three centipoise over the temperature range of interest. While this is high on a percentage basis, it will not have a significant effect on the pressure loss—a few kilopascals more or less are not significant to the design of a pipeline. The viscosity of oil, however, is very much dependent on temperature to the point where it is very important to the overall pressure loss—the viscosity of heavy oil can change by orders of magnitude over the temperature range of interest.

In HOGS I, C-FER gathered oil viscosity data from several participants in the JIP. The densities of the samples from which this data was derived ranged from 9-13.3°API. API gravity is the standard density measurement used in the oil industry. 10°API is the same density at 15°C as water; smaller API gravities indicate heavier oils. At 15°C, the relationship between the API gravity and the specific gravity (SG) is:

$$API = \frac{141.5}{SG} - 131.5 \quad (2.43)$$

Figure 2.3 shows the viscosity of each of the samples tested over the range of temperatures for which they were tested. As would be expected, the lighter the oil the less viscous it is in general, but this is not always the case as is also evident on the graph. Each sample decreased in viscosity as the temperature increased. The scale is a logarithmic scale, so the decrease in viscosity is significant (approximately two orders of magnitude over the 50°C range plotted).

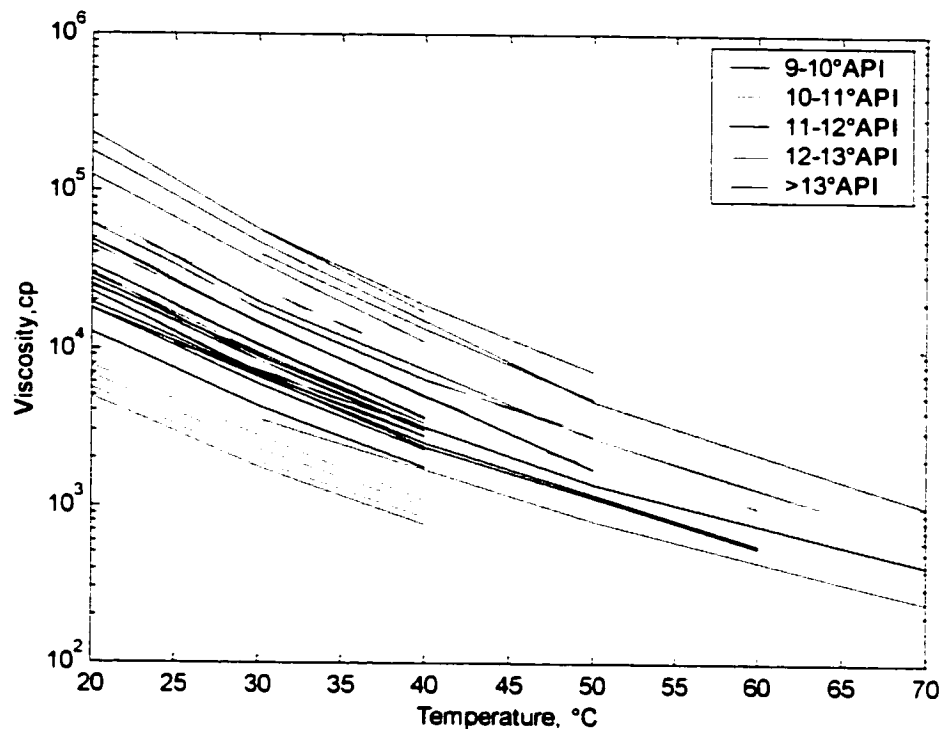


Figure 2.3 Viscosity vs. temperature relationship of Western Canadian heavy oils

Any computation which will require knowing the viscosity of the fluid at arbitrary temperatures must use a correlation of viscosity against temperature. Traditional correlations in the oil industry have been based on API gravity and temperature, and could be used as a good approximation of viscosity even if no test data from a sample was available. This is much less true in heavy oil, and is even worse in Western Canada than in other heavy oil fields around the world. To have any expectation of accuracy, a sample of oil must be tested and then this data can be

fitted to a specific correlation. One correlation that has been used historically, and is quite successful is the assumption that the logarithm of the logarithm of viscosity is a linear function of temperature. Historically, an offset of one centipoise is applied to the relationship, but this is insignificant in the present case, as the viscosities are so high, so this will not be used here. This was applied to the previous data, and is shown in Figure 2.4.

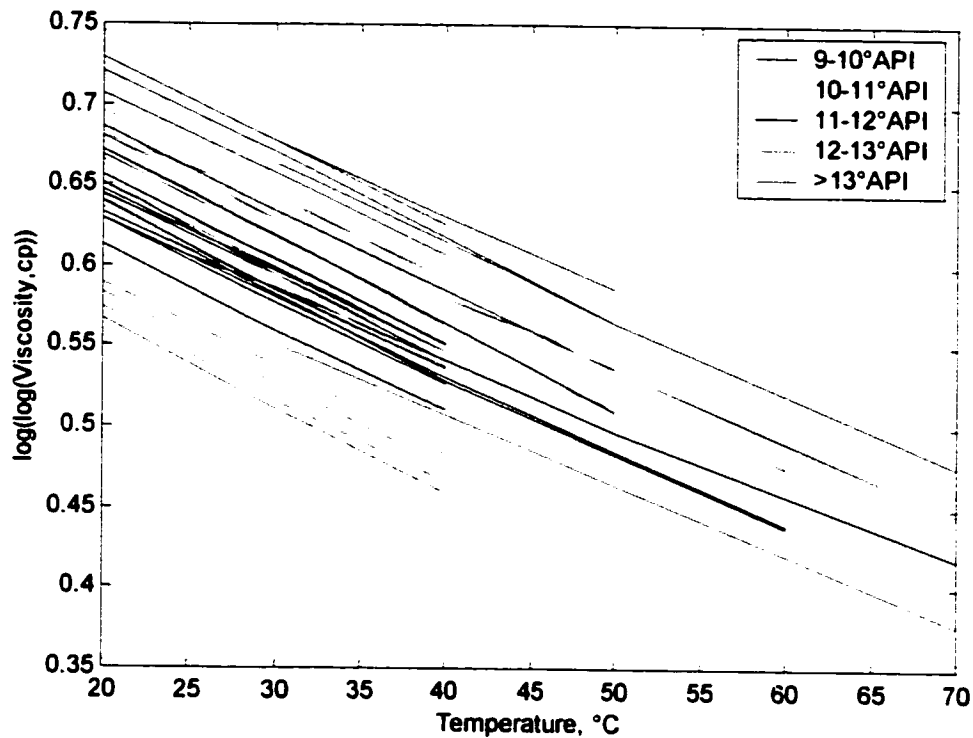


Figure 2.4. Linearized relationship between viscosity and temperature

Figure 2.4 shows that this is a valid correlation for this type of oil, as the plotted lines are very nearly straight. The viscosity correlation is then (with viscosity in centipoise):

$$\log_{10}(\log_{10}(\mu)) = A + BT \quad (2.44)$$

The A and B coefficients are determined from sample data. If there are two sample points at different temperatures, the A and B can be solved for by solving two equations for two unknowns. If there are more points, a least-squares

regression can be used to determine the two parameters. At least two sample points must normally be available to determine the values of A and B .

There are two reasons why a linearized equation for viscosity is valuable, as compared to another form (e.g. polynomial fit). First, note that the lines in Figure 2.4 are roughly parallel. This means that if only one point is available for a specific oil, we can use it to determine the value of A , while assuming that the value of B is the same as for other similar oils. Second, some types of curve fit methods (e.g. polynomials) can give very inaccurate results when extrapolated beyond the range of the data used to generate the curve fit. While extrapolation should never be recommended, a linearized equation can be extrapolated with much more confidence than other methods. It should be noted that of the 137 data points collected by C-FER in phase I of the HOGS project, none were at temperatures below 20°C; in a buried pipeline, it is quite likely that the temperature could go below this.

Figure 2.5 is a parity plot for this correlation, using the data collected by C-FER. The correlation is applied to each oil sample individually. Only samples with three or more data points are plotted here, as correlations calculated based on only two points would be exact for those two points.

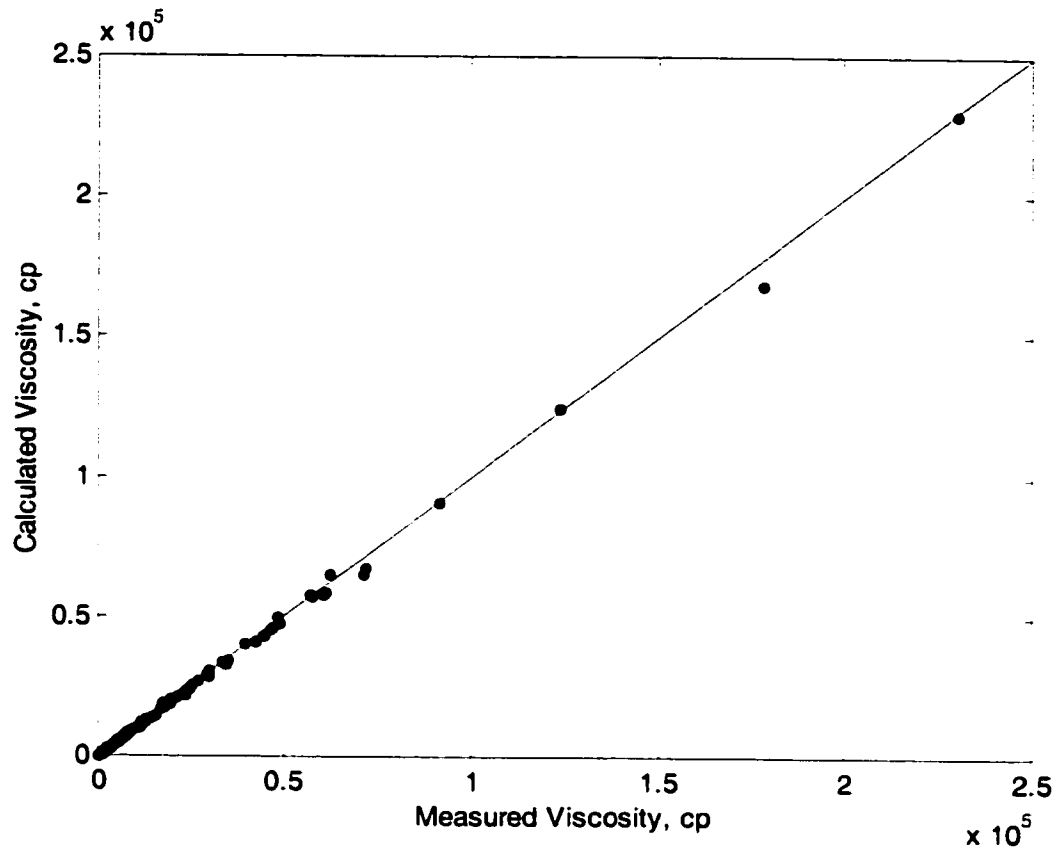


Figure 2.5 Parity plot for viscosity correlation

It can be seen that this equation is quite accurate when used for individual samples.

In HOGS I, C-FER developed a correlation based on the viscosity tests plotted in the above figures[1]. This correlation relates viscosity to temperature and API gravity. It is preferable to always use test data from a well or wells under consideration, but when performing sensitivity analyses, it is easier to have a single parameter to vary (in this case API gravity). The correlation is:

$$X = 1.6194 - 0.83991 \log(API) - 0.0045692 T \quad (2.45)$$

$$\mu = 10^{10^X}$$

The viscosity given by this is in centipoise, so must be divided by 1000 to obtain pascal-seconds. This is in the same form as the previous equation, where a

constant value of B is used, and A varies based on API gravity. This correlation should only be used for Western Canadian heavy crude oils with API gravities ranging from 9-13.3°API. It gave a median error of 5.3%, with a standard deviation of 36%. For comparison, four other commonly-used correlations were also tested against the same data set; of these, the best had a median error of 56.6% with a standard deviation of 86% [1].

2.3.2 Pressure Loss, Considering Effect of Temperature

As was shown in Section 2.1.1, when the properties are constant throughout a pipe and the flow is laminar, the pressure loss will be proportional to the fluid viscosity. This means that the effect of temperature on pressure loss is going to be proportional to the effect of viscosity on pressure loss, so long as the flow is laminar. The flow of oil of these viscosities in the context of a gathering system (i.e. low flow rates in small diameter pipes) will almost always be laminar. For example, 200 m³/d of oil with a viscosity of 1000 cp, and a density of 1000 kg/m³ flowing through a pipe with an internal diameter of 100 mm will have a Reynolds number of about 29.5. This is fully two orders of magnitude below the transition to turbulent flow. Turbulent flow should only occur when the water fraction is high. (This is not considering the possibility of a water-assisted flow regime.)

Over the length of a pipeline, the temperature could change significantly. Therefore the oil viscosity could change considerably. This invalidates the assumption of constant properties in the pressure loss equation. There are two ways around this in laminar flow, only one of which can be easily generalized to the other possible flow regimes. In laminar flow (as discussed in Section 2.1.1), the pressure loss was given simply by:

$$\Delta P = \frac{128 \mu L Q}{\pi D^4} \quad (2.46)$$

Of the quantities in this equation, only the viscosity is changing. As stated in the previous section, the viscosity, in pascal-seconds is given by:

$$\log_{10}(\log_{10}(1000 \mu)) = A + BT \quad (2.47)$$

or:

$$\mu = \frac{10^{10^{A+BT}}}{1000} \quad (2.48)$$

The temperature is still required, and this is given by the following equation (see Section 2.2):

$$T = T_g + (T_f - T_g) \exp\left(-\frac{x}{\hat{R} m c}\right) \quad (2.49)$$

The thermal resistance is well defined and constant over the length of the pipeline for laminar flow, assuming that the ground, pipe, insulation and fluid have constant thermal conductivity, density and specific heat (i.e., these properties do not change with temperature).

Consider an elemental length of the pipeline. The pressure loss is given by:

$$dP = \frac{128 \mu Q}{\pi D^4} dx \quad (2.50)$$

Substituting the viscosity:

$$dP = \frac{128 \times 10^{10^{A+BT}} Q}{1000 \pi D^4} dx \quad (2.51)$$

Integrate this over the length of the pipeline from 0 to L :

$$\Delta P = \frac{128 Q}{1000 \pi D^4} \int_0^L 10^{10^{A+BT}} dx \quad (2.52)$$

The viscosity term could not be removed from inside the integral, since it is a function of position. Finally, the pressure loss for laminar flow of oil is given by:

$$\Delta P = \frac{128 Q}{1000 \pi D^4} \int_0^L 10^{10^{A+BT_g + (T_f - T_g) \exp\left(-\frac{x}{\hat{R} m c}\right)}} dx \quad (2.53)$$

This integral must be solved numerically. Note also that this result is in pascals. It must be divided again by 1000 to convert to kilopascals, if desired.

The other, more general, method of calculating the pressure loss is to split the pipeline into a number of segments. The length of each individual segment should be short enough to ensure that the viscosity changes very little over its length. The pressure loss is calculated based on the temperature at the start of the segment. The temperature at the end of the segment is then determined, and this temperature is used to determine the viscosity in the next segment. This method will also work in turbulent flow, or one of the more exotic flow regimes, as it does in laminar flow, and is preferred for that reason. This method was used in arriving at the results which appear in Chapter 6.

The accuracy can be improved somewhat by calculating the temperature at the end of the segment before calculating the pressure loss. The viscosity can then be evaluated at the average of the temperatures at the beginning and end of the segment. This can be further improved by using a weighted average to consider the fact that the viscosity is not a linear function of temperature.

2.3.3 Effects of Viscous Heating

Pressure loss in a flowing system is caused by fluid friction; both internal to the fluid and at the fluid/wall interface. Conservation of energy clearly applies, so the energy in the form of pressure which is lost must be converted to a different form of energy. This is heat. In most systems, this is neglected because it is a small amount and has no significant effect on the system. In a heavy oil pipeline, however, it may be significant.

Consider rate of energy dissipation (i.e., power). The power lost due to flow pressure from an incompressible fluid [21] is given by:

$$\dot{W} = \Delta P Q \quad (2.54)$$

This power is converted to heat within the fluid (conservation of energy):

$$\dot{q} = \dot{W} \quad (2.55)$$

The temperature increase in a fluid caused by a given rate of heat input is:

$$\Delta T = \frac{\dot{q}}{\dot{m} c} \quad (2.56)$$

Therefore the temperature increase is related to the pressure loss by:

$$\Delta T = \frac{\Delta P Q}{\dot{m} c} \quad (2.57)$$

The mass flow rate and volume flow rate are related by:

$$\dot{m} = \rho Q \quad (2.58)$$

So:

$$\Delta T = \frac{\Delta P Q}{\rho Q c} \quad (2.59)$$

or:

$$\Delta T = \frac{\Delta P}{\rho c} \quad (2.60)$$

As an example, an oil with a density of 950 kg/m³ and a specific heat of 2000 J/kg·K, flowing in a perfectly insulated pipe in which it has a pressure loss of 1000 psi (6.895×10⁶ Pa), will have a temperature increase of 3.6°C. This temperature rise is significant in the calculation of pressure losses in a viscous oil.

This effect, while not significant in typical liquid flows (e.g. water), is also important in other fields, such as the high speed flow of gases [21]. A significant non-dimensional parameter in these fields is the Eckert number:

$$Ec = \frac{v^2}{c(T_s - T_\infty)} \quad (2.61)$$

Ref. 2 lists sources for further reference with respect to the Eckert number.

2.3.4 Analysis of Steady State Results

In the following analyses, the effects of viscous heating are not considered, unless specifically described, despite the significance shown above. This will give somewhat larger values for pressure losses than would be expected, and is therefore a conservative result for pipeline design.

First, a single case is considered over a range of flow rates. The values used for the other quantities are given in Table 2.1.

Table 2.1 Base case values

Pipe outer diameter, in.	3.5
Pipe wall thickness, in.	0.216
Insulation thickness, in.	1.5
Pipe depth, ft.	4
Pipeline length, km	2
Inlet temperature, °C	70
Surface temperature, °C	2
Oil density, kg/m ³	950
Oil conductivity, W/m·K	0.11
Oil specific heat, J/kg·K	2000
Oil test temperature 1, °C	30
Oil viscosity at test 1, cp	25000
Oil test temperature 2, °C	70
Oil viscosity at test 2, cp	800
Pipe conductivity, W/m·K	60
Insulation conductivity, W/m·K	0.04
Ground conductivity, W/m·K	0.5

The A and B parameters from Eq. 2.44 are calculated from the temperatures and viscosities in the above table to be 0.7785 and -0.004510 , respectively.

The pressure loss over a range of flow rates is given in Figure 2.6 below.

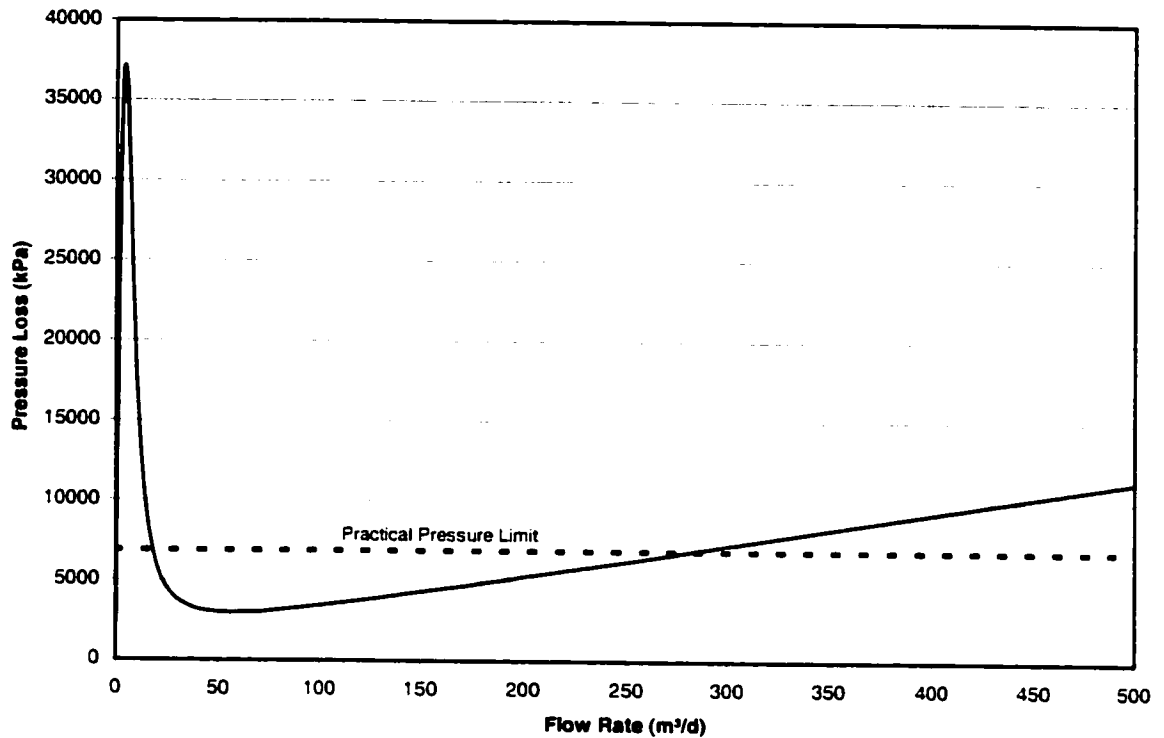


Figure 2.6 Relationship of pressure loss to flow rate

The most obvious thing about this graph is that it is not monotonically increasing as would be expected on a typical pressure loss versus flow rate graph. The reason for this is the temperature loss. Clearly at zero flow rate there is zero pressure loss; as the flow rate increases from zero, the pressure loss grows very rapidly. This is because the fluid is essentially at the ground temperature of 2°C everywhere (the fluid loses its initial temperature very quickly). At 2°C, the viscosity correlation yields a viscosity of 762,000 cp. As the flow rate increases, the fluid is able to retain proportionately more energy for a longer portion of the pipeline, so the increase in pressure loss for each incremental increase in flow rate gets smaller and smaller. Eventually, the effect of retaining temperature on the viscosity outweighs the increased velocity, and the pressure loss actually decreases with increased flow rate. When the flow rates get even higher, the pipeline will not be able to retain more temperature for an increase in flow rate

(i.e., the temperature is nearly constant throughout the pipeline, and increasing the flow rate further will not change this), and once again the increase in velocity becomes dominant and the pressure loss increases with flow rate.

It should be noted that these calculations do not take into account the limits of any pumping equipment or the pipeline itself. No company would actually install a pipeline or pump in a heavy oil gathering system which had an operating limit of over 35000 kPa (the maximum pressure in Figure 2.6. This particular size of pipe would be applicable up to 20,000-30,000 kPa when pumping heavy oil in rural areas, according to the calculations mandated by CSA Z183 [22], assuming a grade of steel with a yield stress in the 40-60 ksi range, and not considering any corrosion or erosion allowances. Most oil companies, however, would not normally be willing in such an application to install a transfer pump with a rating of over 1000 psi (6900 kPa), due to the high capital and operating costs. This pressure limit is marked on Figure 2.6

It is very important that a pipeline be designed so that its intended operating point is somewhere to the right of the local minimum value of pressure loss. The slope to the left of this point is extreme—a slight reduction in flow rate will lead to a large increase in pressure loss.

Variations in the other parameters will also have an effect in the results. One way to look at the effect of these is to vary one parameter at a time from the base values in the table above and look at the results in the form of a tornado chart. A tornado chart is a useful way of visualizing which parameters, when changed, can have a large or small effect on the overall results of a calculation. Two tornado charts are shown below, one using a base flow rate of 200 m³/d and the other using a base flow rate of 20 m³/d. From Figure 2.6 above, it can be seen that these two flow rates will result in a very similar pressure loss, but that they are on

opposite sides of the local minimum. The tornado charts are organized so the parameters with the greatest effect are at the top. The labels beside each level of the chart describe the parameter and the range of values used. The format [x...y...z] is used, where x is the value of the parameter which resulted in the minimum pressure loss, y is the base value (used when any other parameter is being varied), and z is the value which produced the largest pressure loss.

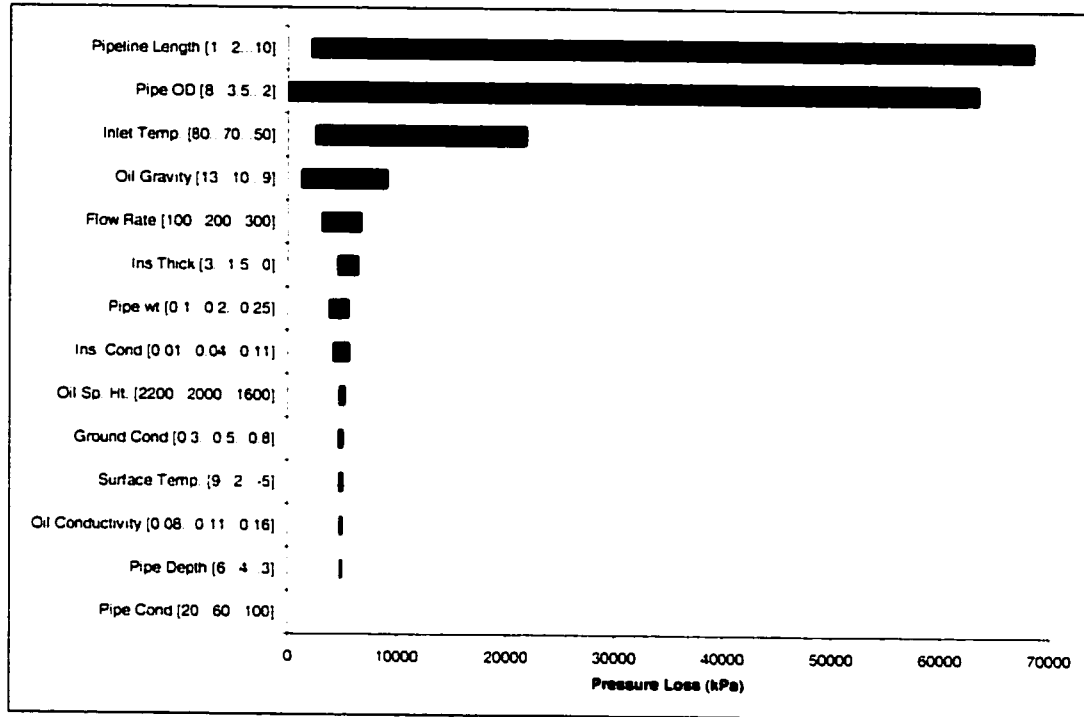


Figure 2.7 Tornado chart for base flow rate of 200 m³/d

It can be seen from Figure 2.7 that the pipeline length, pipe diameter, inlet temperature and oil gravity are the most significant parameters when the flow rate is on the right side of the local minimum in the chart in Figure 2.6. Longer pipelines, smaller pipes and denser (i.e. more viscous) oil all lead to larger pressure losses.

It is worth briefly discussing the effect of pipe wall thickness. This appears to have a significant effect (about the same as insulation thickness), which is contrary to intuitive reasoning, which indicates that since the pipe has such a high

conductivity, a change in its thickness should not have a large effect on the results. This reasoning is supported by the very small effect of pipe conductivity on pressure loss (so small that the line is not visible in the figure). The reason that the wall thickness has a significant effect on pressure loss is that the pipe's inside diameter is calculated from the pipe's OD and the wall thickness. The pipe's ID is very important (raised to a factor of 4 in the pressure loss equation) in calculating flow loss.

It might be expected from these graphs that the solution to extreme pressure loss is simply to use larger pipe. It is true that in most cases, larger pipes could reduce the steady state flow losses. Unfortunately, they cost much more to purchase, insulate and install, so the economics will usually support smaller pipes—just one more case in engineering where physical and economic constraints work in opposite directions. There are also questions as to what happens in transient conditions (start-ups and shutdowns) with larger pipes. Even in steady state conditions, in some cases the larger pipes could actually cause larger pressure losses, depending on how the local minimum point on the pressure loss graph is affected by the change in pipe size.

Clearly the inlet temperature is very important. Economic factors come into play here as well. It may not be economical to heat a tank to 80°C—it may actually cost less to heat a tank to 70°C and pump at a greater pressure.

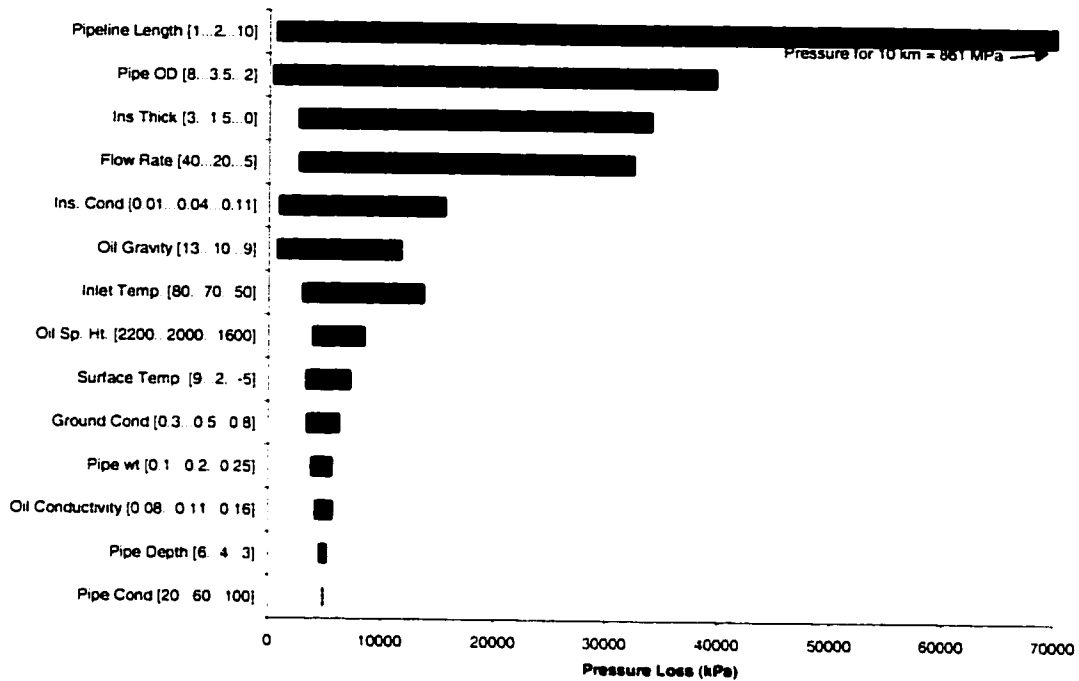


Figure 2.8 Tornado chart for base flow rate of 20 m³/d

In Figure 2.8 it can be seen that changes in more parameters lead to significant changes in the pressure loss, and that the changes are larger than in the 200 m³/d case. This is not surprising, remembering the slope of the pressure loss versus flow rate graph at 20 m³/d as compared to the slope at 200 m³/d. In this region (flow rates below the flow rate which gives a minimum pressure loss—around 55 m³/d in this case), it may become economical to spend the extra money during construction to reduce the pressure loss during operation. For example a larger diameter pipe, or thicker insulation may be justified.

2.3.5 Transient Effects

Effects of thermal transients have not been considered to this point. Calculating thermal transients requires the calculation of the thermal history of the ground around the entire pipeline over the history of the pipeline. This requires a numerical solution; a method of calculating this will be described in Chapter 4.

Transients which are of interest to the operation of viscous oil pipelines include the following:

- **Initial start-up of the pipeline.** The ground is cold but the fluid is warm. It will take a period of time for the temperatures to stabilize.
- **Seasonal temperature variations.** In Alberta, there is approximately a 40°C temperature difference between average winter and summer temperatures. Pipelines are not buried deeply enough to be unaffected by this. Start-ups and shutdowns will therefore be affected by the time of the year in which they take place. It should be noted, however, that in the tornado charts above, the pressure loss was not greatly affected by changes in the surface temperature. This may indicate that the seasonal temperature variations may not have a large effect on the pressure loss when in continuous operation. No hypothesis regarding the effects of season on start-ups and shutdowns can be supported with this data, however.
- **Shutdowns.** These can be planned (e.g., for pump or pipeline maintenance) or unplanned (e.g., due to power failure). The oil's temperature is very important—the cooler it is permitted to get before reaching the end of the pipeline, the higher the pressure loss will be. If flow is stopped, the oil will cool off and when the operator attempts to restart flow, it may not be possible to achieve the same flow rate. The line may even need to be flushed with water before restarting flow of oil. In some cases an expensive intervention involving steam injection through coiled tubing may be required.

None of these is considered in the steady state calculation shown earlier in this section.

3. Ground Temperature Effects

Before attempting to calculate the effect of a pipeline in the ground, one should understand how the temperature in the ground changes as the seasons change. Because soil is a fairly poor conductor of heat, there will be a difference in temperature between the temperature at the surface and at any depth.

The mean daily temperatures (by month) at Elk Point, Alberta [24] are shown in Figure 3.1. These are air temperatures, as recorded by Environment Canada.

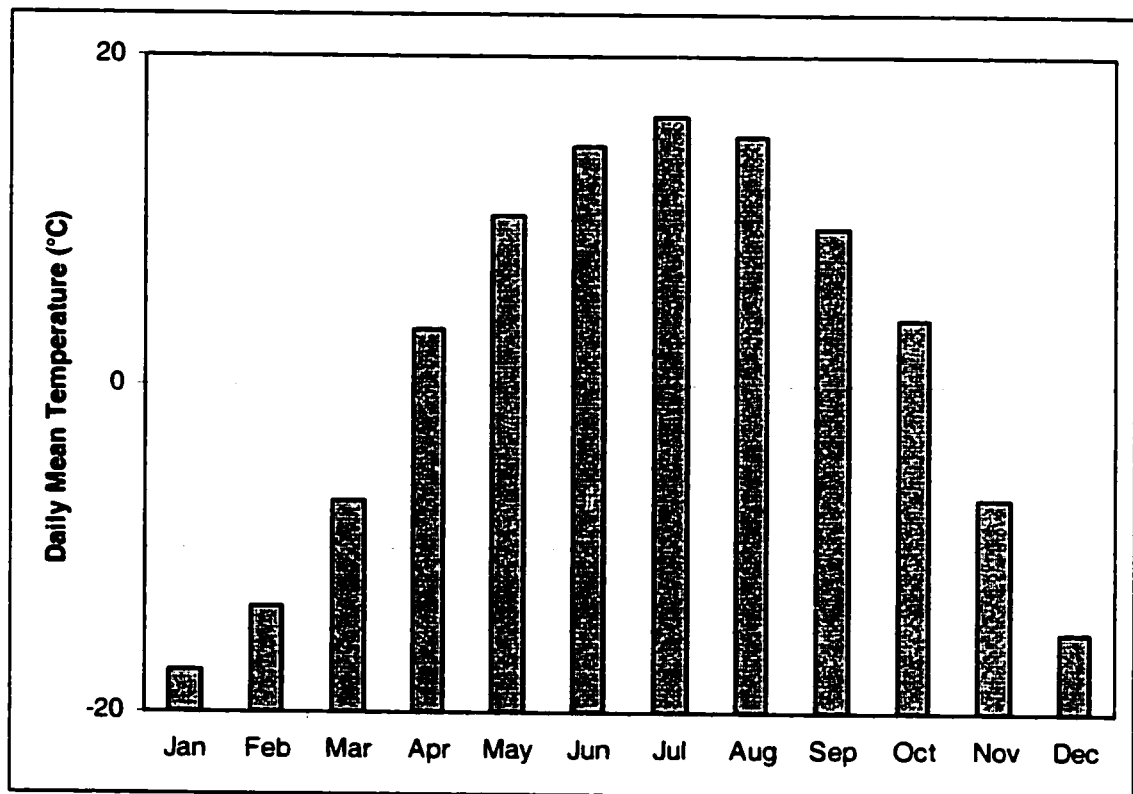


Figure 3.1 Mean Daily Temperature at Elk Point

The temperature at the surface can be assumed to be a sine wave with a period of one year, as an approximation. The rest of the analysis here assumes that one zero point of the sine wave (i.e., where the temperature is an average) occurs close to May 1, the maximum temperature near August 1, and the minimum temperature near February 1. This is shown in Figure 3.2 in Section 3.1.1, where

day 0 is assumed to be May 1. A more rigorous approach would consider solar radiation and convection effects (as was done in the work of Kazemi and Perkins[25]), but this simple approach should be adequate in most cases.

When considering the surface temperature as a sine wave in this way, the temperature at any depth is also a sine wave, but with a reduced amplitude, and a phase delay relative to the surface temperature.

3.1 One-Dimensional Heat Conduction Equation

To determine the temperature in a uniform, semi-infinite medium, the following differential equation [21, 26] is relevant:

$$\kappa \frac{\partial^2 T}{\partial x^2} = \frac{\partial T}{\partial t} \quad (3.1)$$

Where:

κ is thermal diffusivity

T is temperature

t is time

x is depth

Note that in the previous chapter, thermal conductivity was used in the heat transfer equations, and here thermal diffusivity is used. Thermal diffusivity is related to thermal conductivity as:

$$\kappa = \frac{k}{\rho c} \quad (3.2)$$

In steady state calculations, the density and specific heat are not used; when the effects of time are considered, however, these are important.

The boundary condition at the surface can be represented by:

$$T_s = T_{avg} + T_{amp} \cdot \sin(\omega \cdot t) \quad (3.3)$$

Where:

T_s is the temperature at the surface

T_{avg} is the average annual temperature

T_{amp} is the variation from the average of the annual minimum and maximum temperatures

ω is the angular frequency of seasonal variations

Since time is in seconds, the frequency of seasonal variations, ω , is given by:

$$\omega = \frac{2\pi}{86400 \times 365} \quad (3.4)$$

In determining an analytical solution, there are two different options which could be used for the second required boundary condition. The first assumes that the temperature an infinite distance below the surface is the average surface temperature. The second assumes that there is a thermal gradient in the ground, and specifies that a certain distance below the surface (below the deepest point where seasonal variations are noticeable) is a constant temperature which is somewhat different from the average surface temperature.

3.1.1 Analytical Solutions

In solving this differential equation (Eq. 3.1), the initial conditions are not relevant—desired is a solution that is applicable a very long time after the initial condition has passed. The two variations have solutions [26, 27] as follows:

$$T = T_{avg} + B \exp\left[-x \sqrt{\frac{\omega}{2\kappa}}\right] \sin\left[\omega t - x \sqrt{\frac{\omega}{2\kappa}}\right] \quad (3.5)$$

and

$$T = T_{avg} + \frac{x}{x_1} (T_1 - T_{avg}) - \text{Im} \left[B \frac{\sin\left(x_1 - x \sqrt{i \frac{\omega}{\kappa}}\right)}{\sin\left(x_1 \sqrt{i \frac{\omega}{\kappa}}\right)} \exp(-i\kappa x) \right] \quad (3.6)$$

In the second variation, x_1 is some depth at which there are no noticeable seasonal variations in temperature, and T_1 is the constant temperature at that depth. These have been derived analytically, although the derivations are not given by the

references. These were verified to be correct by comparing with a numerical solution.

Figure 3.2, below, shows a comparison between the surface temperature ($T_{avg} = 2^{\circ}\text{C}$ and $B = 20^{\circ}\text{C}$) and the ground temperature at a depth of 1.2 m in a soil with a thermal diffusivity of $1.413 \times 10^{-7} \text{ m}^2/\text{s}$ for both boundary conditions (this value is based on data from [21], and is a reference to dry soil). In the second boundary condition, the temperature was set to be 2.55°C at 15 m, which corresponds to a typical thermal gradient in Alberta and a 2°C average surface temperature. The two curves for the different boundary conditions differ only by the difference in the average temperature of the ground at 1.2 m (0.044°C) with the two different boundary conditions. These two curves are indistinguishable from one another in the figure.

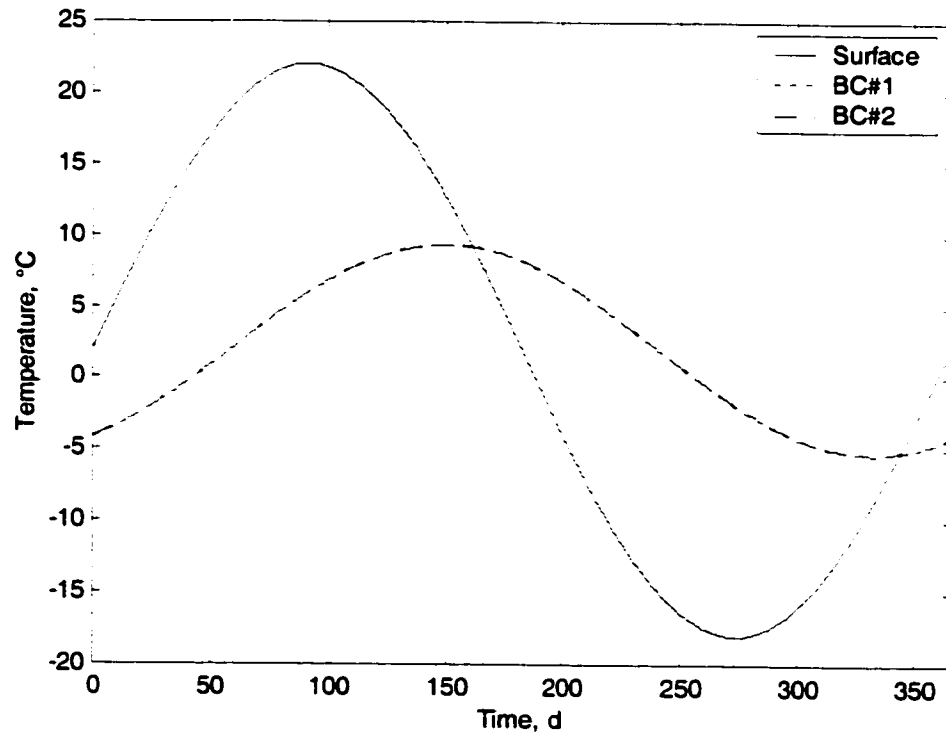


Figure 3.2 Surface and ground temperatures through one year.

For the purposes of the present work it should be irrelevant which of the two boundary conditions is used. This one dimensional formulation will be used in establishing boundary conditions for the two-dimensional model used in the calculation of the temperature of the ground surrounding the pipeline. As such, it will be recalculated for several depths at each time step used in the final model. Since it makes essentially no difference in terms of results which of the two boundary conditions is used, it makes sense to use the one which results in fewer computations being done. The assumption being made here is that the thermal gradient in the ground is not extreme.

From Figure 3.2, it is immediately obvious that there are two significant differences between the temperature at surface and the temperature below the ground. Firstly, the amplitude of the periodic (seasonal) variations in temperature is attenuated. The degree of attenuation decreases as the thermal diffusivity of the ground increases and increases with the depth. Secondly, there is a phase delay. The phase delay increases as the thermal diffusivity of the ground decreases and the depth increases. This means that the ground at depth is coldest not when the air temperature is the coldest, but sometime after that. The delay could be two or three months (or more in some cases). Practically speaking this means that a pipeline operator who wishes to start the pipeline or perform a planned shutdown (e.g. for maintenance) when the ground is as warm as possible should not do so in the hot days of summer, but wait until fall, as this is when the ground at depth is warmest.

The effects of day and night are not considered. Using the principle of superposition, the effects of day and night can be considered using Eq. 3.5. If the period of the sine wave is set to be one day, the diffusivity is the same as was used in Figure 3.2, and the difference between the hottest and coldest temperatures in a day is 10°C , then the difference between the minimum and

maximum daily temperatures at 1 metre of depth is $4.4 \times 10^{-8} \text{ }^\circ\text{C}$. The difference decreases exponentially with depth. At any reasonable pipeline depth, the error introduced by not considering the daily fluctuations in temperature will be negligible.

3.1.2 Numerical Solutions

In some cases, an analytical solution may not be available. This could be the case if the ground properties were not constant, or if the boundary or initial conditions were changed, for example. A finite difference model of the above case can be easily assembled. In these cases, a numerical solution is necessary. There are two ways to derive a finite difference model for such a case. The first is to apply a discretization to the differential equation, and the second is to do an energy balance on a node. (These methods are described briefly below, and in more detail in Section 4.2.) These two methods will result in the same equation, depending on the time difference discretization in the first method. The differential equation is:

$$\kappa \frac{\partial^2 T}{\partial x^2} = \frac{\partial T}{\partial t} \quad (3.7)$$

This is discretized at node i as [21]:

$$\kappa \frac{T_{i-1}^* - 2T_i^* + T_{i+1}^*}{(\Delta x)^2} = \frac{T_i^{t+\Delta t} - T_i^t}{\Delta t} \quad (3.8)$$

Where terms with an asterisk "*" on them can be referenced to time t (explicit) or $t+\Delta t$ (implicit). The advantage of the explicit formulation is that the temperature of each node can be determined based on data which is already known (i.e. the temperature of the node and surrounding nodes at the previous time step). Its disadvantage is that it has a stability criterion, which limits the size of the time step. The implicit method requires that a system of equations be solved simultaneously, but does not have a limit on the time step to ensure numerical stability. Because of the inherent stability of the implicit method, it is preferred

here. Arranging the equation into a form suitable for solving a system of simultaneous equations:

$$T_i^{i+1} - \frac{\kappa \Delta t}{(\Delta x)^2} (T_{i-1}^{i+1} - 2T_i^{i+1} + T_{i+1}^{i+1}) = T_i^i \quad (3.9)$$

Rearranging:

$$\left(-\frac{\kappa \cdot \Delta t}{(\Delta x)^2} \right) T_{i-1}^{i+1} + \left(1 + \frac{2\kappa \Delta t}{(\Delta x)^2} \right) T_i^{i+1} + \left(-\frac{\kappa \Delta t}{(\Delta x)^2} \right) T_{i+1}^{i+1} = T_i^i \quad (3.10)$$

Implementing this scheme over a 15 metre depth, with the bottom boundary set to the average annual temperature, and the top boundary being the periodic surface temperature, and using a spatial discretization (Δx) of 0.2 m, and a time step of a half-day, with the initial temperature set to be the average annual temperature throughout, gives the results shown in Figure 3.3 (as compared to the analytical solution in Section 3.1.1 above):

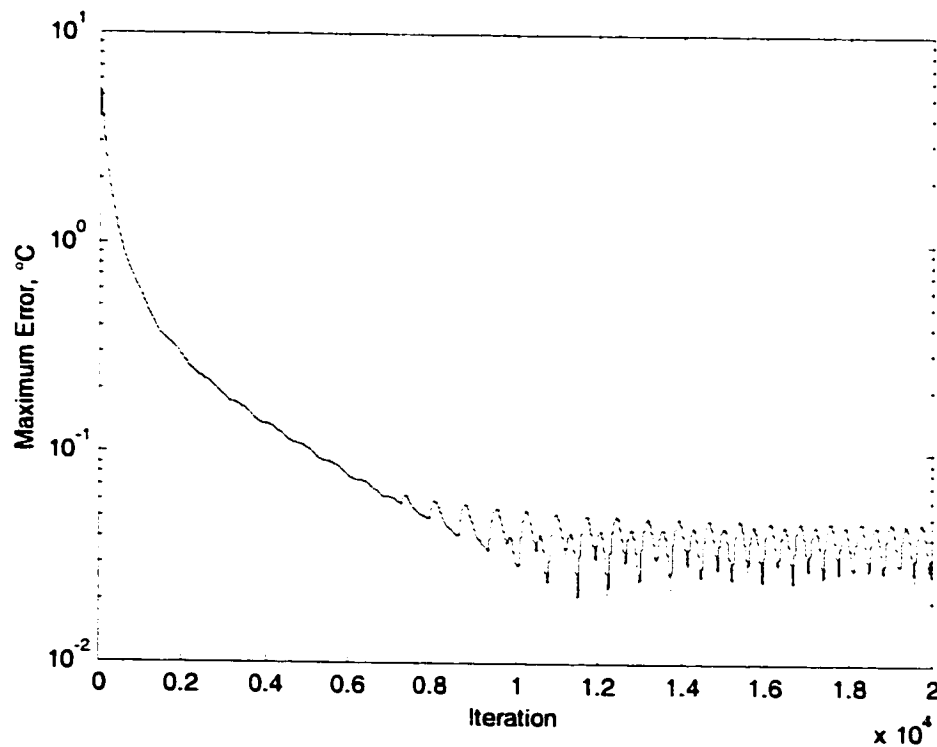


Figure 3.3 Comparison of analytical and numerical solutions

After approximately 10,000 iterations (i.e. 5000 days, or about 14 years), the error settles down to a periodic value, oscillating around 0.04°C. The first 14 years of simulated time are required for the initial condition to become irrelevant to the numerical solution (remembering that the analytical solution already removed the effects of the initial condition). Figure 3.2 only showed one year of calculation because the effect of the initial condition was considered to have completely died out; the temperature at any depth then has a period of one year. Figure 3.3 shows a much longer time period because the effects of the initial condition are considered; the longer time shows how these effects die out with time.

A smaller time step or a smaller spatial discretization would reduce the value around which the error oscillates after the initial condition is no longer relevant. Using the analytical solution at time 0 as an initial condition would remove the error shown in the first 10,000 iterations of the plot.

3.2 Effects of Different Boundary Conditions

The results shown above specified the temperature at the surface as a boundary condition. The properties of the ground were uniform and constant throughout time. Some variations on this can also be considered.

3.2.1 Convection at the Surface

Convection is easily considered at the surface using a finite difference scheme. All the nodes below the ground use exactly the same nodal equation as before; only the surface node changes. A new node must be added to the grid, however, to account for the temperature of the air at the surface. The implicit formulation is shown below:

$$\frac{2\kappa\Delta t}{(\Delta x)^2}(T_1^{i+1} - T_0^{i+1}) + \frac{2h\Delta t}{\Delta x\rho c}(T_\infty - T_0^{i+1}) = T_0^{i+1} - T_0^i \quad (3.11)$$

Rearranging:

$$-\frac{2h\Delta t}{\Delta x \rho c} \cdot T_{\infty} + \left(1 + \frac{2\kappa\Delta t}{(\Delta x)^2} + \frac{2h\Delta t}{\Delta x \rho c}\right) T_0^{t+1} - \frac{2\kappa\Delta t}{(\Delta x)^2} \cdot T_1^{t+1} = T_0^t \quad (3.12)$$

For sufficiently high values of the convective coefficient (h), there is very little difference between the results for this case and for the case where the surface temperature was set equal to the air temperature.

Any covering on the ground will likely have an effect on the heat transfer between the air and the ground. Grain fields on the surface of the ground could reduce the convective coefficient by breaking up the air flow, although it is unlikely that stubble on the fields in spring and autumn would have a significant effect on the heat transfer. Pipelines built through bushy or forested areas would certainly have a reduced convective coefficient because there is less wind at ground level in these areas. While the bush is cleared for the installation of the pipeline, not only will it grow back (to some extent: pipeline corridors are kept reasonably clear), but its presence a few metres away will almost certainly break up the wind, reducing the value of the convective coefficient. Figure 3.5 in Section 3.2.2 shows a comparison of some different values of the convective coefficient. It can be seen that decreasing the convective coefficient will reduce the amplitude of the temperature oscillations at depth and increase the phase difference between the oscillations and those at surface. Depending on the expected value of the convective coefficient it may or may not be reasonable to neglect the effect of convection (i.e., use the specified surface temperature formulations above). For comparison, [25] uses 2.5-5 BTU/hr-ft²-°F (14-28 W/m²-K) for a convection coefficient in Alaska. In Figure 3.5, it can be seen that there is very little difference in ground temperature when a convection coefficient is 25 W/m²-K on bare ground as when it is infinite on bare ground.

3.2.2 Insulating Layer at Surface

The next issue regarding ground cover is snow. Snow acts as a good insulator, especially when it is light, dry snow, as is typically found in cold regions such as

Western Canada. In [21], the thermal conductivity of snow is listed as 0.049 for a density of 110 kg/m³ (loose) and 0.19 for a density of 500 kg/m³ (packed). The presence of a significant snow layer could significantly effect the temperature of the ground below the surface. This could easily be modelled with a finite difference scheme, using a layer of nodes with different thermal properties.

To account for a new layer in the finite difference model, the node at the interface must be considered specially. Note that the nodes within the two regions are considered exactly the same way as before, except that the values of κ and Δx will be (or could be) different in each of the regions. The interface node, and the node immediately on each side of it are shown in Figure 3.4.

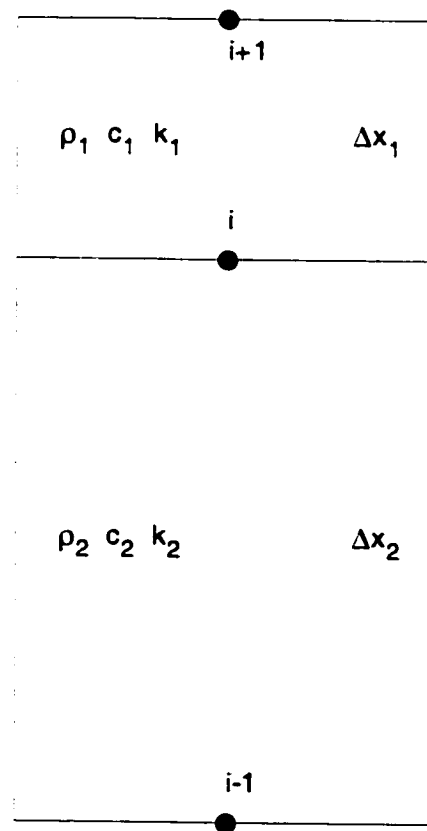


Figure 3.4 Finite difference model on boundary of two regions

The equation at the interface node is:

$$\frac{\frac{2k_1 \Delta t}{\Delta x_1} (T_{i+1}^{t+1} - T_i^{t+1}) + \frac{2k_2 \Delta t}{\Delta x_2} (T_{i-1}^{t+1} - T_i^{t+1})}{\rho_1 c_1 \Delta x_1 + \rho_2 c_2 \Delta x_2} = T_i^{t+1} - T_i^t \quad (3.13)$$

Rearranged:

$$\left(\frac{-\frac{2k_1 \Delta t}{\Delta x_1}}{\rho_1 c_1 \Delta x_1 + \rho_2 c_2 \Delta x_2} \right) T_{i+1}^{t+1} + \left(1 + \frac{\frac{2k_1 \Delta t}{\Delta x_1} + \frac{2k_2 \Delta t}{\Delta x_2}}{\rho_1 c_1 \Delta x_1 + \rho_2 c_2 \Delta x_2} \right) T_i^{t+1} + \left(\frac{-\frac{2k_2 \Delta t}{\Delta x_2}}{\rho_1 c_1 \Delta x_1 + \rho_2 c_2 \Delta x_2} \right) T_{i-1}^{t+1} = T_i^t \quad (3.14)$$

Clearly if the physical properties and the discretization is the same in both regions, this reduces to the simple nodal equation above, noting that:

$$\kappa = \frac{k}{\rho c} \quad (3.15)$$

Figure 3.5 shows a comparison of five different conditions. The data plotted is the temperature at a depth of 1.2 metres below the surface over a period of one year.

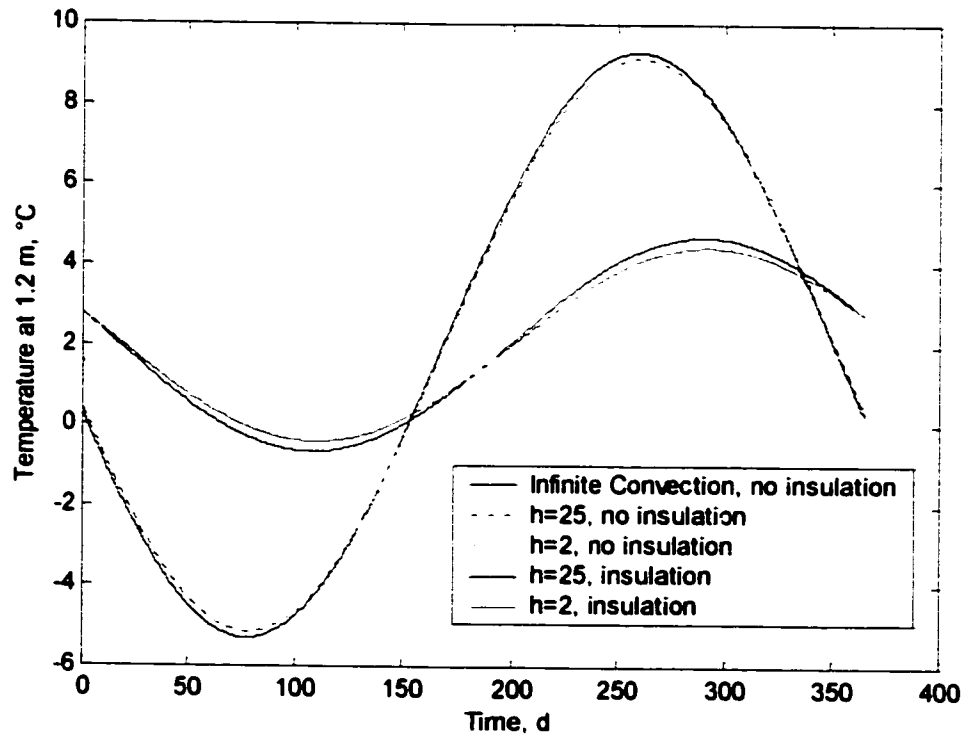


Figure 3.5 Effect of convective coefficient and insulating surface layer.

The insulation represents snow, although it is considered to be on the ground all year, even above 0°C—this plot is simply an illustration of the effect of an insulating layer on the ground. The depth of the insulation layer was 15 cm; the thermal conductivity, density and specific heat were 0.049 W/m·K, 110 kg/m³ and 2040 J/kg·K, respectively. It is immediately evident that either reducing the convective coefficient or adding an insulating layer (e.g. of snow) will serve both to increase the attenuation of the change in temperature at depth and to increase the phase delay.

3.2.3 Radiation

Heat can be lost from the ground by radiation as well as by convection. If radiation is considered rigorously, the difference between night and day needs to be considered, along with the angle of the sun and lengths of the day at different times of the year. A less rigorous approach was used by [25], who applied a sine wave formulation of the sun's radiant energy as incident on the ground in their area of interest (the Alaskan north slope). Radiation effects are neglected in the current work.

3.2.4 Moisture in the Ground

In real soil there will almost always be some degree of moisture. As the ground temperature drops to the freezing point it is incapable of dropping lower until the water freezes, regardless of the surface temperature. Likewise, when the ground starts to warm up, the temperature cannot rise above the freezing point until all the ice has melted. Because the latent energy of the ice-water phase change is so high, this effect can cause a large phase delay and attenuation of the seasonal temperature variations below the surface of the ground.

A simple finite difference scheme can represent this behaviour. The ground within each node contains a certain amount of moisture, which must freeze (or

melt) before the temperature of the node can go below (or above) the freezing point. The equation for the energy balance [26] at a node is:

$$\frac{\rho c \Delta x}{\Delta t} (T_i^{t+1} - T_i^t) = \frac{k}{\Delta x} (T_{i-1} - 2T_i + T_{i+1}) + \frac{L m_w}{\Delta t} \quad (3.16)$$

The latent heat of fusion, L , for water is approximately 333,000 J/kg. Note that m_w is the mass of water per unit volume *to change phase* during the time step (positive for freezing, negative for melting).

This is more easily solved using an explicit scheme, unlike the previous formulations which could be solved with an implicit scheme. This is because the mass of water to change phase is unknown and must be calculated for each layer at each time step. As described earlier, the biggest disadvantage of using an explicit scheme is the limit placed on the time step by the need for stability. The explicit form of the equation is:

$$T_i^{t+1} = T_i^t + \frac{\kappa \Delta t}{(\Delta x)^2} (T_{i-1}^t - 2T_i^t + T_{i+1}^t) + \frac{L m_w}{\rho c \Delta x} \quad (3.17)$$

At the surface node it is:

$$T_0^{t+1} = \frac{2\kappa \Delta t}{(\Delta x)^2} (T_1^t - T_0^t) + \frac{2h \Delta t}{\Delta x \rho c} (T_\infty - T_0^t) + T_0^t + \frac{L m_w}{\rho c \Delta x} \quad (3.18)$$

To implement this in a model, the program will have to keep track of the proportion of the water contained within each node which is liquid and solid. If this value at any node is not 0 or 1 (i.e., all water is solid or liquid, respectively), then the nodal temperature must be 0°C. The calculations will have to be iterative in some cases—for each time step, the program will have to calculate a new temperature at each node, assuming $m_w = 0$, and ensure that node did not cross the 0°C barrier. If the nodal temperature changes sign, a value for m_w will have to be calculated, and a new proportion of frozen water will be calculated. The initial version of the model will assume that the thermal properties of the ground are the same, regardless of whether the water is in a liquid or solid phase—if the moisture

content of the ground is very low, this assumption is reasonable. When the moisture content is higher, however, the change in properties must be considered.

In an explicit formulation, there is a stability criterion to consider. If the effect of the phase change is not considered, and the case has a convective boundary, then the stability criterion [21] is based on the Fourier number (Fo) and the Biot number (Bi):

$$Fo(1 + Bi) \leq \frac{1}{2} \quad (3.19)$$

Where:

$$Fo = \frac{\kappa \Delta t}{(\Delta x)^2} \quad (3.20)$$

$$Bi = \frac{h \Delta x}{k} \quad (3.21)$$

The maximum time step that can be used for a given case is then:

$$\Delta t \leq \frac{\frac{1}{2}}{\frac{\kappa}{(\Delta x)^2} + \frac{\kappa h}{\Delta x k}} \quad (3.22)$$

The results can be seen in Figure 3.6.

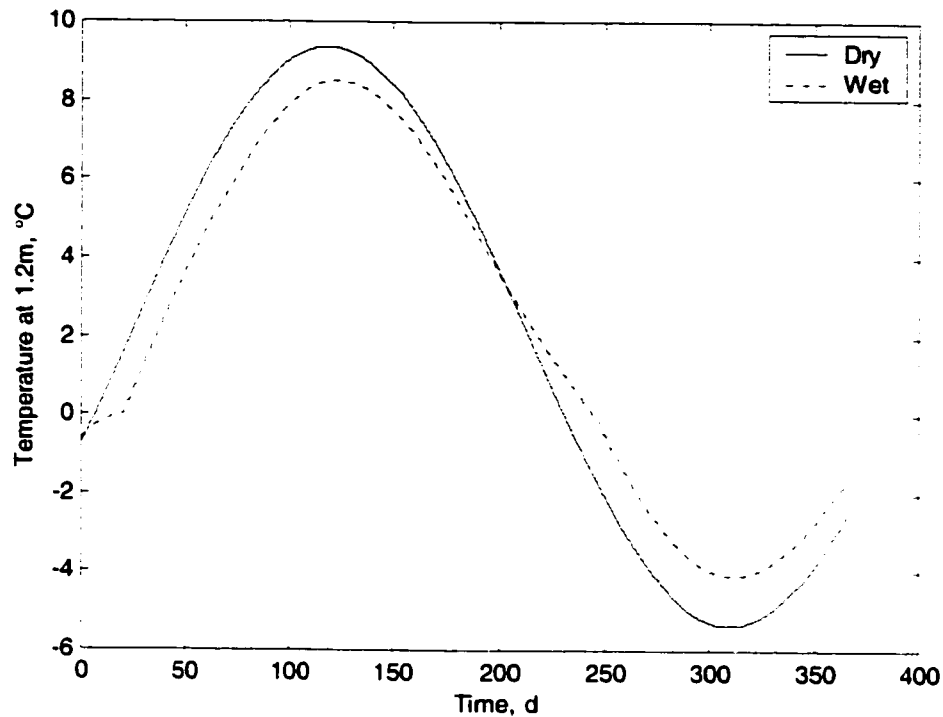


Figure 3.6 Seasonal ground temperature variation for dry and moist ground.

This plot shows a one year period after the conditions have had time to stabilize from the initial condition. As might be expected, there is attenuation of the temperature variation, since the latent heat of the water acts as a buffer. There is clearly a change in the behaviour of the curve as it crosses 0°C in each direction. This is because the ground is not permitted by the calculation algorithm to be at any temperature other than 0°C while there is both liquid and solid water present. It should be noted that this is an approximation: [26] states that liquid water can exist below 0°C and solid water can exist above 0°C while in the porous medium of the ground.

While not plotted, it is evident that increasing the water content in the ground will increase the attenuation. At what point this becomes a significant issue to the calculation of the temperatures in a buried pipeline is undetermined at this time. Figure 3.6, above, is for soil with 50 kg of water per cubic metre of soil. Even at

this very low water content (about 2.5% by mass), it can be seen that there is a significant effect. For any higher water content, as would be expected in moist ground, the assumption that freezing and thawing have an insignificant effect on the total rate of heat transfer to and from any buried pipeline will most likely be invalid.

4. Transient Heat Loss Calculations

In order to determine the heat loss from a pipeline at any moment in time, in the midst of transient conditions, the temperature distribution in the ground surrounding the pipeline must be known. This requires that the thermal history of the ground be calculated.

4.1 Transient Heat Conduction Equation

The differential equation governing two-dimensional transient heat transfer in Cartesian coordinates [21, 26] is:

$$\frac{1}{\kappa} \frac{\partial T}{\partial t} = \frac{\partial^2 T}{\partial x^2} + \frac{\partial^2 T}{\partial y^2} \quad (4.1)$$

This assumes a constant value of κ throughout the domain. This assumption is carried through the rest of this work unless otherwise specified. There is only a very limited range of applications for which this equation can be solved analytically. Most cases will require a numerical solution.

4.2 Finite Difference Method

In a finite difference model, the domain of interest is divided into regions, each of which is centred around a node. The results are calculated at the nodes. A nodal temperature at a given time is based on the temperature of the nodes around it, and its own temperature at an earlier time. There are two ways of deriving a finite difference equation for a given problem. The first is to simply apply numerical derivative equations to the known differential equation, and the second is to take a step further back and apply physical principles. Numerical derivatives [21] which can be applied to the above equation are:

$$\frac{\partial T}{\partial t} = \frac{T^{t+\Delta t} - T^t}{\Delta t} \quad \text{and} \quad \frac{\partial^2 T}{\partial x^2} = \frac{T_{t-\Delta x} - 2T_t + T_{t+\Delta x}}{(\Delta x)^2} \quad (4.2, 4.3)$$

Other formulations are available, some of which may increase accuracy, but these are simple and are adequate for most cases.

Applying these to the two dimensional transient heat transfer differential equation gives the following results:

$$\frac{1}{\kappa} \frac{T^{t+\Delta t} - T^t}{\Delta t} = \frac{T_{x-\Delta x} - 2T_x + T_{x+\Delta x}}{(\Delta x)^2} + \frac{T_{y-\Delta y} - 2T_y + T_{y+\Delta y}}{(\Delta y)^2} \quad (4.4)$$

The problem remaining is that in each of the three terms, the temperature is referred to only one of the two dimensions, and the terms on the right hand side are not referred to a time. Consider a node (i,j) , where a change in the first parameter refers to a change in the x direction and a change in the second parameter refers to a change in the y direction. The equation is now:

$$\frac{1}{\kappa} \frac{T_{i,j}^{t+\Delta t} - T_{i,j}^t}{\Delta t} = \frac{T_{i+1,j} - 2T_{i,j} + T_{i-1,j}}{(\Delta x)^2} + \frac{T_{i,j+1} - 2T_{i,j} + T_{i,j-1}}{(\Delta y)^2} \quad (4.5)$$

The terms on the right hand side are still not referred to a time. There are two choices: t and $t+\Delta t$. If t is chosen then it is possible to solve for each $T^{t+\Delta t}$ independently of the others (this is called the explicit method). This is easily implemented in a computer program. Unfortunately, this simplicity comes at a cost. If the size of the time step (Δt) is too large, the calculation becomes numerically unstable (i.e., the error increases at each step). The maximum value of the time step depends on the values of Δx , Δy , and κ . If $t+\Delta t$ is chosen, however, the calculation is inherently stable, regardless of the size of the time step, but the result at any node cannot be calculated independently from the results at the other nodes (this is called the implicit method). Note that oscillations in the solution can still occur (especially at larger time steps), but these are damped out with increasing time. Smaller time steps will also lead to increased accuracy. Because of the inherent stability of the implicit method, it will be used exclusively in this work.

In an implicit formulation, the difference equation is:

$$\frac{1}{\kappa} \frac{T_{i,j}^{t+\Delta t} - T_{i,j}^t}{\Delta t} = \frac{T_{i+1,j}^{t+\Delta t} - 2T_{i,j}^{t+\Delta t} + T_{i-1,j}^{t+\Delta t}}{(\Delta x)^2} + \frac{T_{i,j+1}^{t+\Delta t} - 2T_{i,j}^{t+\Delta t} + T_{i,j-1}^{t+\Delta t}}{(\Delta y)^2} \quad (4.6)$$

There is such an equation for every node in the system. This results in a system of equations which must be solved simultaneously. Written in a matrix-vector form, this is:

$$[A]\{T^{t+\Delta t}\} = \{T^t\} \quad (4.7)$$

[A] is a $n \times n$ matrix, and the $\{T\}$ terms are $n \times 1$ column vectors. The value of [A] must be determined from the finite difference equation. At a given node, the equation can be rewritten as:

$$T_{i,j}^{t+\Delta t} - T_{i,j}^t = \frac{\kappa \Delta t}{(\Delta x)^2} (T_{i+1,j}^{t+\Delta t} - 2T_{i,j}^{t+\Delta t} + T_{i-1,j}^{t+\Delta t}) + \frac{\kappa \Delta t}{(\Delta y)^2} (T_{i,j+1}^{t+\Delta t} - 2T_{i,j}^{t+\Delta t} + T_{i,j-1}^{t+\Delta t})$$

$$T_{i,j}^{t+\Delta t} - \frac{\kappa \Delta t}{(\Delta x)^2} (T_{i+1,j}^{t+\Delta t} - 2T_{i,j}^{t+\Delta t} + T_{i-1,j}^{t+\Delta t}) - \frac{\kappa \Delta t}{(\Delta y)^2} (T_{i,j+1}^{t+\Delta t} - 2T_{i,j}^{t+\Delta t} + T_{i,j-1}^{t+\Delta t}) = T_{i,j}^t$$

Finally:

$$-\frac{\kappa \Delta t}{(\Delta y)^2} T_{i,j-1}^{t+\Delta t} - \frac{\kappa \Delta t}{(\Delta x)^2} T_{i-1,j}^{t+\Delta t} + \left(1 + 2\frac{\kappa \Delta t}{(\Delta x)^2} + 2\frac{\kappa \Delta t}{(\Delta y)^2} \right) T_{i,j}^{t+\Delta t} - \frac{\kappa \Delta t}{(\Delta x)^2} T_{i+1,j}^{t+\Delta t} - \frac{\kappa \Delta t}{(\Delta y)^2} T_{i,j+1}^{t+\Delta t} = T_{i,j}^t \quad (4.8)$$

This is now in a form that can be easily converted to a matrix-vector form as above. All that remains is a bookkeeping issue, since there are two dimensions of nodes which must be stored in a one-dimensional vector.

The second method of deriving the finite difference equation is based on physical principles. Consider node (i, j) , surrounded by nodes $(i-1, j)$, $(i+1, j)$, $(i, j-1)$, and $(i, j+1)$, as shown below.

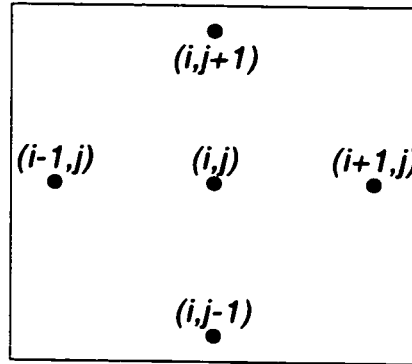


Figure 4.1 Node numbering

At any instant in time the heat flowing from node $(i-1, j)$ into node (i, j) is given by:

$$\dot{q} = \frac{k A}{\Delta x} \Delta T \quad (4.9)$$

If the two dimensional domain is assumed to have a depth of L in the third dimension, then this is:

$$\dot{q} = \frac{k L \Delta y}{\Delta x} (T_{i-1,j} - T_{i,j}) \quad (4.10)$$

If the time step is short enough so that the temperatures of the two nodes do not change significantly, the total amount of energy to flow between the nodes is:

$$q = \dot{q} \Delta t = \frac{k L \Delta y \Delta t}{\Delta x} (T_{i-1,j} - T_{i,j}) \quad (4.11)$$

Similar equations can be written for the heat flow from the other nodes during the time step. The change in temperature of node (i,j) is given by:

$$\Delta T = T_{i,j}^{t+\Delta t} - T_{i,j}^t = \frac{q}{\rho V c} = \frac{q}{\rho \Delta x \Delta y L c} \quad (4.12)$$

This can be combined into one equation for the node:

$$T_{i,j}^{t+\Delta t} - T_{i,j}^t = \frac{\frac{k L \Delta y \Delta t}{\Delta x} (T_{i-1,j} - T_{i,j}) + \frac{k L \Delta y \Delta t}{\Delta x} (T_{i+1,j} - T_{i,j}) + \frac{k L \Delta x \Delta t}{\Delta y} (T_{i,j-1} - T_{i,j}) + \frac{k L \Delta x \Delta t}{\Delta y} (T_{i,j+1} - T_{i,j})}{\rho \Delta x \Delta y L c} \quad (4.13)$$

Simplifying:

$$T'_{i,j}{}^{t+\Delta t} - T'_{i,j}{}^t = \frac{k \Delta t}{\rho c} \frac{\frac{\Delta y}{\Delta x} (T_{i-1,j} - T_{i,j}) + \frac{\Delta y}{\Delta x} (T_{i+1,j} - T_{i,j}) + \frac{\Delta x}{\Delta y} (T_{i,j-1} - T_{i,j}) + \frac{\Delta x}{\Delta y} (T_{i,j+1} - T_{i,j})}{\Delta x \Delta y}$$

$$T'_{i,j}{}^{t+\Delta t} - T'_{i,j}{}^t = \kappa \Delta t \left(\frac{1}{(\Delta x)^2} (T_{i-1,j} - T_{i,j}) + \frac{1}{(\Delta x)^2} (T_{i+1,j} - T_{i,j}) + \frac{1}{(\Delta y)^2} (T_{i,j-1} - T_{i,j}) + \frac{1}{(\Delta y)^2} (T_{i,j+1} - T_{i,j}) \right)$$

Finally:

$$T'_{i,j}{}^{t+\Delta t} - T'_{i,j}{}^t = \frac{\kappa \Delta t}{(\Delta x)^2} (T_{i-1,j} - 2T_{i,j} + T_{i+1,j}) + \frac{\kappa \Delta t}{(\Delta y)^2} (T_{i,j-1} - 2T_{i,j} + T_{i,j+1}) \quad (4.14)$$

This is the same result as was obtained above.

This formulation of the finite difference method is in the Cartesian coordinate system. It is therefore best applied in situations which have straight lines at right angles to one another. A pipeline buried in ground (considering a cross-section only) is essentially a circle in a semi-infinite plane. The circle is actually comprised of one or two hollow annuli (the pipe wall and possibly a layer of insulation). These regions were illustrated in Figure 2.1. Representing this in a Cartesian coordinate system would require a very large number of nodes. Alternatively, the heat conduction equation can be transformed to other coordinate systems.

4.2.1 Derivation of Radial Coordinate System Equations

The transient heat conduction equation in a radial coordinate system is the following [21]:

$$\frac{1}{\kappa} \frac{\partial T}{\partial t} = \frac{1}{r} \frac{\partial T}{\partial r} + \frac{\partial^2 T}{\partial r^2} \quad (4.15)$$

In the same way as for the Cartesian version, there are more than one way to derive a finite difference approximation to this equation.

4.2.1.1 Method Using Assumption of Small Discretization

The simplest method of creating a finite difference equation is to apply the numerical derivative formulae as was done above for the Cartesian version of the equation. In this case, the formulae are:

$$\frac{\partial T}{\partial t} = \frac{T_{r,\theta}^{t+\Delta t} - T_{r,\theta}^t}{\Delta t} \quad (4.16)$$

$$\frac{\partial T}{\partial r} = \frac{T_{r+\Delta r,\theta} - T_{r-\Delta r,\theta}}{2\Delta r} \quad (4.17)$$

$$\frac{\partial^2 T}{\partial r^2} = \frac{T_{r+\Delta r,\theta} - 2T_{r,\theta} + T_{r-\Delta r,\theta}}{(\Delta r)^2} \quad (4.18)$$

As before, the terms in the two spatial derivatives can be evaluated at time t (explicit method) or at time $t+\Delta t$ (implicit method). Again, there are different formulations for these derivatives which can be used. Using these ones will give the same result as for a physical derivation, under an assumption of small discretization.

Consider a node (r,θ) with neighbours $(r+\Delta r,\theta)$, $(r-\Delta r,\theta)$, $(r,\theta+\Delta\theta)$, and $(r,\theta-\Delta\theta)$, as illustrated in Figure 4.2.

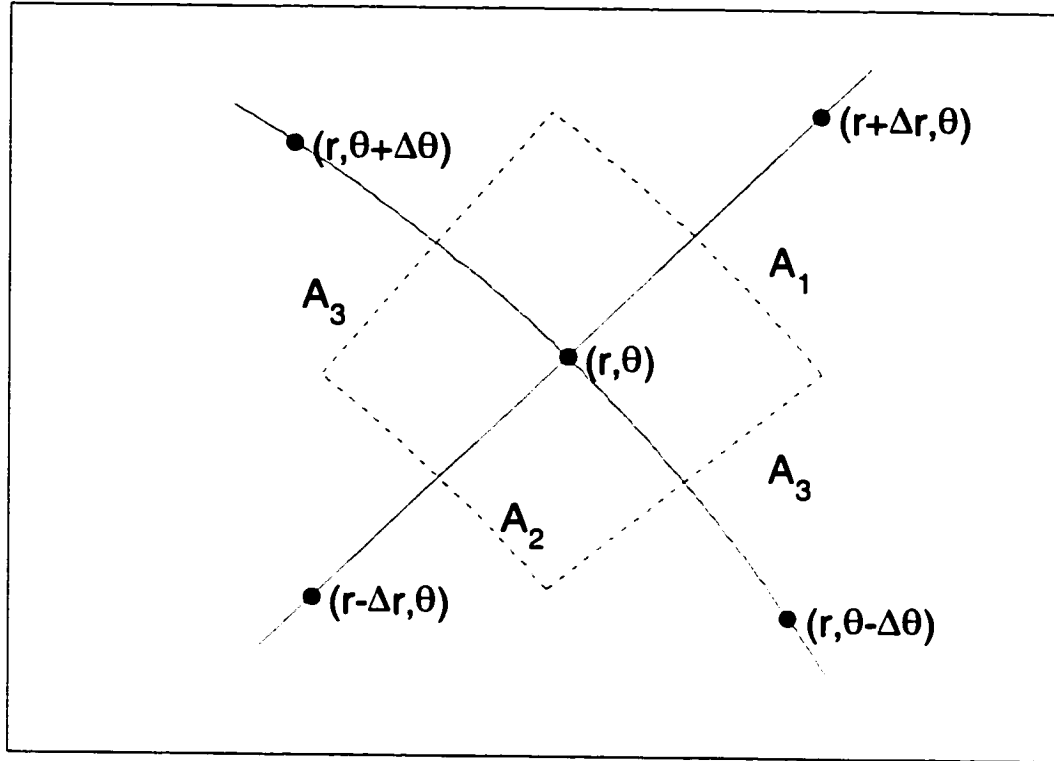


Figure 4.2 Nodal geometry in radial system

Temperature is considered to vary only in two dimensions: in order to ensure that the units are correct, however, a third dimension must be considered. The thickness of the two dimensional domain in this third dimension is L . The surface area between nodes (r, θ) and $(r+\Delta r, \theta)$ is A_1 , between nodes (r, θ) and $(r-\Delta r, \theta)$ is A_2 , and between nodes (r, θ) and $(r, \theta+\Delta \theta)$ or $(r, \theta-\Delta \theta)$ is A_3 . The volume represented by node (r, θ) is V . These quantities are:

$$V = L \Delta \theta r \Delta r \quad (4.19)$$

$$A_1 = L \Delta \theta \left(r + \frac{\Delta r}{2} \right) \quad (4.20)$$

$$A_2 = L \Delta \theta \left(r - \frac{\Delta r}{2} \right) \quad (4.21)$$

$$A_3 = L \Delta r \quad (4.22)$$

The heat transfer between any two nodes in the radial direction in a given time period is:

$$q = \frac{k A \Delta T}{\Delta r} \Delta t \quad (4.23)$$

Between two nodes in the angular direction the heat transfer is:

$$q = \frac{k A \Delta T}{r \Delta \theta} \Delta t \quad (4.24)$$

There is an assumption in these formulae that the radial discretization (Δr) is small relative to the radius, and that the temperatures do not change significantly during the time step. The change in temperature of the node in this time is:

$$\Delta T = \frac{q}{\rho V c} \quad (4.25)$$

If these terms are all put together and expressed in an implicit form, the following expression is obtained:

$$T_{r-\Delta r, \theta}^{i+\Delta t} (-A) + T_{r, \theta-\Delta \theta}^{i+\Delta t} (-B) + T_{r, \theta}^{i+\Delta t} (1 + A + 2B + C) + T_{r, \theta+\Delta \theta}^{i+\Delta t} (-B) + T_{r+\Delta r, \theta}^{i+\Delta t} (-C) = T_{r, \theta}^i \quad (4.26)$$

Where:

$$A = \frac{\kappa \Delta t \left(r - \frac{\Delta r}{2} \right)}{r (\Delta r)^2} \quad (4.27)$$

$$B = \frac{\kappa \Delta t}{r^2 (\Delta \theta)^2} \quad (4.28)$$

$$C = \frac{\kappa \Delta t \left(r + \frac{\Delta r}{2} \right)}{r (\Delta r)^2} \quad (4.29)$$

This is exactly the same equation as would be obtained using the numerical derivative method with the formulations shown above.

4.2.1.2 Method Without Using Assumption of Small Discretization

The above method assumed that the radial discretization was small relative to the radius. This assumption can be avoided if the heat transfer in the radial direction is expressed as follows [21] for the inner and outer nodes, respectively:

$$q = \frac{k L \Delta \theta \Delta T}{\ln\left(\frac{r}{r - \Delta r}\right)} \Delta t \quad \text{or} \quad q = \frac{k L \Delta \theta \Delta T}{\ln\left(\frac{r + \Delta r}{r}\right)} \Delta t \quad (4.30, 4.31)$$

Using this formulation, the equation obtained is:

$$T_{r-\Delta r, \theta}^{i+\Delta t} (-A) + T_{r, \theta-\Delta \theta}^{i+\Delta t} (-B) + T_{r, \theta}^{i+\Delta t} (1 + A + 2B + C) + T_{r, \theta+\Delta \theta}^{i+\Delta t} (-B) + T_{r+\Delta r, \theta}^{i+\Delta t} (-C) = T_{r, \theta}^i \quad (4.32)$$

Where:

$$A = \frac{\kappa \Delta t}{r \Delta r \ln\left(\frac{r}{r - \Delta r}\right)} \quad (4.33)$$

$$B = \frac{\kappa \Delta t}{r^2 (\Delta \theta)^2} \quad (4.34)$$

$$C = \frac{\kappa \Delta t}{r \Delta r \ln\left(\frac{r + \Delta r}{r}\right)} \quad (4.35)$$

4.2.1.3 Comparison

Both of these methods give satisfactory results when the discretization is small. Figure 4.3 shows the maximum error at any point in the domain in each, as compared to an analytical solution from [28]. The physical situation is that of a steel pipe, forced to a temperature of 70°C on the inside surface and 5°C on the outside surface. The large error at the start is due to a finite number of terms used in the analytical solution (which is the sum of an infinite series); i.e., the bulk of the error at the start is actually in the computation of the analytical solution, not the finite difference solution.

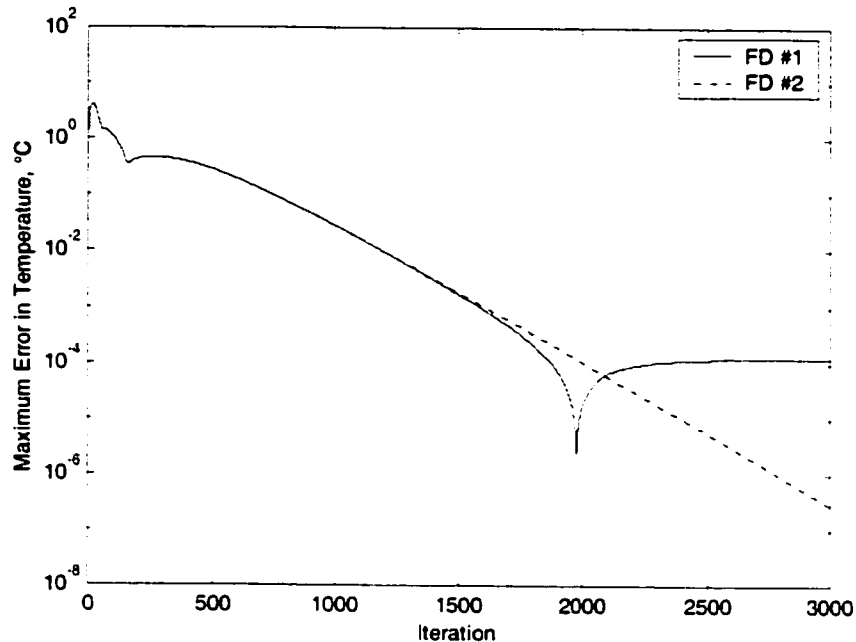


Figure 4.3 Error in radial finite differences

For the first period of time, there is very little difference between the two methods. It is only as a steady state is approached that a difference becomes obvious. In fact, it is easily verified that the second method approaches the analytical steady state solution (which can easily be obtained) exactly, while the first does not. As discretization increases, the difference between the two methods decrease. (This makes sense, since as discretization increases, the assumption used in deriving the first method becomes more and more valid.) Since there is no good reason not to use the second method, it should be used.

4.2.1.4 Symmetry Boundary Condition

The system that is being considered in this work (i.e. a pipe buried in the ground) has a line of symmetry which is a vertical line passing through the centre of the cylinder. This means that only half of the cylinder needs to be considered in any finite difference calculation scheme. The nodal equation is:

$$T_{r-\Delta r,\theta}^{i+\Delta t}(-A) + T_{r,\theta-\Delta\theta}^{i+\Delta t}(-B) + T_{r,\theta}^{i+\Delta t}(1 + A + 2B + C) + T_{r,\theta+\Delta\theta}^{i+\Delta t}(-B) + T_{r+\Delta r,\theta}^{i+\Delta t}(-C) = T_{r,\theta}^i \quad (4.36)$$

The cylinder now has nodes in the angular (θ) direction only from $-\pi/2$ to $\pi/2$ (assuming the right hand side of the line of symmetry is being considered), instead of over a full circle. This means that the node at the top ($\pi/2$) position does not have a corresponding $\theta + \Delta\theta$ node as required in the equation. However, because of symmetry, the temperature at any given radius will be the same at nodes $\pi/2 + \Delta\theta$ and $\pi/2 - \Delta\theta$. Therefore the nodal equation for nodes at $\theta = \pi/2$ is:

$$T_{r-\Delta r,\theta}^{i+\Delta t}(-A) + T_{r,\theta-\Delta\theta}^{i+\Delta t}(-2B) + T_{r,\theta}^{i+\Delta t}(1 + A + 2B + C) + T_{r+\Delta r,\theta}^{i+\Delta t}(-C) = T_{r,\theta}^i \quad (4.37)$$

Similarly, at the bottom ($-\pi/2$) position, the nodal equation is:

$$T_{r-\Delta r,\theta}^{i+\Delta t}(-A) + T_{r,\theta}^{i+\Delta t}(1 + A + 2B + C) + T_{r,\theta+\Delta\theta}^{i+\Delta t}(-2B) + T_{r+\Delta r,\theta}^{i+\Delta t}(-C) = T_{r,\theta}^i \quad (4.38)$$

4.2.1.5 Connection of Two Radial Systems

The above methods work if there is a homogeneous cylindrical system. If two different cylindrical regions are connected (e.g., a pipe and insulation around it), the boundary between these two regions must be specially considered. Note that the above formulations will still work at nodes other than those on the boundary. (This and the following derivation requires that there be nodes on the boundary itself.)

Figure 4.4 illustrates a node on the boundary between two different cylindrical regions. These regions may have different properties and different radial discretization. (The angular discretization must be the same in both regions.)

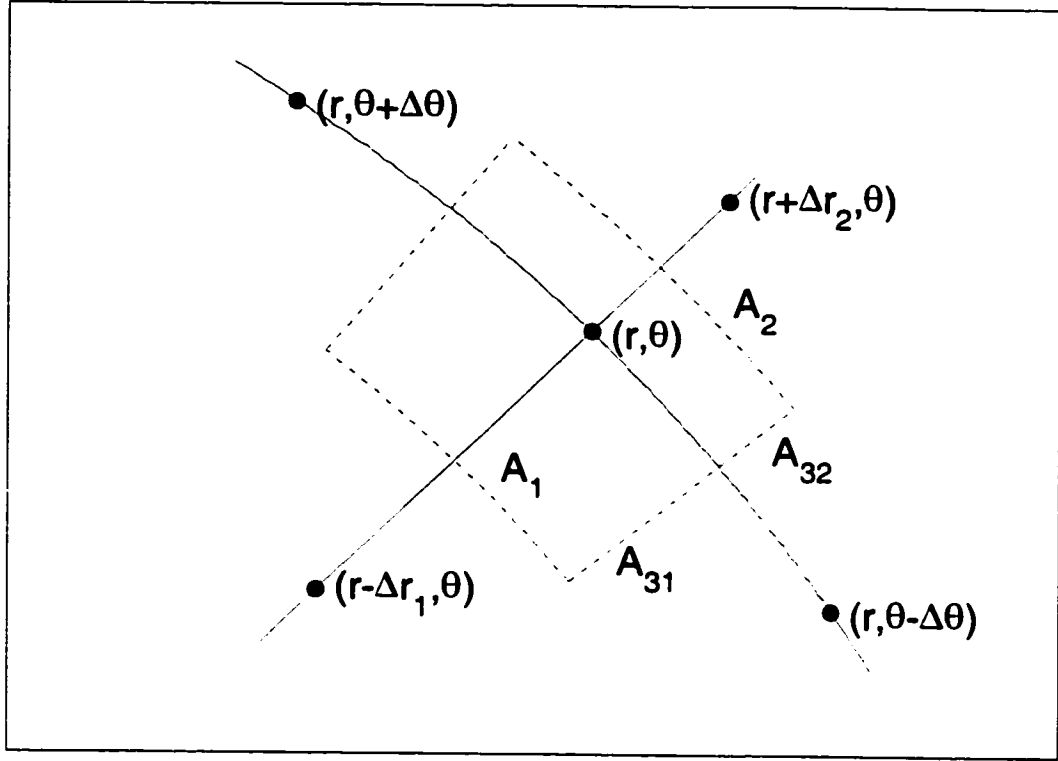


Figure 4.4 A node at the intersection of two cylindrical regions

As before, the thickness of the two dimensional domain is L . The surface area between nodes (r, θ) and $(r + \Delta r_2, \theta)$ is A_2 , between nodes (r, θ) and $(r - \Delta r_1, \theta)$ is A_1 , and between nodes (r, θ) and $(r, \theta + \Delta \theta)$ or $(r, \theta - \Delta \theta)$ is A_{31} on the first side of the boundary and A_{32} on the second side. The volume represented by node (r, θ) is V , which is comprised of V_1 and V_2 . These quantities are:

$$V = V_1 + V_2 = L \Delta \theta \left[\left(r - \frac{\Delta r_1}{4} \right) \frac{\Delta r_1}{2} + \left(r + \frac{\Delta r_2}{4} \right) \frac{\Delta r_2}{2} \right] \quad (4.39)$$

$$A_1 = L \Delta \theta \left(r - \frac{\Delta r_1}{2} \right) \quad (4.40)$$

$$A_2 = L \Delta \theta \left(r + \frac{\Delta r_2}{2} \right) \quad (4.41)$$

$$A_{31} = L \frac{\Delta r_1}{2} \quad (4.42)$$

$$A_{32} = L \frac{\Delta r_2}{2} \quad (4.43)$$

Using the small discretization assumption, the following equations are the same as in the above case.

The heat transfer between any two nodes in the radial direction in a given time period is:

$$q = \frac{k A \Delta T}{\Delta r} \Delta t \quad (4.44)$$

Between two nodes in the angular direction the heat transfer is:

$$q = \frac{k A \Delta T}{r \Delta \theta} \Delta t \quad (4.45)$$

Considering that the thermal conductivity, density and specific heat in the two regions may be different, the change in temperature of the node in this time is:

$$\Delta T = \frac{q}{\rho_1 V_1 c_1 + \rho_2 V_2 c_2} \quad (4.46)$$

The following result is obtained:

$$\begin{aligned} \frac{(T_{r,\theta}^{i+\Delta t} - T_{r,\theta}^i)(\rho_1 V_1 c_1 + \rho_2 V_2 c_2)}{\Delta t} = & \frac{k_2 A_2 (T_{r+\Delta r_2,\theta} - T_{r,\theta})}{\Delta r_2} + \frac{k_1 A_1 (T_{r-\Delta r_1,\theta} - T_{r,\theta})}{\Delta r_1} \\ & + \frac{k_1 A_{31} (T_{r,\theta-\Delta \theta} - T_{r,\theta})}{r \cdot \Delta \theta} + \frac{k_2 A_{32} (T_{r,\theta-\Delta \theta} - T_{r,\theta})}{r \cdot \Delta \theta} \\ & + \frac{k_1 A_{31} (T_{r,\theta+\Delta \theta} - T_{r,\theta})}{r \Delta \theta} + \frac{k_2 A_{32} (T_{r,\theta+\Delta \theta} - T_{r,\theta})}{r \Delta \theta} \end{aligned} \quad (4.47)$$

This can be simplified to the following:

$$T_{r-\Delta r_1,\theta}^{i+\Delta t} (-A) + T_{r,\theta-\Delta \theta}^{i+\Delta t} (-B) + T_{r,\theta}^{i+\Delta t} (1 + A + 2B + C) + T_{r,\theta+\Delta \theta}^{i+\Delta t} (-B) + T_{r+\Delta r_2,\theta}^{i+\Delta t} (-C) = T_{r,\theta}^i \quad (4.48)$$

Where:

$$A = \frac{k_1 A_1}{\Delta r_1} \frac{\Delta t}{(\rho_1 V_1 c_1 + \rho_2 V_2 c_2)} \quad (4.49)$$

$$B = \frac{(k_1 A_{31} + k_2 A_{32}) \Delta t}{r \Delta \theta (\rho_1 V_1 c_1 + \rho_2 V_2 c_2)} \quad (4.50)$$

$$C = \frac{k_2 A_2 \Delta t}{\Delta r_2 (\rho_1 V_1 c_1 + \rho_2 V_2 c_2)} \quad (4.51)$$

Substituting where possible, and further simplifying:

$$A = \frac{k_1 \left(r - \frac{\Delta r_1}{2} \right) \Delta t}{\Delta r_1 \left(\rho_1 \left(r - \frac{\Delta r_1}{4} \right) \frac{\Delta r_1}{2} c_1 + \rho_2 \left(r + \frac{\Delta r_2}{4} \right) \frac{\Delta r_2}{2} c_2 \right)} \quad (4.52)$$

$$B = \frac{(k_1 \Delta r_1 + k_2 \Delta r_2) \Delta t}{r (\Delta \theta)^2 \left(\rho_1 \left(r - \frac{\Delta r_1}{4} \right) \frac{\Delta r_1}{2} c_1 + \rho_2 \left(r + \frac{\Delta r_2}{4} \right) \frac{\Delta r_2}{2} c_2 \right)} \quad (4.53)$$

$$C = \frac{k_2 \left(r + \frac{\Delta r_2}{2} \right) \Delta t}{\Delta r_2 \left(\rho_1 \left(r - \frac{\Delta r_1}{4} \right) \frac{\Delta r_1}{2} c_1 + \rho_2 \left(r + \frac{\Delta r_2}{4} \right) \frac{\Delta r_2}{2} c_2 \right)} \quad (4.54)$$

Preferably, the assumption of small discretization should not be used. The alternative derivation uses the following equations for heat flow between two radially adjacent nodes:

$$q = \frac{k L \Delta \theta \Delta T}{\ln \left(\frac{r}{r - \Delta r} \right)} \Delta t \quad \text{or} \quad q = \frac{k L \Delta \theta \Delta T}{\ln \left(\frac{r + \Delta r}{r} \right)} \Delta t \quad (4.55, 4.56)$$

The following result is obtained:

$$\begin{aligned} (T_{r,\theta}^{t+\Delta t} - T_{r,\theta}^t) \frac{(\rho_1 V_1 c_1 + \rho_2 V_2 c_2)}{\Delta t} &= \frac{k_2 L \Delta \theta (T_{r+\Delta r_2,\theta} - T_{r,\theta})}{\ln \left(\frac{r + \Delta r_2}{r} \right)} + \frac{k_1 L \Delta \theta (T_{r-\Delta r_1,\theta} - T_{r,\theta})}{\ln \left(\frac{r}{r - \Delta r_1} \right)} \\ &+ \frac{k_1 A_{31} (T_{r,\theta-\Delta \theta} - T_{r,\theta})}{r \Delta \theta} + \frac{k_2 A_{32} (T_{r,\theta-\Delta \theta} - T_{r,\theta})}{r \Delta \theta} \\ &+ \frac{k_1 A_{31} (T_{r,\theta+\Delta \theta} - T_{r,\theta})}{r \Delta \theta} + \frac{k_2 A_{32} (T_{r,\theta+\Delta \theta} - T_{r,\theta})}{r \Delta \theta} \end{aligned} \quad (4.57)$$

As above, this can be simplified into:

$$T_{r-\Delta r_1, \theta}^{i+\Delta t}(-A) + T_{r, \theta-\Delta \theta}^{i+\Delta t}(-B) + T_{r, \theta}^{i+\Delta t}(1+A+2B+C) + T_{r, \theta+\Delta \theta}^{i+\Delta t}(-B) + T_{r+\Delta r_2, \theta}^{i+\Delta t}(-C) = T_{r, \theta}^i \quad (4.58)$$

Where:

$$A = \frac{k_1 L \Delta \theta}{\ln\left(\frac{r}{r-\Delta r_1}\right)} \frac{\Delta t}{(\rho_1 V_1 c_1 + \rho_2 V_2 c_2)} \quad (4.59)$$

$$B = \frac{(k_1 A_{31} + k_2 A_{32})}{r \Delta \theta} \frac{\Delta t}{(\rho_1 V_1 c_1 + \rho_2 V_2 c_2)} \quad (4.60)$$

$$C = \frac{k_2 L \Delta \theta}{\ln\left(\frac{r+\Delta r_2}{r}\right)} \frac{\Delta t}{(\rho_1 V_1 c_1 + \rho_2 V_2 c_2)} \quad (4.61)$$

Substituting where possible, and further simplifying:

$$A = \frac{k_1 \Delta t}{\ln\left(\frac{r}{r-\Delta r_1}\right) \left(\rho_1 \left(r - \frac{\Delta r_1}{4} \right) \frac{\Delta r_1}{2} c_1 + \rho_2 \left(r + \frac{\Delta r_2}{4} \right) \frac{\Delta r_2}{2} c_2 \right)} \quad (4.62)$$

$$B = \frac{(k_1 \Delta r_1 + k_2 \Delta r_2) \Delta t}{r (\Delta \theta)^2 \left(\rho_1 \left(r - \frac{\Delta r_1}{4} \right) \frac{\Delta r_1}{2} c_1 + \rho_2 \left(r + \frac{\Delta r_2}{4} \right) \frac{\Delta r_2}{2} c_2 \right)} \quad (4.63)$$

$$C = \frac{k_2 \Delta t}{\ln\left(\frac{r+\Delta r_2}{r}\right) \left(\rho_1 \left(r - \frac{\Delta r_1}{4} \right) \frac{\Delta r_1}{2} c_1 + \rho_2 \left(r + \frac{\Delta r_2}{4} \right) \frac{\Delta r_2}{2} c_2 \right)} \quad (4.64)$$

4.2.1.6 Convective Boundary Conditions

The inside surface of the inner radial system (representing the pipe wall) is exposed to the fluid within the pipe. In the present case, the fluid would normally be warmer than the surroundings, and therefore heat is transferred from the fluid to the pipe wall. The convective heat loss equation is described in Section 2.2. This equation removes the assumption that the fluid temperature doesn't change over the segment length. The traditional finite difference methods for convective

boundaries also use this assumption, so they will have to be rewritten to remove the assumption, as was done for the basic equation in Section 2.2.

The formulation described in Section 2.2 makes an assumption of the existence of a steady state. This will frequently not be acceptable in a transient heat transfer calculation. At some points in a calculation, a quasi steady state may exist, and at these times, the steady state formulation may be acceptable. At other times, a different formulation will be required. The steady state formulation presented in Section 2.2 is:

$$\dot{q} = (T_f - T_g) \left(1 - \exp\left(-\frac{L}{\hat{R} \dot{m} c}\right) \right) \dot{m} c \quad (4.65)$$

The transient formulation that will be used is derived in a similar way to this. It considers a fixed element of fluid mass as it travels from one point in the pipeline to another. The change in temperature of this element in the time period [21] is:

$$dT = -\frac{\dot{q}}{m c} dt \quad (4.66)$$

The heat flow (considering that the surroundings have a constant temperature) is:

$$\dot{q} = \frac{T - T_g}{R} \quad (4.67)$$

These terms can be combined as:

$$dT = -\frac{T - T_g}{R m c} dt \quad (4.68)$$

$$\frac{dT}{T - T_g} = -\frac{dt}{R m c} \quad (4.69)$$

Integrate:

$$\ln(T - T_g) = \frac{-t}{R m c} + C \quad (4.70)$$

$$T - T_g = k \exp\left(\frac{-t}{R m c}\right)$$

To solve for the arbitrary constant (k), a boundary condition is applied. The temperature of the fluid at the start of the time period ($t = 0$) is known to be T_f . Therefore, the following is true:

$$T_f - T_s = k \quad (4.71)$$

This is now inserted into the equation to arrive at:

$$T - T_s = (T_f - T_s) \exp\left(\frac{-\Delta t}{R m c}\right) \quad (4.72)$$

To determine the heat flow, the following equation is applied:

$$\dot{q} = (T_f - T) \frac{m c}{\Delta t} \quad (4.73)$$

Substituting the temperature at the end of the time period:

$$\begin{aligned} \dot{q} &= \left(T_f - \left[T_s + (T_f - T_s) \exp\left(\frac{-\Delta t}{R m c}\right) \right] \right) \frac{m c}{\Delta t} \\ &= (T_f - T_s) \left[1 - \exp\left(\frac{-\Delta t}{R m c}\right) \right] \frac{m c}{\Delta t} \end{aligned} \quad (4.74)$$

So the two formulations for heat loss are now:

$$\text{Quasi steady state} \quad \dot{q} = (T_f - T_s) \left(1 - \exp\left(-\frac{L}{\hat{R} \dot{m} c}\right) \right) \dot{m} c \quad (4.75)$$

$$\text{Transient} \quad \dot{q} = (T_f - T_s) \left[1 - \exp\left(\frac{-\Delta t}{R m c}\right) \right] \frac{m c}{\Delta t} \quad (4.76)$$

The form of these two equations are very similar, as could be expected. They are also dimensionally equivalent, as required. Note that the transient equation can also be used to calculate heat flow in a steady state case. The case where the two forms are equivalent is when the time step (Δt) is the time for the fluid to travel the length of the segment (L). In this case, the following equations are true (where D is the inside diameter of the pipe):

$$m = L \rho \frac{\pi}{4} D^2 \quad (4.77)$$

$$\dot{m} = Q \rho \quad (4.78)$$

$$\Delta t = \frac{L\pi D^2}{4Q} \quad (4.79)$$

$$R' = RL \quad (4.80)$$

The steady state equation then reduces to:

$$\begin{aligned} \dot{q} &= (T_f - T_s) \left(1 - \exp\left(-\frac{L}{RLQ\rho c}\right) \right) Q\rho c \\ &= (T_f - T_s) \left(1 - \exp\left(-\frac{1}{RQ\rho c}\right) \right) Q\rho c \end{aligned} \quad (4.81)$$

The transient equation is:

$$\begin{aligned} \dot{q} &= (T_f - T_s) \left[1 - \exp\left(\frac{-\frac{L\pi D^2}{4Q}}{RL\rho\frac{\pi}{4}D^2c}\right) \right] \frac{L\rho\frac{\pi}{4}D^2c}{\frac{L\pi D^2}{4Q}} \\ &= (T_f - T_s) \left[1 - \exp\left(\frac{-1}{RQ\rho c}\right) \right] \rho Qc \end{aligned} \quad (4.82)$$

In this case, the two equations are identical. In practise, there will be times when it is more appropriate to use one or the other. This will be discussed further in Section 5.1.

These two heat flow equations must now be expressed in appropriate form for use in a finite difference equation. First they will be expressed slightly differently:

$$\text{Steady State} \quad \dot{q} = (T_f - T_s) \left(1 - \exp\left(-\frac{L}{R'Q\rho}\right) \right) Q\rho c \quad (4.83)$$

$$\text{Transient} \quad \dot{q} = (T_f - T_s) \left[1 - \exp\left(\frac{-\Delta t}{R\rho\pi r_i^2 Lc}\right) \right] \frac{\rho\pi r_i^2 Lc}{\Delta t} \quad (4.84)$$

In both cases, the thermal resistance is only the resistance to the next node, and so will only encompass the convection portion, or:

$$R = \frac{1}{2h\pi r_i L} \quad R' = \frac{1}{2h\pi r_i} \quad (4.85a, 4.85b)$$

So the heat flow equations are then:

$$\text{Steady State} \quad \dot{q} = (T_f - T_s) \left(1 - \exp\left(-\frac{2Lh\pi r_i}{Q\rho c}\right) \right) Q\rho c \quad (4.86)$$

$$\text{Transient} \quad \dot{q} = (T_f - T_s) \left[1 - \exp\left(\frac{-2\Delta t h}{\rho r_i c}\right) \right] \frac{\rho\pi r_i^2 L}{\Delta t} \quad (4.87)$$

The system to be resolved is shown in Figure 4.5.

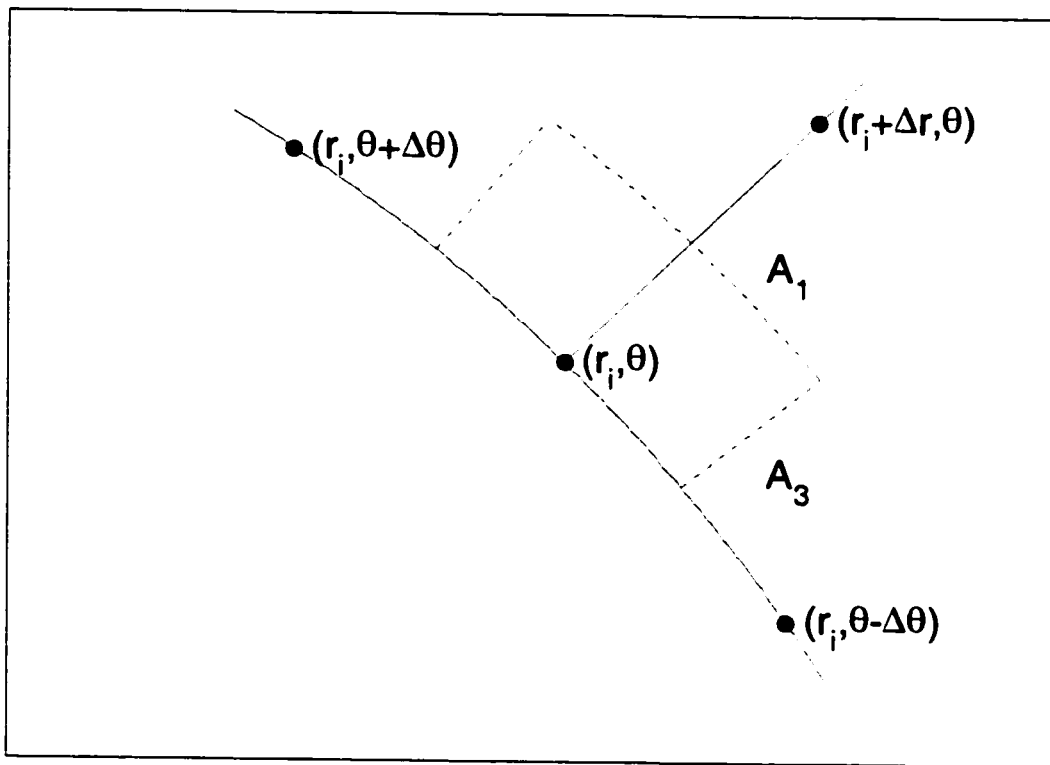


Figure 4.5 Nodes used in convective boundary with finite difference method

The depth of the two dimensional domain in the third dimension is L . The surface area between nodes (r, θ) and $(r + \Delta r, \theta)$ is A_1 , and between nodes (r, θ) and $(r, \theta + \Delta \theta)$ or $(r, \theta - \Delta \theta)$ is A_3 . The volume represented by node (r, θ) is V . These quantities are:

$$V = L\Delta\theta \frac{\Delta r}{2} \left(r_i + \frac{\Delta r}{4} \right) \quad (4.88)$$

$$A_1 = L \Delta \theta \left(r_i + \frac{\Delta r}{2} \right) \quad (4.89)$$

$$A_3 = \frac{L \Delta r}{2} \quad (4.90)$$

The heat transfer between any two nodes in the radial direction in a given time period is:

$$q = \frac{k A_1 \Delta T}{\Delta r} \Delta t \quad (4.91)$$

Between two nodes in the angular direction the heat transfer is:

$$q = \frac{k A_3 \Delta T}{r_i \Delta \theta} \Delta t \quad (4.92)$$

There is an assumption in these terms that the radial discretization (Δr) is small relative to the radius, and that the temperatures do not change significantly during the time step.

The change in temperature of the node in this time is:

$$\Delta T = \frac{q}{\rho V c} \quad (4.93)$$

The fluid temperature at the start of the segment (steady state) or at the start of the time step (transient) is T_f . Note that the heat transfer equations above for convection are for the heat transfer over the entire inside surface of the pipe. This must be scaled by a factor to account for the proportion of this heat entering each node. Assuming the heat transfer is evenly distributed over the inside surface of the pipe, the above convective equations can be multiplied by a factor as follows:

$$q_{nodal} = q \frac{\Delta \theta}{2\pi} \quad (4.94)$$

The equation for the steady state method can be built as:

$$\begin{aligned}
(T_{r,\theta}^{i+\Delta t} - T_{r,\theta}^i) \rho c L \Delta \theta \frac{\Delta r}{2} \left(r + \frac{\Delta r}{4} \right) &= (T_f - T_{r,\theta}^i) \left(1 - \exp \left(-\frac{L h 2 \pi r_i}{Q \rho_f c_f} \right) \right) Q \rho_f c_f \Delta t \frac{\Delta \theta}{2 \pi} \\
&+ (T_{r,\theta-\Delta \theta} - 2 T_{r,\theta} + T_{r,\theta+\Delta \theta}) \frac{k}{r \Delta \theta} \frac{L \Delta r}{2} \Delta t \\
&+ (T_{r+\Delta r,\theta} - T_{r,\theta}) \frac{k}{\Delta r} L \Delta \theta \left(r + \frac{\Delta r}{2} \right) \Delta t
\end{aligned} \tag{4.95}$$

This can be expressed in an implicit form as:

$$T_f (-A) + T_{r,\theta-\Delta \theta}^{i+\Delta t} (-B) + T_{r,\theta}^{i+\Delta t} (1 + A + 2B + C) + T_{r,\theta+\Delta \theta}^{i+\Delta t} (-B) + T_{r+\Delta r,\theta}^{i+\Delta t} (-C) = T_{r,\theta}^i \tag{4.96}$$

Where:

$$A = \frac{\left(1 - \exp \left(-\frac{L h 2 \pi r_i}{Q \rho_f c_f} \right) \right) Q \rho_f c_f \frac{\Delta \theta}{2 \pi} \Delta t}{\rho c L \Delta \theta \frac{\Delta r}{2} \left(r + \frac{\Delta r}{4} \right)} \tag{4.97}$$

$$= \frac{\left(1 - \exp \left(-\frac{L h 2 \pi r_i}{Q \rho_f c_f} \right) \right) Q \rho_f c_f \Delta t}{\rho c L \Delta r \pi \left(r + \frac{\Delta r}{4} \right)}$$

$$B = \frac{\frac{k}{r \Delta \theta} \frac{L \Delta r}{2} \Delta t}{\rho c L \Delta \theta \frac{\Delta r}{2} \left(r + \frac{\Delta r}{4} \right)} \tag{4.98}$$

$$= \frac{\kappa \Delta t}{(\Delta \theta)^2 r \left(r + \frac{\Delta r}{4} \right)}$$

$$\begin{aligned}
C &= \frac{\frac{k}{\Delta r} L \cdot \Delta \theta \left(r + \frac{\Delta r}{2} \right) \Delta t}{\rho c L \Delta \theta \frac{\Delta r}{2} \left(r + \frac{\Delta r}{4} \right)} \\
&= \frac{2\kappa \left(r + \frac{\Delta r}{2} \right) \Delta t}{(\Delta r)^2 \left(r + \frac{\Delta r}{4} \right)}
\end{aligned} \tag{4.99}$$

Alternatively, the form of the transient version of the equation results in a change only to the A parameter:

$$A = \frac{\left(1 - \exp\left(-\frac{\Delta t h 2}{r_i \rho_f c_f} \right) \right) r_i^2 L \rho_f c_f}{\rho c L \Delta r \left(r + \frac{\Delta r}{4} \right)} \tag{4.100}$$

To derive these forms without assuming a small discretization, once again the radial heat flow must be expressed as:

$$q = \frac{k L \Delta \theta \Delta T}{\ln\left(\frac{r + \Delta r}{r} \right)} \Delta t \tag{4.101}$$

The nodal equation is then:

$$\begin{aligned}
(T_{r,\theta}^{i+\Delta t} - T_{r,\theta}^i) \rho c L \Delta \theta \frac{\Delta r}{2} \left(r + \frac{\Delta r}{4} \right) &= (T_f - T_{r,\theta}^i) \left(1 - \exp\left(-\frac{L h 2 \pi r_i}{Q \rho_f c_f} \right) \right) Q \rho_f c_f \Delta t \frac{\Delta \theta}{2 \pi} \\
&+ (T_{r,\theta-\Delta \theta}^i - T_{r,\theta}^i + T_{r,\theta+\Delta \theta}^i) \frac{\Delta t k L \Delta r}{r \Delta \theta \cdot 2} \\
&+ (T_{r,\theta+\Delta r}^i - T_{r,\theta}^i) \frac{k L \Delta \theta \Delta t}{\ln\left(\frac{r + \Delta r}{r} \right)}
\end{aligned} \tag{4.102}$$

This can be expressed in an implicit form as:

$$T_f (-A) + T_{r,\theta-\Delta \theta}^{i+\Delta t} (-B) + T_{r,\theta}^{i+\Delta t} (1 + A + 2B + C) + T_{r,\theta+\Delta \theta}^{i+\Delta t} (-B) + T_{r,\theta+\Delta r}^{i+\Delta t} (-C) = T_{r,\theta}^i \tag{4.103}$$

Where:

$$A = \frac{\left(1 - \exp\left(-\frac{Lh2\pi r_i}{Q\rho_f c_f}\right)\right) Q\rho_f c_f \Delta t}{\rho c L \Delta r \pi \left(r + \frac{\Delta r}{4}\right)} \quad (4.104)$$

$$B = \frac{\kappa \Delta t}{(\Delta\theta)^2 r \left(r + \frac{\Delta r}{4}\right)} \quad (4.105)$$

$$C = \frac{\kappa \Delta t}{\ln\left(\frac{\Delta r + r}{r}\right) \frac{\Delta r}{2} \left(r + \frac{\Delta r}{4}\right)} \quad (4.106)$$

Only the C term has changed from the previous formulation. For the transient convective case, the A term is the same as when the small discretization assumption was used.

4.2.2 Derivation of Ground Coordinate System Equations

The coordinate system used to describe the heat transfer in the ground is an adaptation of the methods described by Archer and O'Sullivan [29], Martin and Sadhal [30], and Chung et al [31]. The heat transfer from the outside edge of the cylindrical system (i.e., the outside of the pipe or insulation) to the surface of the ground is considered.

4.2.2.1 Transformation of Variables

The transformation of variables which is used to describe the new coordinate system is [30]:

$$x + iy = c \coth\left(\frac{\alpha + i\beta}{2}\right) \quad (4.107)$$

Where:

$$\phi = \frac{Z}{r_o} \quad (4.108)$$

$$\alpha_o = \cosh^{-1}(\phi) \quad (4.109)$$

$$c = r_o \sinh(\alpha_o) \quad (4.110)$$

The half domain (symmetry applies for the other half) is defined by the range:

$$0 \leq \alpha \leq \alpha_o$$

$$0 \leq \beta \leq \pi$$

It can be shown (see Appendix A) that the transformation reduces to:

$$x = c \left[\frac{\sinh \alpha}{\cosh \alpha - \cos \beta} \right] \quad (4.111)$$

$$y = c \left[\frac{\sin \beta}{\cosh \alpha - \cos \beta} \right] \quad (4.112)$$

This is referred to as a bipolar or bicylindrical coordinate system by Martin and Sadhal [30].

In the Cartesian coordinate system, x represents the vertical distance below the ground, and $-y$ represents the horizontal distance from the plane of symmetry (y is negative). For example, the pipe centreline is at $x = Z$, $y = 0$. In the transformed coordinate system, $\alpha = \alpha_o$ represents the boundary of the pipe surface, $\alpha = 0$ represents the surface of the ground, $\beta = 0$ is the plane of symmetry below the pipe, and $\beta = \pi$ represents the plane of symmetry above the pipe. This is shown in Figure 4.6, where solid lines represent lines of constant α and dashed lines represent lines of constant β .

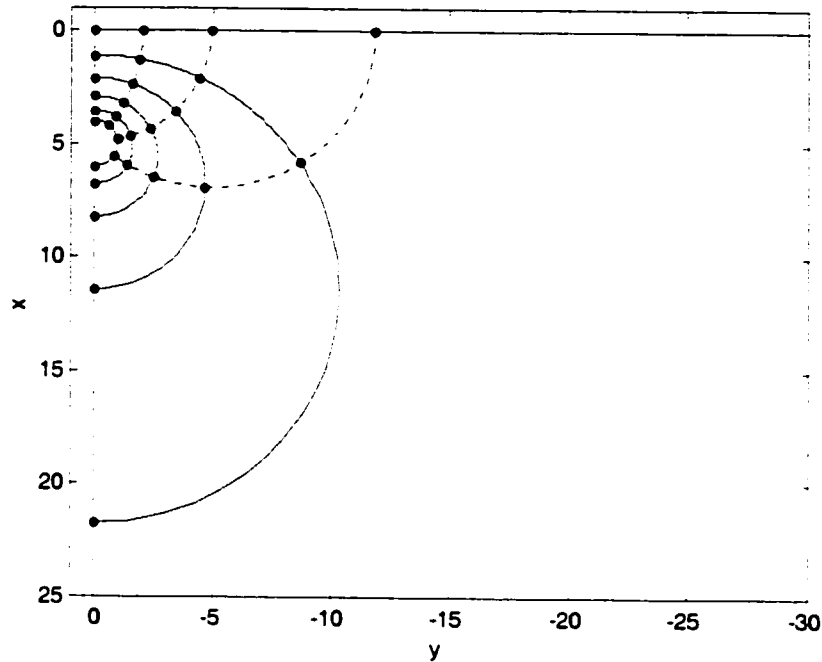


Figure 4.6 Coordinate system used in the ground

There is one node not shown in the plot. Looking at the result of the hyperbolic cotangent function over the range of possible α and β , it is evident that a problem occurs when α and β are both equal to zero, since $\coth(0)$ is undefined. More accurately:

$$\lim_{x \rightarrow 0} [\coth(x)] = \infty \quad (4.113)$$

This means there is a node at infinity which is not plotted in the above figure. This point is considered to lie both on the $\alpha = 0$ line, which runs along the surface, and the $\beta = 0$ line, which runs down into the ground from the bottom of the pipe.

4.2.2.2 Transformation of Conduction Equation

The heat conduction equation in the x - y plane is transformed into the α - β plane:

$$\frac{1}{\kappa} \frac{\partial T}{\partial t} = \left(\frac{\cosh \alpha - \cos \beta}{c} \right)^2 \times \left(\frac{\partial^2 T}{\partial \alpha^2} + \frac{\partial^2 T}{\partial \beta^2} \right) \quad (4.114)$$

(See Appendix B for a derivation of this.)

The steady state solution to this equation, with constant temperature boundary conditions applied at the surface of the ground (T_s) and the surface of the pipe (T_p) is:

$$T = T_s + (T_p - T_s) \frac{\alpha}{\alpha_0} \quad (4.115)$$

The transformed heat equation can easily be implemented in a finite difference scheme. It is also easily verified that after a long period of time, the finite difference model approaches the steady state solution shown above. However, it should be noted that the further away a node is from the pipe, the longer it takes for it to reach the steady state result.

4.2.2.3 Finite Difference Model

The finite difference equation, set up into an implicit format is:

$$T_{\alpha-\Delta\alpha,\beta}^{i+\Delta t} (-A) + T_{\alpha+\Delta\alpha,\beta}^{i+\Delta t} (-A) + T_{\alpha,\beta}^{i+\Delta t} (1 + 2A + 2C) + T_{\alpha,\beta-\Delta\beta}^{i+\Delta t} (-C) + T_{\alpha,\beta+\Delta\beta}^{i+\Delta t} (-C) = T_{\alpha,\beta}^i \quad (4.116)$$

Where:

$$A = \frac{\kappa \Delta t}{(\Delta\alpha)^2} \left(\frac{\cosh \alpha - \cos \beta}{c} \right)^2 \quad (4.117)$$

$$C = \frac{\kappa \Delta t}{(\Delta\beta)^2} \left(\frac{\cosh \alpha - \cos \beta}{c} \right)^2 \quad (4.118)$$

Special consideration is required at the symmetry boundaries. At these nodes, either the $(\alpha, \beta + \Delta\beta)$ or $(\alpha, \beta - \Delta\beta)$ node will not exist (depending on whether it is the $\beta = 0$ or $\beta = \pi$ boundary under consideration). Due to symmetry, however it is known that at these boundaries:

$$T_{\alpha,\beta-\Delta\beta} = T_{\alpha,\beta+\Delta\beta} \quad (4.119)$$

Which can be used to fill the necessary terms of the finite difference equations for those nodes.

This scheme was tested with a fairly small discretization (five nodes in the α direction and four nodes in the β direction). The thermal diffusivity was $1.4 \times 10^{-7} \text{ m}^2/\text{s}$, and the cylinder had a diameter of 15 cm. The temperature of the surface of the cylinder was 70°C and the temperature of the surface of the ground was 5°C . The maximum error (where error is defined as difference relative to steady state value as described above) is plotted in Figure 4.7.

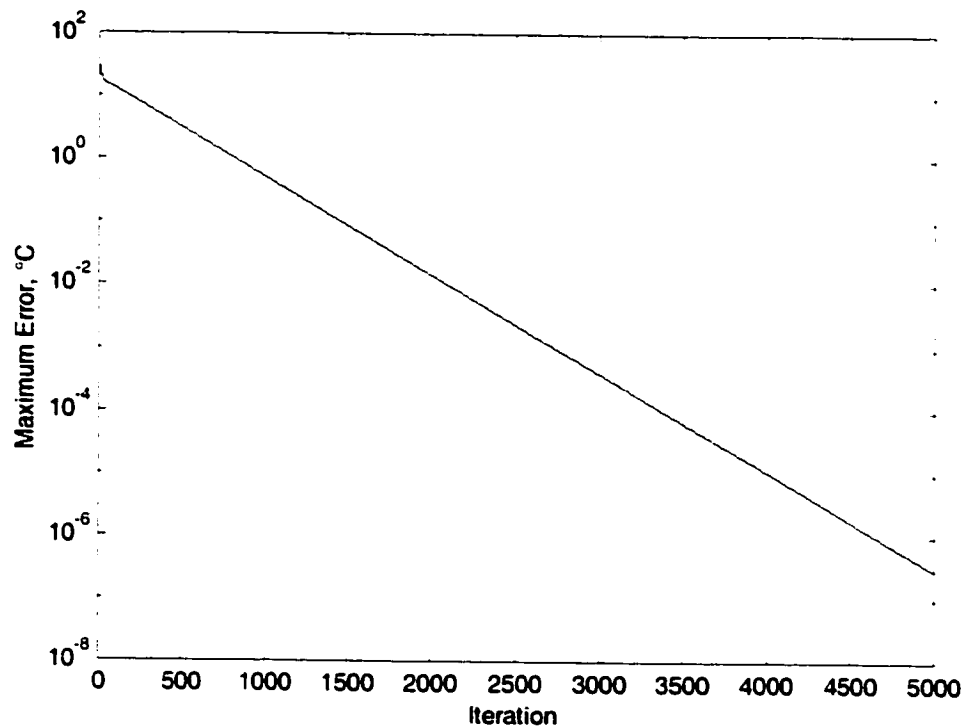


Figure 4.7 Convergence of finite difference calculation

It is evident that the results do converge towards the theoretical steady state value, as expected.

4.2.3 Connection of Ground System to Radial System

The pipe and insulation are based in a cylindrical coordinate system, and the ground uses a bipolar coordinate system. These two systems do not match up to one another perfectly. It can be seen that although the bipolar coordinate system gives a perfect circle on the boundary between the two systems, the nodes are not evenly spaced on this circle, as they are in the cylindrical system. This is shown in Figure 4.8.

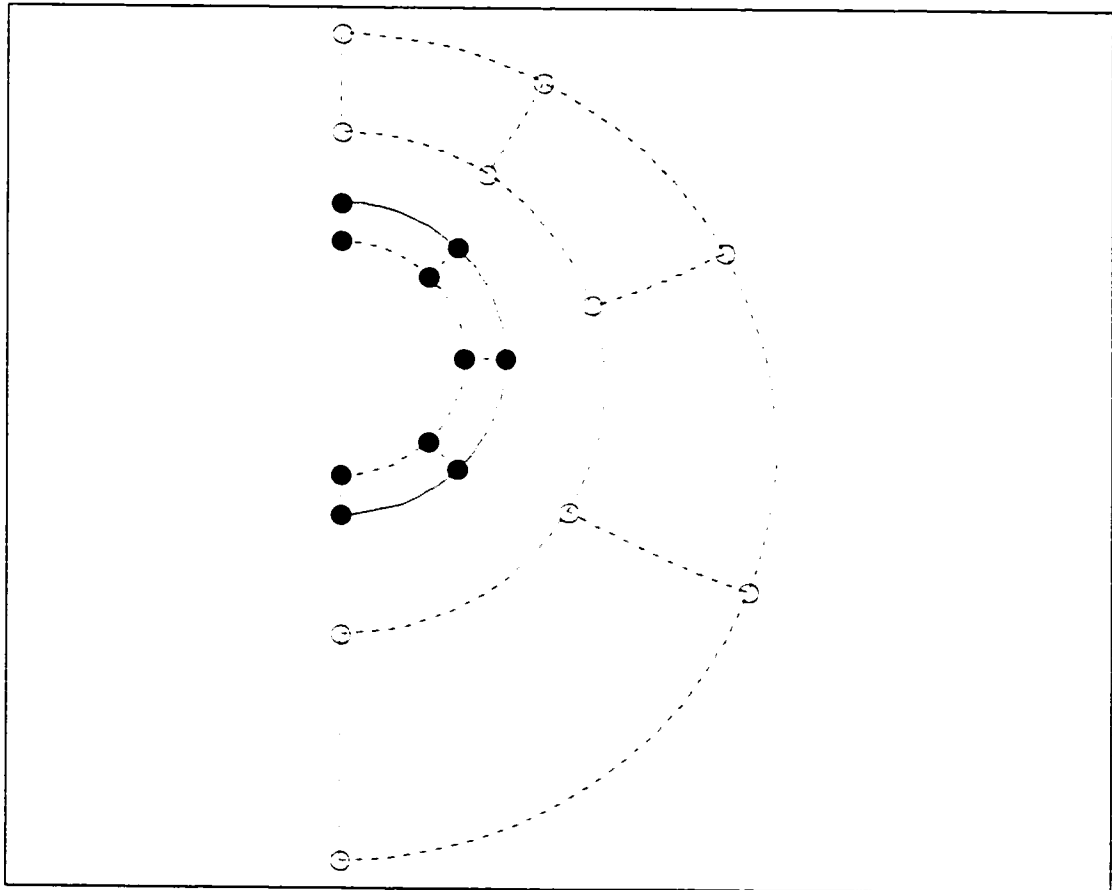


Figure 4.8 Connection of radial and bicylindrical coordinate systems

The figure shows the outer nodes on the insulation (solid circles), including the boundary, and the first two layers of nodes in the ground (hollow circles). It can be seen that the two coordinate systems do not line up with one another at the boundary. Therefore, the finite difference method used to connect the two systems must consist of an approximation.

The finite difference equation in an implicit form is:

$$T^{i+\Delta t} (1 + A + B + 2C) + T_{r-}^{i+\Delta t} (-A) + T_{\alpha+}^{i+\Delta t} (-B) + T_{\theta-}^{i+\Delta t} (-C) + T_{\theta+}^{i+\Delta t} (-C) = T^i \quad (4.120)$$

Where:

$$A = \frac{2 \Delta t \left[\frac{k_c (r - \frac{1}{2} \Delta r_c)}{\Delta r_c} \right]}{\rho_t c_t (\frac{1}{2} \Delta r_t (r + \frac{1}{4} \Delta r_t)) + \rho_c c_c (\frac{1}{2} \Delta r_c (r - \frac{1}{4} \Delta r_c))} \quad (4.121)$$

(Small discretization assumption)

$$A = \frac{\frac{2 \Delta t k_c}{\ln \left(\frac{r}{r - \Delta r_c} \right)}}{\rho_t c_t (\frac{1}{2} \Delta r_t (r + \frac{1}{4} \Delta r_t)) + \rho_c c_c (\frac{1}{2} \Delta r_c (r - \frac{1}{4} \Delta r_c))} \quad (4.122)$$

(No small discretization assumption)

$$B = \frac{2 \Delta t \left[\frac{k_t (r + \frac{1}{2} \Delta r_t)}{\Delta r_t'} \right]}{\rho_t c_t (\frac{1}{2} \Delta r_t (r + \frac{1}{4} \Delta r_t)) + \rho_c c_c (\frac{1}{2} \Delta r_c (r - \frac{1}{4} \Delta r_c))} \quad (4.123)$$

$$C = \frac{2 \Delta t \left[\frac{(k_t \frac{1}{2} \Delta r_t + k_c \frac{1}{2} \Delta r_c)}{r (\Delta \theta)^2} \right]}{\rho_t c_t (\frac{1}{2} \Delta r_t (r + \frac{1}{4} \Delta r_t)) + \rho_c c_c (\frac{1}{2} \Delta r_c (r - \frac{1}{4} \Delta r_c))} \quad (4.124)$$

Where:

Subscript c represents the radial (cylindrical) region (the insulation)

Subscript t represents the transformed region (the ground)

$\frac{1}{2} \Delta r_t$ is the distance from a node on the border to a point at $\frac{\Delta \alpha}{2}$ to the next

transformed node

$\frac{1}{2} \Delta r_t'$ is half the distance from the node on the border to the next transformed

node.

This approximation becomes more and more accurate as the discretization increases (i.e. the space between nodes becomes smaller). More important, however, is the ratio of the outside diameter of the pipe and the burial depth of the pipe. As this ratio decreases (i.e., smaller pipe or deeper burial), the accuracy of the approximation increases. Unfortunately, this ratio is controlled by the physical geometry of the problem and cannot be adjusted in the same way that discretization can be. A finite element method removes this approximation, but adds others (e.g., the representation of curved lines by multiple straight line segments). Whether a finite element method can improve the accuracy of the calculation will be examined in Chapter 8.

5. Calculation Algorithm

5.1 Construction of Model

Chapter 2 covered issues relating to flow losses; Chapter 3 discussed the issues surrounding ground temperature in undisturbed ground; and Chapter 4 described the two dimensional finite difference model for calculating transient temperature distributions in the geometry of interest. In order to calculate the pressure losses in a viscous oil pipeline over time, these issues must all be combined into a comprehensive calculation model.

An initial condition must be assumed, both in the fluid and in the ground temperature distribution. The ground temperature distribution could be assigned based on the results of a previous calculation, or it could be assumed simply to be the temperature of undisturbed ground, which can be obtained from the analytical solutions shown in Section 3.1.1. The fluid present in the pipeline at start-up (time zero) can also be determined from the result of a previous calculation if it is not a first-time use of the pipeline. Otherwise, it can be assumed that the fluid is water (left in the pipeline from the hydrostatic pressure test required by law), and is at the temperature of the ground around it.

Unless the calculation is to be continued from a previous calculation with no discontinuity added in the fluid, it should be assumed that there is a discontinuity introduced into the pipeline at time zero. In the case of a pipeline pre-filled with cold water, when heated oil starts to flow into the pipeline, there will be a sharp discontinuity both in fluid type (and flow regime) and in temperature. Chapter 4 described two methods of calculating the convective heat transfer: transient and (quasi) steady state. The transient method must be used if there is any fluid discontinuity in the pipeline. Fluid discontinuities are caused by events such as the following:

- start-up or shut down
- change in flow regime (e.g., transition from water-in-oil emulsion to oil-in-water emulsion)
- sharp change in inlet temperature
- sharp change in flow rate
- sharp change in water fraction

For the last three, the determination of what is a “sharp change” is subjective. When written into a computer program, this would ideally be left to the user to specify. In some cases, the user may want any change in these conditions to be considered a discontinuity, and in other cases a 5% or 10% instantaneous change could be acceptable, depending on the accuracy required.

The length of the pipeline is divided into segments; each segment is the same length. This is done because when there is a discontinuity in the pipeline, “blocks” of fluid are tracked as they move through the pipeline. It would be very difficult to account for blocks of different sizes moving through the pipeline. If it was known that there would never be discontinuities in the pipeline, then the segments could be different lengths—this would actually be computationally more efficient because the segment size could reflect the expected thermal gradient. Normally, the thermal gradient will be higher at the start of the pipeline, where the oil is hottest. As it cools off through the length of the pipe, the temperature difference between the oil and the surface of the ground decreases, and so the amount of temperature lost in the oil decreases over a unit length. For maximum computational efficiency, the segment length would be shortest where the thermal gradient is the highest. Unfortunately, the possibility of the presence of discontinuities means that a generic algorithm is limited to equal segment lengths.

In the calculation algorithm it is assumed that the temperature along the length of each segment is constant (although it changes from segment to segment). Note that there are two dimensional temperature variations within each segment; only the dimension along the length is not allowed to vary. The shorter each segment is, the more accurate this assumption will be (but the more memory and computational time will be required). No heat transfer is considered from one segment to the next, other than through the fluid.

In the transient case, the discontinuities must be tracked as they move through the pipeline. The time step is specified to be exactly the time for a fluid boundary to move one segment length through the pipeline. In theory, the time step could be the time for a fluid boundary to move an integer number of segment lengths through the pipeline. In this method, the heat transfer through each fluid block passing through the segment in the time step would be summed, and the result applied to the ground temperature calculation. It was found, however, that this method produced severe oscillations at times when there was a steep thermal gradient in the fluid (e.g. at the start of hot oil flowing into a cold pipeline). While these oscillations were found to be stable (i.e., they would dissipate in time), they were quite severe in some cases. It was determined that the shorter time step (and therefore a longer calculation time) would be preferable to the possibility of having severe numerical oscillations in the results.

There is one problem with forcing the time step to be equal to the time it takes for a fluid boundary to move one segment length. If the flow rate is very low, this time can be quite long. The ground surface temperature, liquid flow rate and water fraction are evaluated only at the start of the time step. If the time step is very long, these could change significantly during the time step, causing erroneous results. For this reason, it is best to force a limit on the time step—the algorithm will not proceed if it is determined that the time step would exceed a

predetermined maximum. In this case, a higher flow rate or shorter segment length would have to be used.

In the quasi steady state case, there is no restriction on the time step or on the segment length. It is not convenient, however, to change the segment length once established. The time step can be easily changed when the steady state convection calculation is used. Just as in the transient case, it is unwise to make the time step too long, as the ground surface temperature, liquid flow rate and water fraction are evaluated only at the start of the time step. The maximum time step allowed can be the same in both the transient and steady state methods. (This would be determined based on factors such as the maximum expected rate of change of the flow rate, water fraction or ground surface temperature.)

While there is probably no reason that the maximum time step could not be used immediately after it is determined that there are no discontinuities in the pipeline, it is thought that a gradual increase in the time step would be more appropriate. A starting point is the last time step size used by the transient method while the discontinuity was present. Once the discontinuity leaves the pipeline, the time step size is increased somewhat at each step until the maximum allowed size is reached.

A typical calculation will start with cold ground and a pipeline filled with water. In this case, the calculation algorithm is as follows:

1. Initialize ground temperatures. This is done based on the time of year and the depth of each node below the surface, assuming undisturbed ground.
2. Note that the pipeline is entirely filled with water at the start.
3. Determine initial flow rate from production data. The initial time step is then the length of time for a fluid boundary to travel the length of one segment.

4. If the calculated time step is above the maximum allowed, abort the calculation.
5. Calculate effective density and specific heat of the fluid in each segment.
6. Perform internal calculation (see below) for each segment.
7. Record outputs for the time step.
8. Determine if there is a discontinuity in the pipe (either a new one entering the pipe, or an old one still in the pipe).
9. Determine flow rates at next point in time.
10. If there is a discontinuity in the pipe, then the time step length is determined based on the flow rate; otherwise it can be set arbitrarily. (Normally it should start at the value of the last time step before the discontinuity left the pipe, and be increased at each step until either a new discontinuity enters the line or the maximum value for the time step is reached.)
11. Calculate pipe fluid temperatures and pressure losses based on the temperatures
12. Recalculate positions of any discontinuities (if present)
13. Return to step 4, until the desired final time has been reached.

The internal calculation algorithm (step 6, above) has the following form:

1. Set temperature boundary conditions (surface nodes, and pipe/fluid boundary nodes).
2. Determine if previously stored coefficient matrix (see Section 5.2) is still valid. It will not be valid if the present calculation is the first one, or if any of the following have changed:
 - a. Type of convection calculation (transient or steady state)
 - b. Water fraction
 - c. Flow rate
 - d. Time step

e. Convective coefficient

3. If the matrix is not valid, rebuild it and perform an LU decomposition factoring step (see Section 5.3) on it.
4. Perform an LU decomposition backsubstitution step on the matrix to calculate the ground temperatures.

This calculation algorithm, when used with the transient convection method, can also be used when the flow in the pipeline is stopped. In this case, the fluid blocks cool off in place in the pipeline (i.e., they are not advanced at each time step). The effects of stopping and restarting flow can then be analysed; this is a matter of high importance to an oil company considering installing a heavy oil pipeline.

The flow calculations can be based on any of the flow regimes discussed in Chapter 2, without changing the main calculation algorithm at all. This is because the segmented method of calculating the pressure loss is used (as opposed to the integration method, which is only applicable to laminar flow). The coefficient matrix, as described below changes, and then only the rows of the matrix referring to the convective boundary change, and the equation used to calculate the change in temperature also changes. Neither of these two changes affects the overall algorithm.

5.2 Coefficient Matrix

In calculating the temperature of the ground in one segment of the pipeline, the finite difference method is used, as described in Chapter 4. There are a number of regions within the two-dimensional section of ground which need to be considered:

- fluid/pipe boundary
- pipe
- pipe/insulation boundary

- insulation
- insulation/ground boundary
- ground
- surface (boundary)

Each of the boundaries has one layer of nodes; the other regions can have any number of layers. Each layer must, however, have exactly the same number of nodes in it. The basic form of the equation at each layer is:

$$BT_{i-1,j}^{t+\Delta t} + CT_{i,j-1}^{t+\Delta t} + DT_{i,j}^{t+\Delta t} + ET_{i,j+1}^{t+\Delta t} + FT_{i+1,j}^{t+\Delta t} = T_{i,j}^t \quad (5.1)$$

This can be written in matrix form as:

$$[A]\{T^{t+\Delta t}\} = \{T^t\} \quad (5.2)$$

There is a two dimensional domain being solved. The temperatures of all of the nodes in these two dimensions must be stored in a one-dimensional vector. The two-dimensional temperature matrix is wrapped into a one dimensional form. The nodes in each layer are kept together, with each subsequent layer added on to the vector after each other. The $i-1, j$ node is always the element before the i, j node in the vector and the $i+1, j$ node is always the element after the i, j node. The $i, j-1$ node is located M elements before the i, j node in the vector and the $i, j+1$ node is always M elements after the i, j node, where there are M elements in each layer of nodes.

This is translated into the coefficient matrix as well. Each row represents one node and its relationship with itself and all the other nodes in the domain over one time step. In each row, there are five non-zero elements (corresponding to one node and its immediate neighbours)—exactly five nodes are referred to in the finite difference equation for each layer. The only exception to this is at the symmetry boundary conditions, where one node is not used; at which point there are four non-zero nodes in the row.

The coefficients in each row are determined based on in which region (from the above list) the node corresponding to the row is located. The coefficients are calculated from one of the sets of coefficients listed in Chapter 4, as appropriate.

The first layer of nodes and the last layer of nodes are used as inputs. These are the boundary conditions referring to the temperature at the surface of the ground, and the temperature of the fluid entering the segment. In the coefficient matrix, the rows referring to these nodes (the first M rows and the last M rows of the matrix, where M is the number of nodes in each layer) contain a one on the diagonal and zeros elsewhere. Therefore, the elements in the temperature vector referring to these nodes will not change in the matrix calculation, but will have an effect on other nodes in the system. The temperatures of these nodes are changed outside the matrix calculation.

5.3 Matrix Solutions

The coefficient matrix is a square matrix of size $N \times N$, and the two temperature vectors (old-known and new-unknown) are column vectors of length N . In order to determine the temperature at the end of the time step, the following equation is solved:

$$[A]\{T^{t+\Delta t}\} = \{T^t\} \quad (5.3)$$

Where A is the vector of coefficients as described in Section 5.2.

5.3.1 Gaussian Elimination

The standard way solving an equation like this is by Gaussian elimination. The simplest method of Gaussian elimination, as found in many introductory numerical methods textbooks [e.g., 32] is not a very efficient method, however. In this, a large number of computations are required at each time step, and no benefit can be derived from the fact that the coefficient matrix may not change at any given time.

5.3.2 Iterative Methods

Iterative methods of matrix solution can often be faster than other methods. The compromise is that they give approximate answers. These methods require the user to specify a tolerance—the algorithm will iterate until the results fall within the tolerance. In cases where an initial estimate is close to the desired solution, iterative methods can be very fast. This may be applicable to the present problem, as the temperature vector should normally change very little over any given time step. The temperature vector at the start of the time step is then used as the initial estimate in determining the temperature vector at the end of the time step.

5.3.3 LU Decomposition

LU decomposition is essentially a form of Gaussian elimination. Its advantage is that it divides the computation into two steps: factoring and decomposition. The factoring step is where the bulk of the computational effort lies, and it depends only upon the coefficient matrix and not upon the temperature vectors. This means that if the coefficient matrix does not change from calculation to calculation, there is no need to repeat the largest part of the computation each time. This can amount to a huge savings in computation time if the coefficient matrix does not frequently change. When the coefficient matrix does change, there is no penalty for having to perform the factoring step, as compared to the computation time required for straight Gaussian elimination. For this reason, most codes available in the public domain use LU decomposition for their standard routines for solving systems of linear equations. Because this method is so popular, a large amount of effort has been invested in optimizing these calculations as much as possible. The difference between the simplest calculation algorithm for Gaussian elimination in an introductory textbook and a highly optimized calculation algorithm in the public domain [33] was seen to be two to three orders of magnitude!

LU decomposition was used in the calculations for which the results are discussed in Chapter 6. This is for several reasons:

- There are highly optimized codes available in the public domain, which can easily be used.
- The coefficient matrix does not change between time steps; the major part of the calculation is only done once. At each time step, only a simple backsubstitution step needs to be carried out.
- The results are accurate to machine precision, even when the thermal profile in the ground is changing rapidly (i.e., at start-up).

5.3.4 Banded Solution Methods

The coefficient matrix for this problem will always be banded. This means that the only non-zero values in the matrix are on or near the diagonal. Algorithms are available which can use this to advantage. Generally, these are best at optimizing memory space (since the zero values which comprise the bulk of the matrix do not need to be stored), but some can improve on calculation time as well. Note that these may not be as efficient in the present case because the band width is quite wide and there are many zeros located within the band. (In each row, there will be non-zero values on the diagonal, the values immediately to the left and right of the diagonal, and at some spacing, M , to the left and right of the diagonal. All other values are zeros; see Section 5.2.) This means that the banded algorithm will still require the storage and manipulation of a large number of zeros; the algorithm will therefore lose some of its efficiency.

5.3.5 Sparse Solution Methods

A sparse matrix is one which contains mostly zeros. Algorithms are available which use this to advantage in the same way that banded solution methods do. Much less memory space is generally required than for methods which assume the matrix is full of non-zeros. Again, these methods generally optimize for memory

space, but in some cases can be faster than full matrix solutions. Sparse LU decomposition solution methods are available and may be the best option for the present application, if one can be found which runs faster than the full matrix LU decomposition algorithms. (In the present application, speed will normally be of greater concern than memory.)

6. Results

6.1 Parametric Studies in Constant Flow

The main purpose of the present work is to link the effects of temperature and viscosity in heavy oil pipelines. Other factors, such as diluent addition or core-annular flow, also affect the pressure loss of the flow of heavy oil. In these cases, temperature is not a significant factor in determining the pressure loss. The temperature of the ground can still be calculated using the techniques described earlier. This can be used if the flow regime reverts to a heavy oil flow. Because pressure loss is not a significant issue in these cases, they will not be examined in detail in the parametric studies presented here.

The effect of viscous heating, as described in Section 2.3.3 is not considered in these calculations. The results will therefore be conservative--the pressures reported will be higher than the actual pressures experienced in the given cases. This helps to ensure that if the program reports that a particular design will not exceed a given pressure, that pressure will not be exceeded in the field, even if some assumptions or estimates of fluid or ground physical properties are not accurate.

In order to gauge the effect of a change in a condition, a range of parameters will be varied, one at a time. The base parameters are as listed in Table 6.1 below. Where applicable, these are the same as were in Table 2.1; the new values are shown in *italics*.

Table 6.1 Base case parameters

Pipe outer diameter, in.	3.5
Pipe wall thickness, in.	0.216
Insulation thickness, in.	1.5
Pipe depth, ft.	4
Pipeline length, km	2
Flow rate, m ³ /d	20
Production start date	<i>May 1</i>
Inlet temperature, °C	70
Mean surface temperature, °C	2
Seasonal temperature variation, °C	20
Oil density, kg/m ³	950
Oil conductivity, W/m·K	0.11
Oil specific heat, J/kg·K	2000
Oil test temperature 1, °C	30
Oil viscosity at test 1, cp	25000
Oil test temperature 2, °C	70
Oil viscosity at test 2, cp	800
Pipe conductivity, W/m·K	60
Insulation conductivity, W/m·K	0.04
Ground conductivity, W/m·K	0.5
Pipe density, kg/m ³	7800
Insulation density, kg/m ³	190
Ground density, kg/m ³	2000
Pipe specific heat, J/kg·K	400
Insulation specific heat, J/kg·K	1000

In the following sections, the more important of these parameters will be varied through a range to determine the effect on the temperature and pressure loss throughout a two year cycle of seasons. The surface temperature is approximated by a sine wave which starts at the mean annual temperature on May 1.

6.1.1 Flow Rate

The flow rate was varied from 5 to 350 m³/d. The maximum pressure, and the maximum pressure for each flow rate after the first 25 days are tabulated in Table 6.2.

Table 6.2 Flow rates and pressures

Flow Rate, m ³ /d	Maximum Pressure, kPa	Max. Pressure After 25 Days, kPa
5	91,513	74,296
10	61,928	26,184
15	30,070	11,330
20	16,976	6728
25	11,135	4753
30	8254	3988
35	6659	3424
50	4838	3096
100	4357	3450
150	5062	4318
200	5963	5260
250	6919	6269
300	7905	7238
350	8902	8252

The maximum (i.e. start-up) pressure is plotted in Figure 6.1.

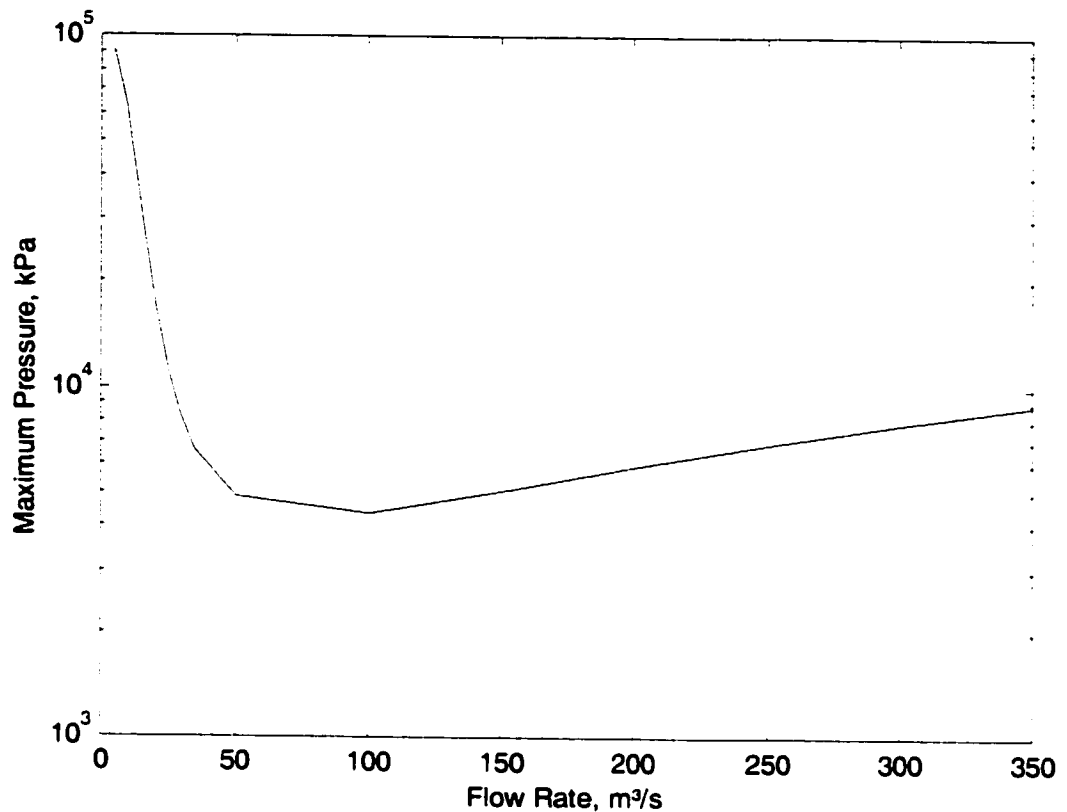


Figure 6.1 Effect of flow rate on pressure loss

At any flow rate in this range, the pressure and temperature responses essentially have the same characteristics: there is a transient period in the first few days when the temperatures of the pipeline and the surrounding ground stabilize, and then there is a sinusoidal region where the pipeline is responding to the seasonal temperature changes. Prior to start-up, the ground is cold and the pipeline is filled with water. During the start-up transient, the hot oil flows into the pipeline, displacing the water, and cooling off as its heat is lost to the ground. As the oil front advances into the pipeline, the pressure loss grows from a very small value (representing the flow losses of water alone). Eventually, the entire pipeline is filled with oil, but this oil has lost much of its heat to the surrounding ground. This point in time will typically be when the highest pressure loss is experienced (for a pipeline with a constant flow rate of oil). After this, the ground warms up

fairly quickly, and as it does, the oil loses less and less heat to the ground. This in turn results in lower pressure losses. The temperature of the ground changes with the seasons and this is what dominates the long term behaviour of the pipeline. As the flow rates increase, proportionately less heat can be lost to the ground in winter or during the start-up transient, or gained from the ground in summer. The higher the flow rate, the less extreme the start-up transient will be, and the less effect the change in the seasons will have.

Two pressures are given in the table above (and those below). These indicate the pressure loss during the start-up transient (which is the overall maximum pressure loss), and the pressure loss during a typical winter after the start-up transient has died out. The smallest value of maximum transient pressure loss occurs somewhere between 50 and 150 m³/d, while the smallest value of maximum seasonal pressure loss occurs somewhere between 35 and 100 m³/d. As was discussed in Chapter 2, the heat loss effects, combined with the high dependence of viscosity on temperature, cause low flow rates to have high pressure losses: the pressure loss versus flow rate curve is non-monotonic, unlike for a fluid in which the viscosity does not change.

All these effects can be seen in the figures below. Figure 6.2 shows two years worth of flow at each of the flow rates in Table 6.2, while Figure 6.3 shows only the first two days of each of these simulations. Figure 6.4 shows start-up for those cases in which the maximum pressure does not exceed 10 MPa, and Figure 6.5 shows a two years of operation of the same cases. The dashed line in Figure 6.2 and subsequent figures in this chapter represents the base case described in Table 6.1.

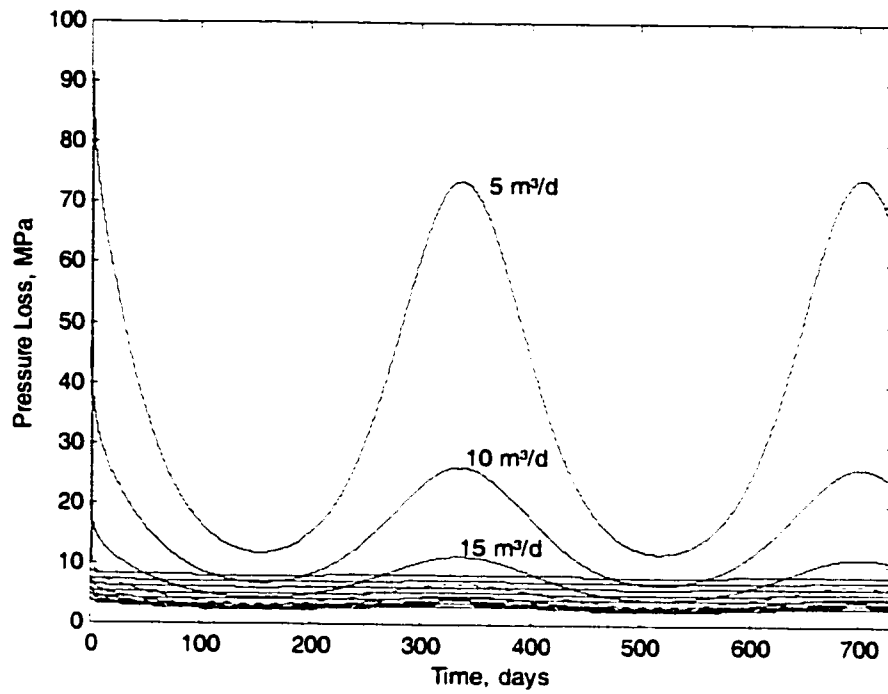


Figure 6.2(a) Pressure loss with varying flow rate

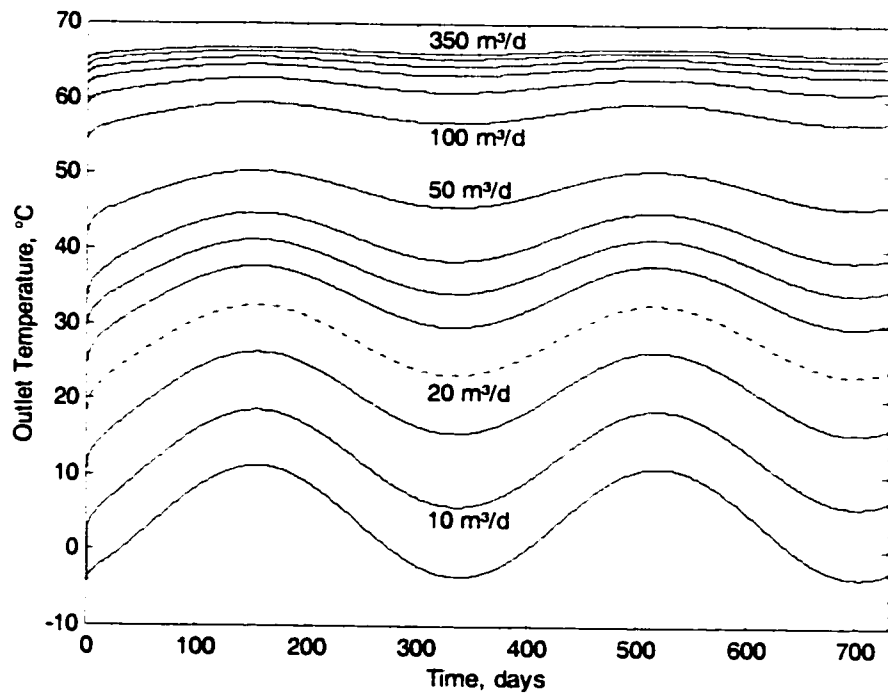


Figure 6.2(b) Temperature with varying flow rate

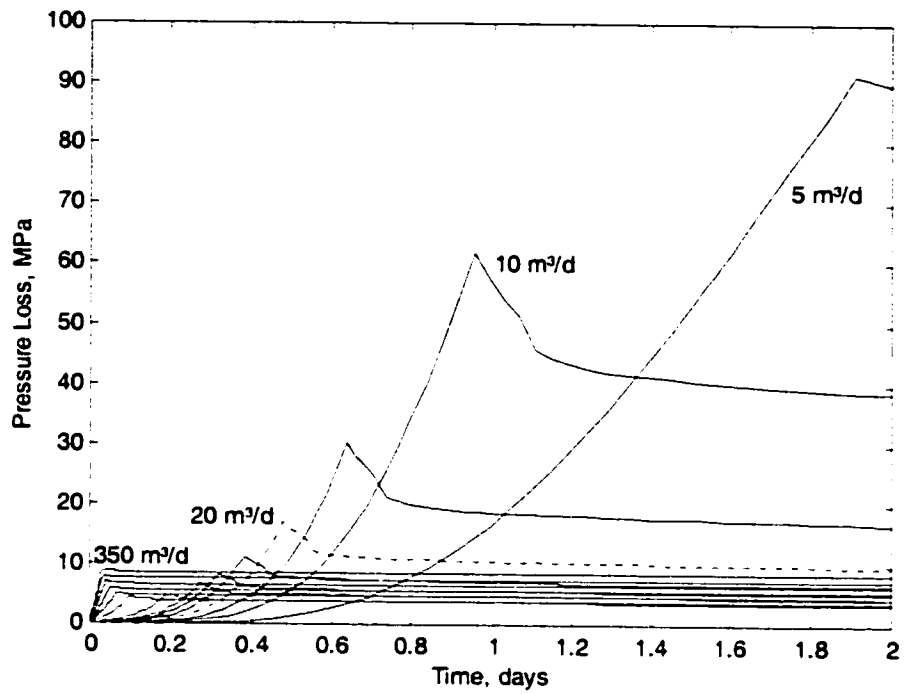


Figure 6.3(a) Pressure loss with varying flow rate

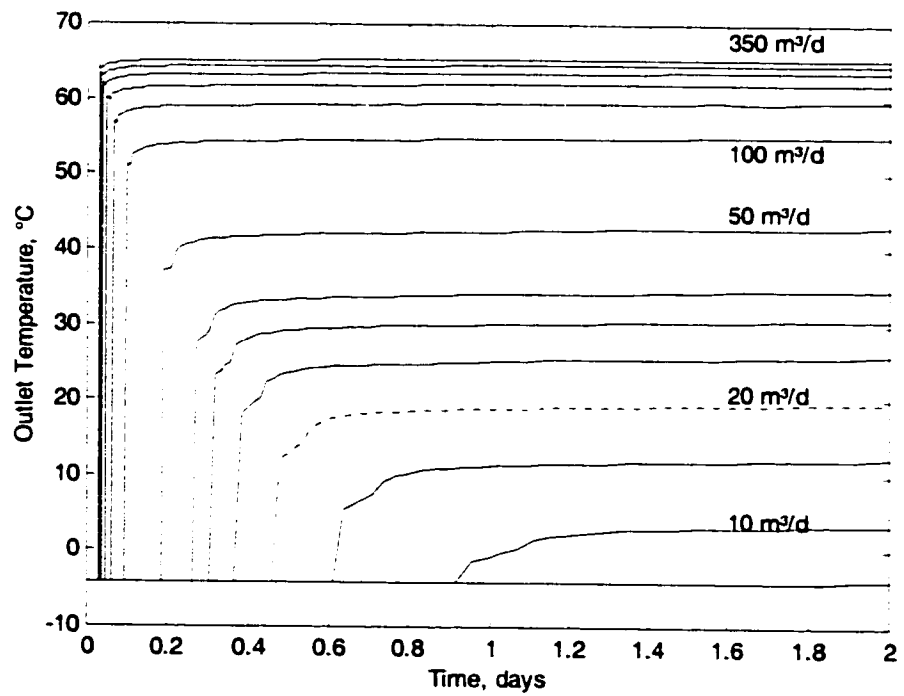


Figure 6.3(b) Temperature with varying flow rate

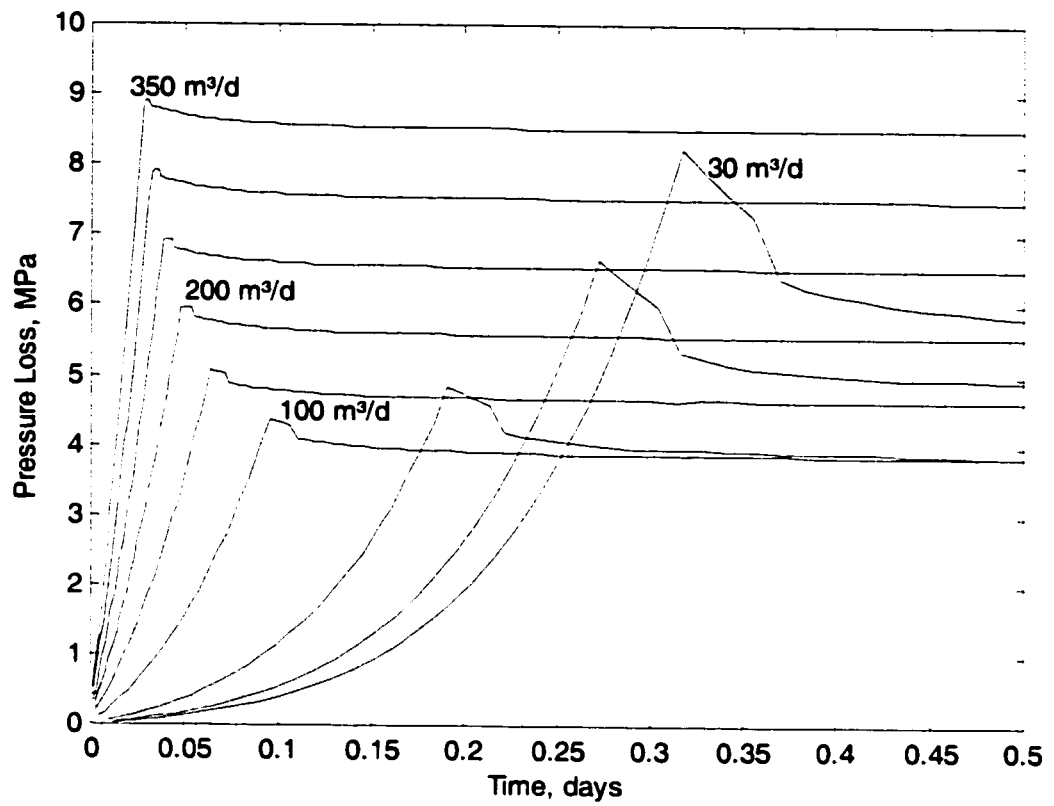


Figure 6.4 Start-up pressures

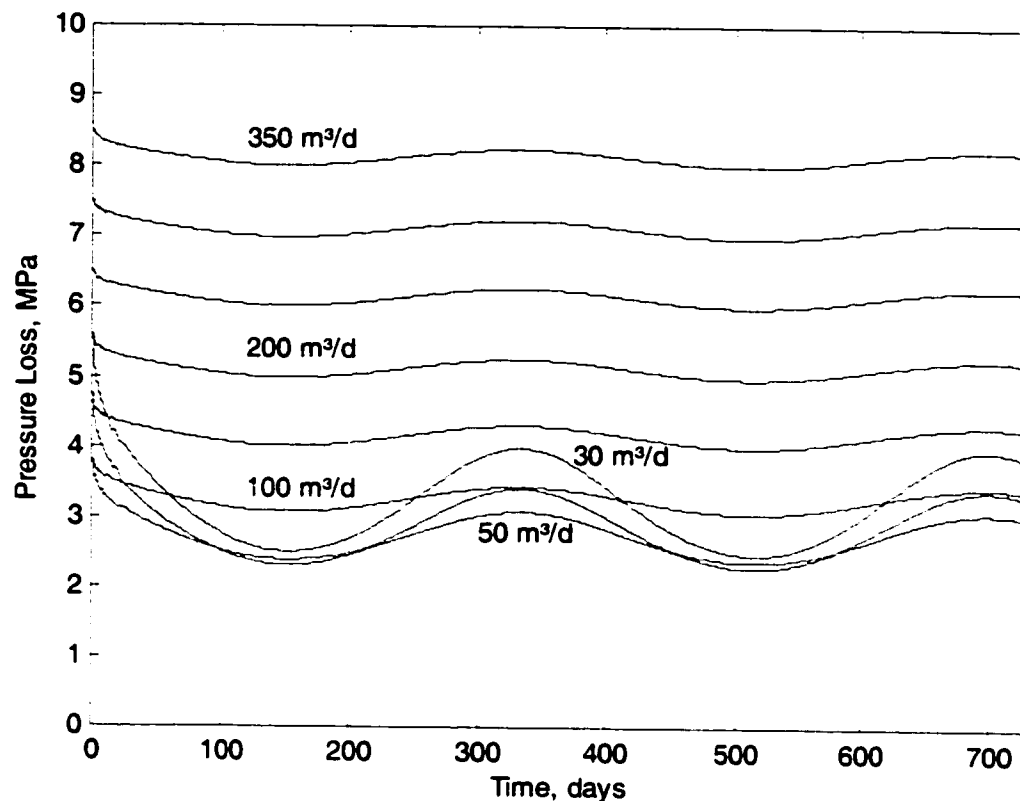


Figure 6.5 Operating pressures

Figure 6.2(a) and Figure 6.5 show the behaviour that is evident in Table 6.1 and Figure 2.6; the pressure loss decreases substantially with increasing flow rate, until a critical point is reached, at which point further increases in flow rate lead to slight increases in pressure loss. It can be seen in Figure 6.3(b), however, that the outlet temperature always increases with increasing flow rate. At higher flow rates, the increase is less: clearly there is an asymptotic limit at the inlet temperature (70°C in this case).

Figures 6.3(a) and (b), and Figure 6.4 show the start-up behaviour described earlier. As the pipeline is filled with hot oil, the cold water is displaced. This causes an increase in pressure as more and more of the pipeline is filled with higher viscosity oil. The temperature at the end of the pipeline cannot change at

all until the oil-water interface arrives at the outlet of the pipeline. Clearly this happens faster with higher flow rates. Once the pipeline is completely filled with oil, the pressure tends to decrease somewhat as the ground surrounding the pipeline tends to warm up.

6.1.2 Pipe Size

In both cases, the pipe size will be varied from 1.5" to 6" nominal (1.900"-6.625" actual), with the pipe wall thickness being adjusted according to commonly used pipes of the appropriate size.

Table 6.3 Pressure losses with varying pipe sizes

Nominal Pipe Size, in.	Actual Outside Diameter, in.	Wall Thickness, in.	Maximum Pressure, kPa	Max. Pressure After 25 Days, kPa
1.5	1.900	0.145	242048	35744
2	2.375	0.154	70379	18717
3	3.5	0.216	16976	6728
4	4.5	0.237	6188	3267
5	5.563	0.258	3795	1794
6	6.625	0.280	2293	1149

Figure 6.6 shows the maximum (i.e. start-up) pressures.

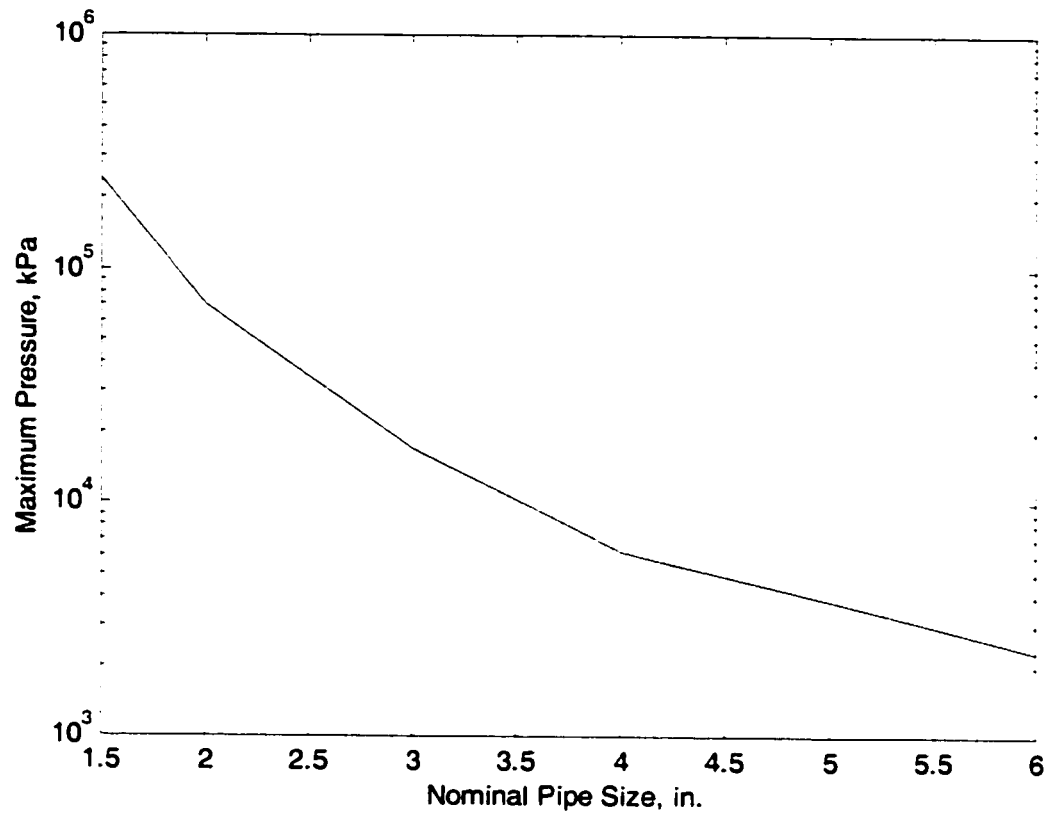


Figure 6.6. Effect of pipe size on pressure loss

Figure 6.7 shows two years worth of flow at each of the pipe sizes in Table 6.3.

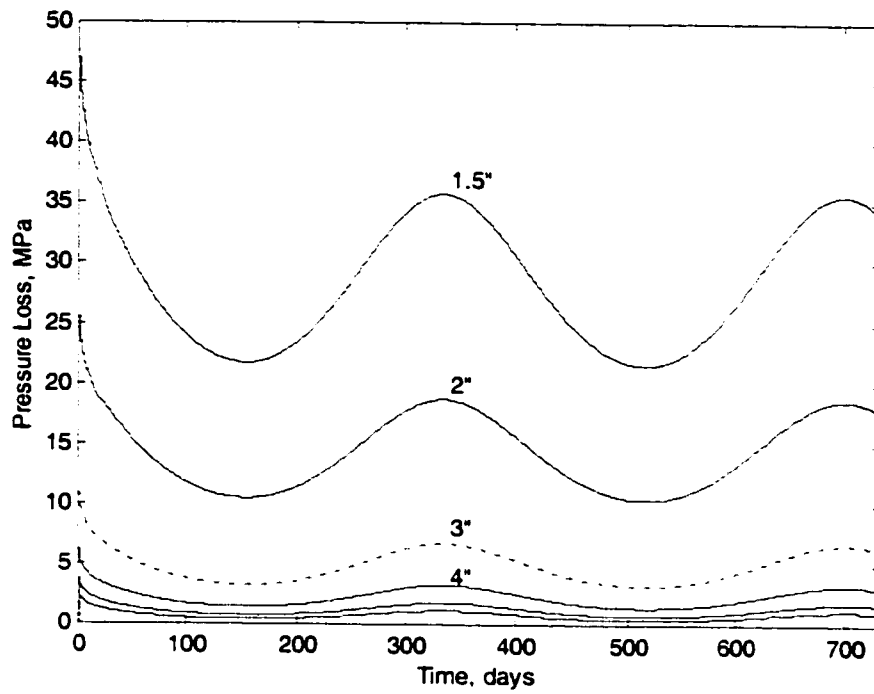


Figure 6.7(a) Pressure loss with varying pipe size

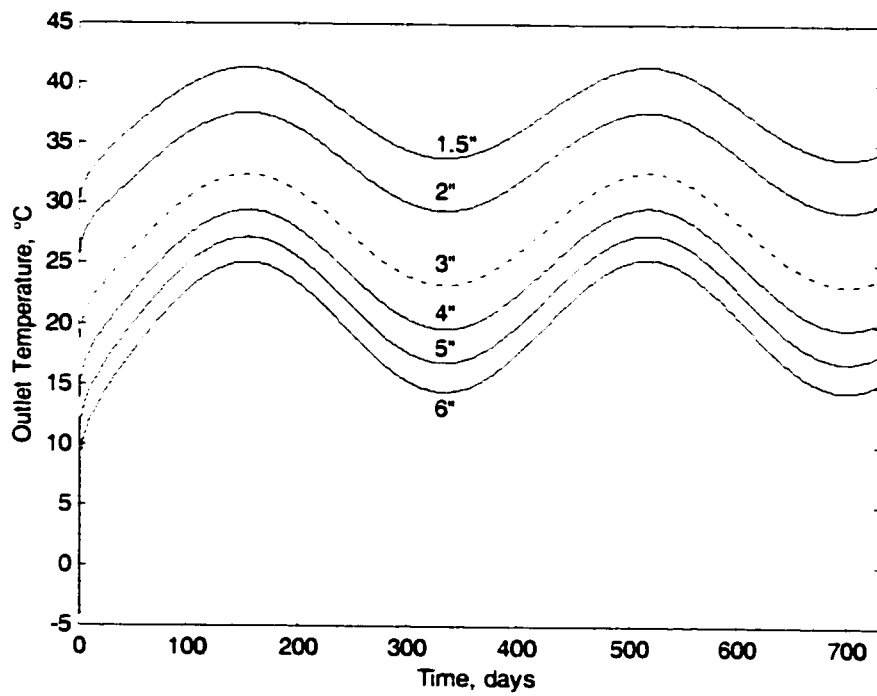


Figure 6.7(b) Temperature with varying pipe size

Decreasing the pipe size in this case leads to increase in both the maximum pressure loss and the maximum pressure loss after 25 days. This will normally be the case. There could be cases, however, in which the situation could be such that a small increase in pipe size could lead to an increase in pressure loss, because of the reduced velocity.

Note that the pressure scale in Figure 6.7(a) has been adjusted to cut off the pressure spikes at start-up for the two smallest pipe sizes. These spikes were indistinguishable from the axis line on the figure. The velocity is higher in the smaller pipes (for the same flow rate), so the duration of any pressure spike at start-up is smaller.

6.1.3 Pipeline Length

Pipeline length was adjusted from 0.5 km to 10 km. The maximum pressure loss (i.e. during the start-up transient) and the maximum pressure loss after 25 days are in Table 6.4.

Table 6.4 Pressure losses with varying pipeline lengths

Pipeline Length, km	Maximum Pressure, kPa	Max. Pressure After 25 Days, kPa
0.5	272	197
1	1433	800
2	16,976	6728
3	84,582	32,463
4	236,731	104,737
6	759,648	497,483
8	1,464,410	1,188,740
10	2,232,240	2,098,600

Figure 6.8 shows the maximum (i.e., start-up) pressure in this table.

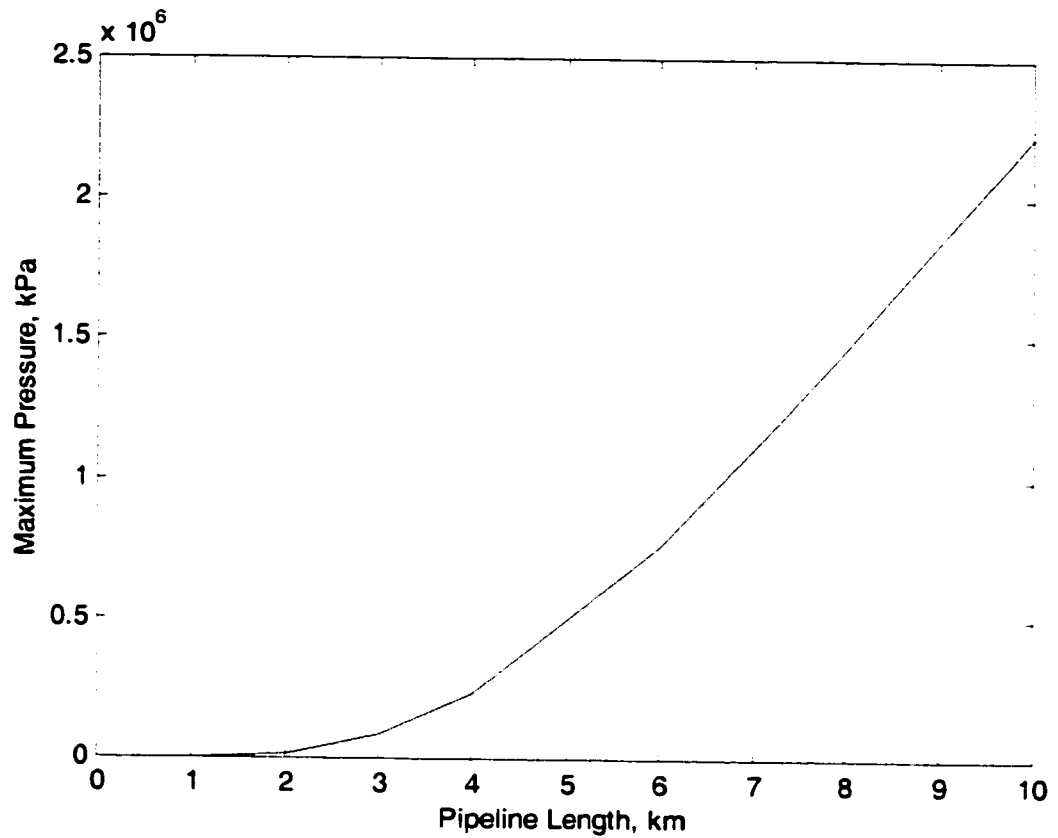


Figure 6.8 Effect of pipeline length on maximum pressure

Pressure increases exponentially with length at smaller lengths, as the increasing heat loss is dominant. After a certain length is reached, the fluid has essentially cooled to ground temperature and further increases in length lead to a linear increase in temperature.

Figure 6.9 shows two years worth of flow at each of the pipeline lengths in Table 6.9.

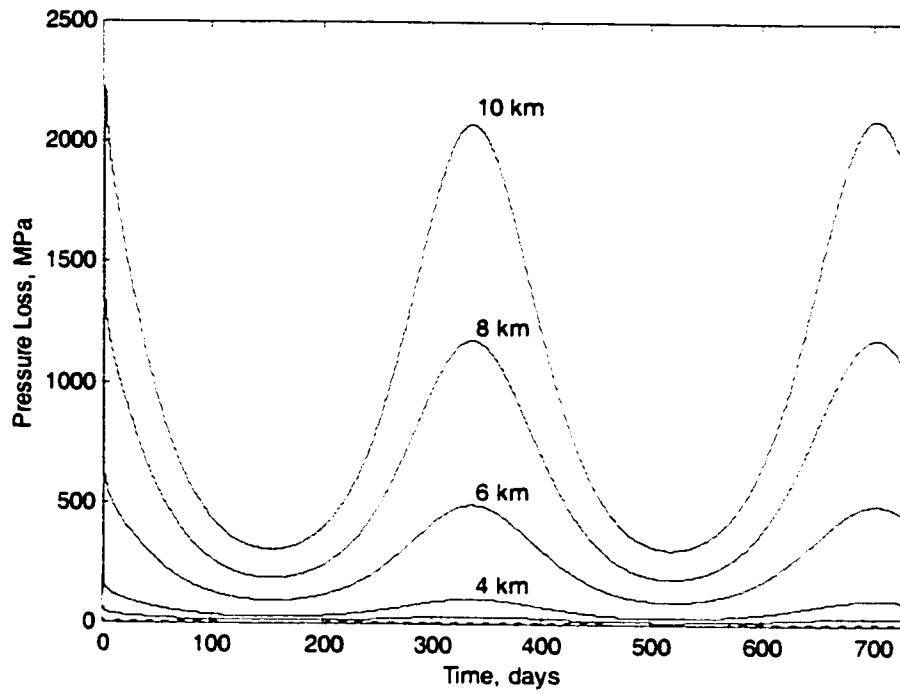


Figure 6.9(a) Pressure loss with varying pipeline length

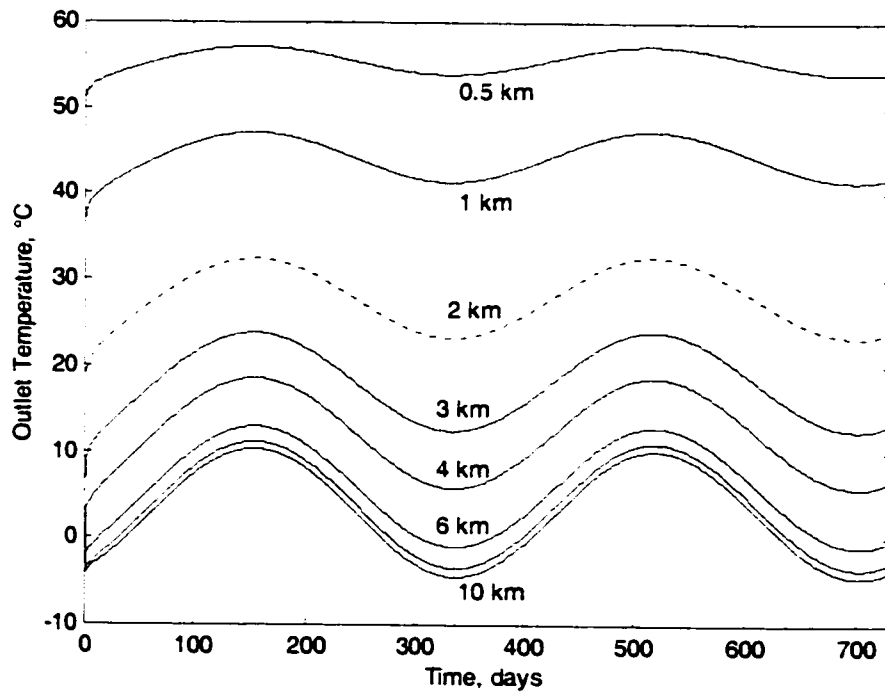


Figure 6.9(b) Temperature with varying pipeline length

Figure 6.10 shows the same data, but only for those lengths with an operating pressure less than 10 MPa.

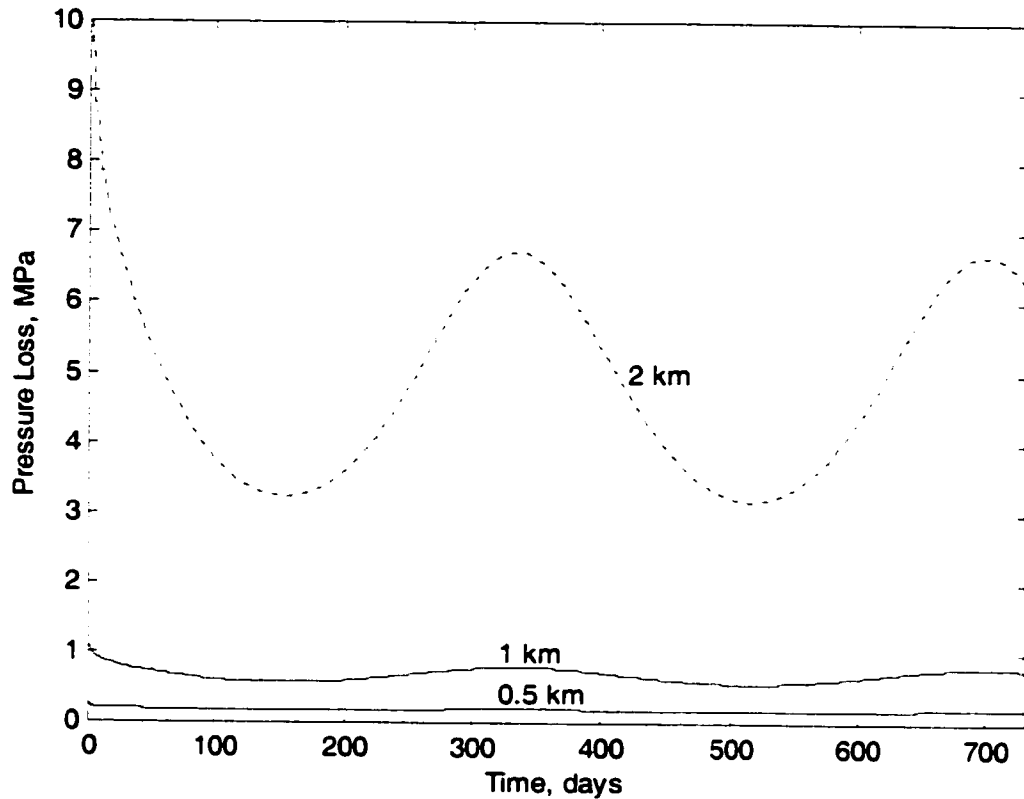


Figure 6.10 Effect of length on pressure

In pumping a hot, viscous oil through a buried pipeline, the shorter the distance, the better. Even when the viscosity is constant, the pressure loss increases in proportion to the length. This is combined here with further cooling of the fluid and the associated increase in viscosity. With this particular configuration, lengths over approximately two kilometres will result in pressure losses that are very high (over 1000 psi). Even at two kilometres, a special start-up procedure may be required to reduce the maximum pressure loss during the start-up transient.

6.1.4 Burial Depth

The pipeline burial depth was adjusted from 1 ft to 9 ft. The maximum pressure loss (i.e. during the start-up transient) and the maximum pressure loss after 100 days are in Table 6.5. 100 days is used in this case, because at deeper depths, the start-up transient lasts longer than at shallow depths, and has not died out after the 25 days used in the other examples in this section.

Table 6.5 Pressure losses with varying burial depths

Burial Depth, ft	Maximum Pressure, kPa	Max. Pressure After 100 Days, kPa
1	14,227	14,054
3	17,317	7961
4	16,976	6728
5	15,913	5948
7	13,597	5120
9	11,930	4891

The maximum pressure (i.e. start-up) data from this table is plotted in Figure 6.11.

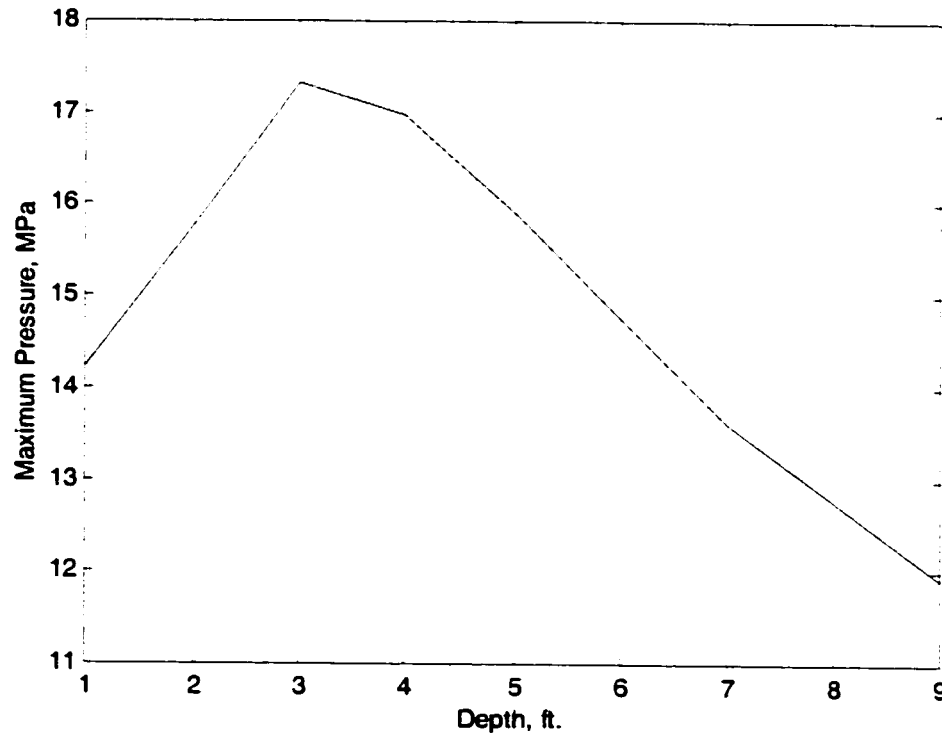


Figure 6.11 Effect of depth on start-up pressure.

While the start-up pressure is less for a 1 ft. burial depth than for a 3 ft. depth, this is due to the seasonal effects; the operating pressure decreases monotonically with increasing depth.

Figure 6.12 shows two years worth of flow at each of the burial depths in Table 6.12.

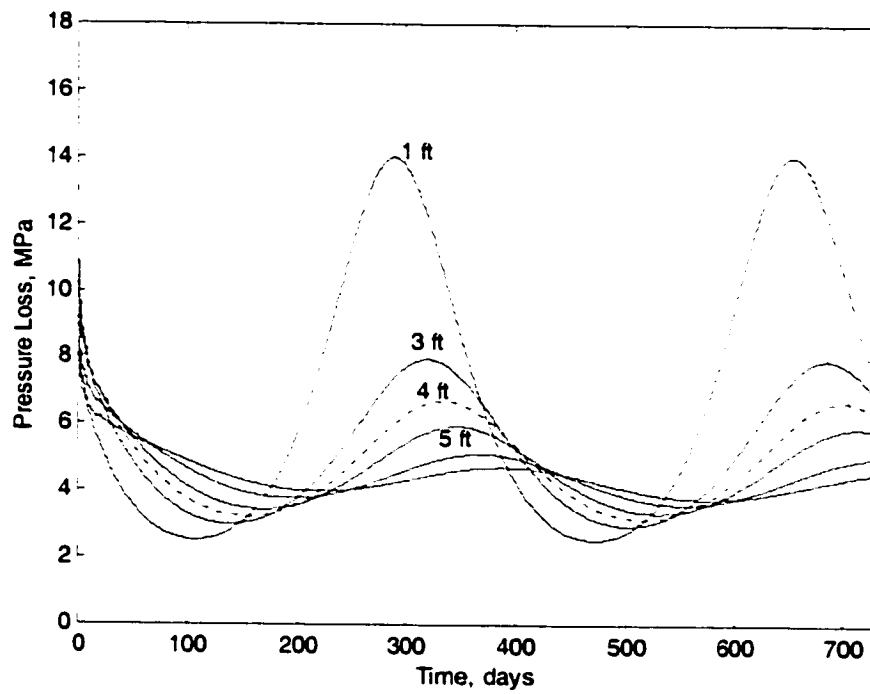


Figure 6.12(a) Pressure loss with varying pipeline depth

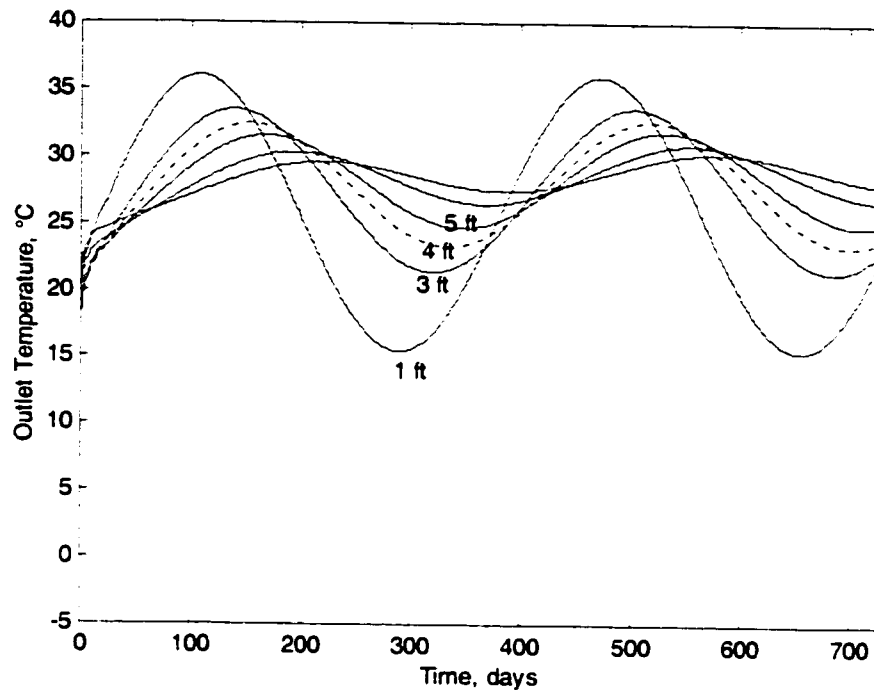


Figure 6.12(b) Temperature with varying pipeline depth

It is evident that the performance of the pipeline is less sensitive to depth than the other parameters examined so far. A heated viscous oil pipeline designer would have to consider other factors when deciding upon a burial depth. It is unlikely that anyone would install a pipeline less than three to four feet below the surface of the ground; at those shallow depths a pipeline is much more susceptible to mechanical damage from activity (e.g. farming) on the surface. Economic factors will also determine how deep a pipeline would be buried.

Evident in Figure 6.12 is the phase difference between the temperature and pressure plots for pipelines of different depths. This is the same phase delay discussed in Section 3.1.1 and is related to the time it takes for effects of surface temperature to be felt at a given depth below the ground—the deeper the location of interest, the more time it takes for a change in surface temperature to be felt.

6.1.5 Insulation Thickness

The insulation thickness was adjusted from 0" to 3". The maximum pressure loss (i.e. during the start-up transient) and the maximum pressure loss after 25 days are in Table 6.6.

Table 6.6 Pressure losses with varying insulation thicknesses

Insulation Thickness, in.	Maximum Pressure, kPa	Max. Pressure After 25 Days, kPa
0	276,814	84,342
0.5	64,853	25,823
1	24,883	11,564
1.5	16,976	6728
2	13,970	4592
2.5	12,578	3430
3	11,861	2729

The maximum pressure data is plotted in Figure 6.13.

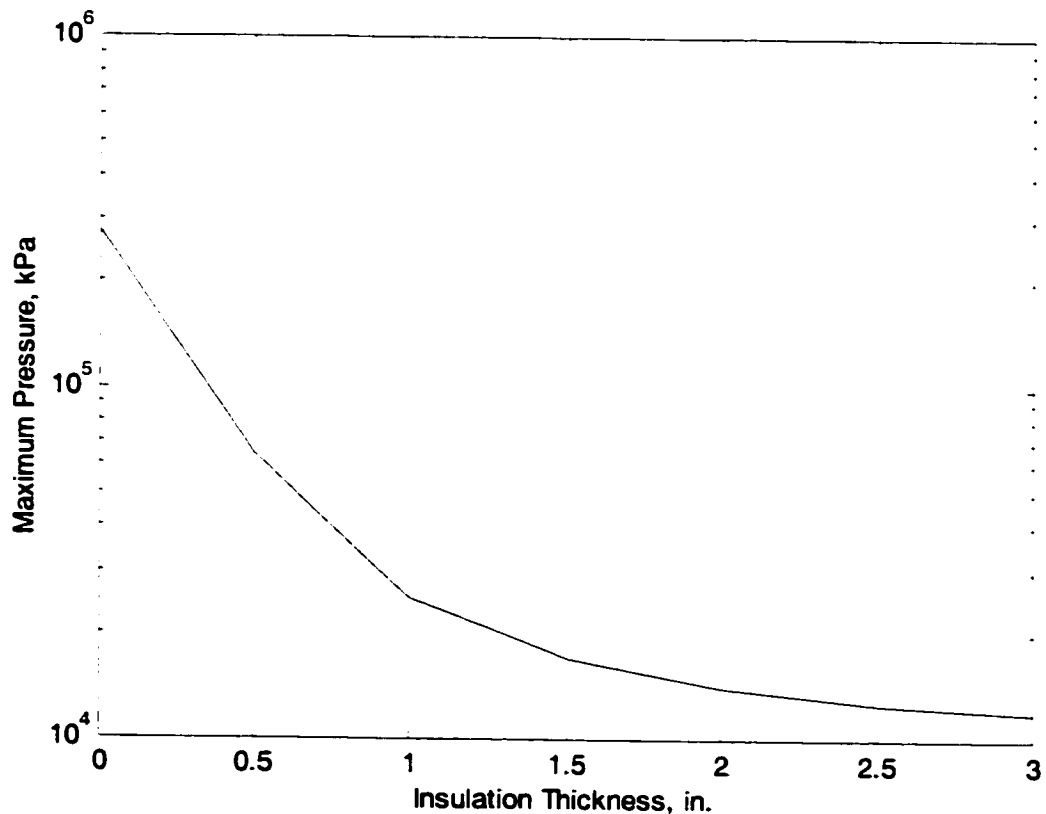


Figure 6.13 Effect of insulation thickness on start-up pressure

Figure 6.14 shows two years worth of flow at each of the insulation thicknesses in Table 6.6.

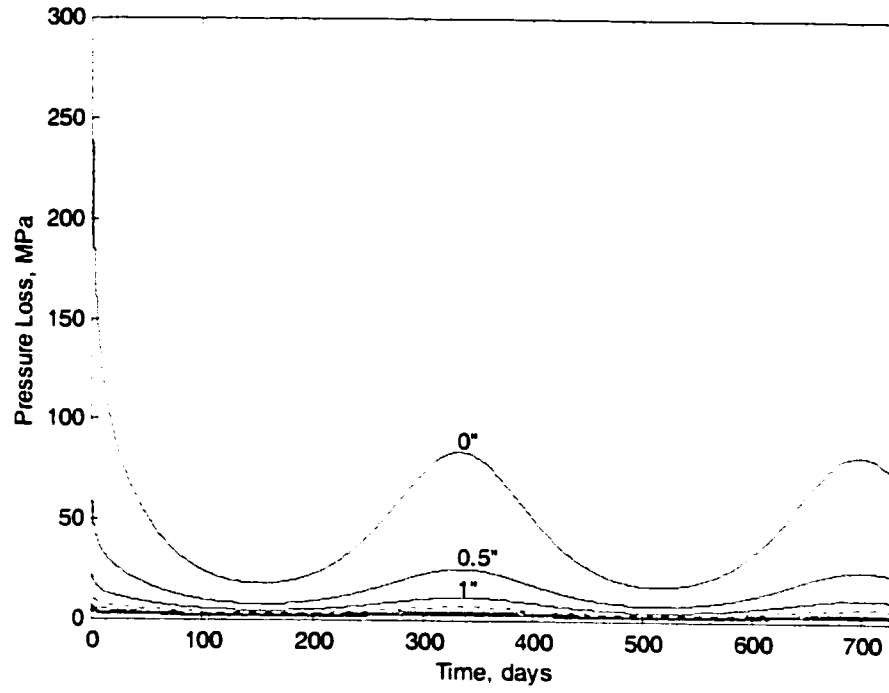


Figure 6.14(a) Pressure loss with varying insulation thickness

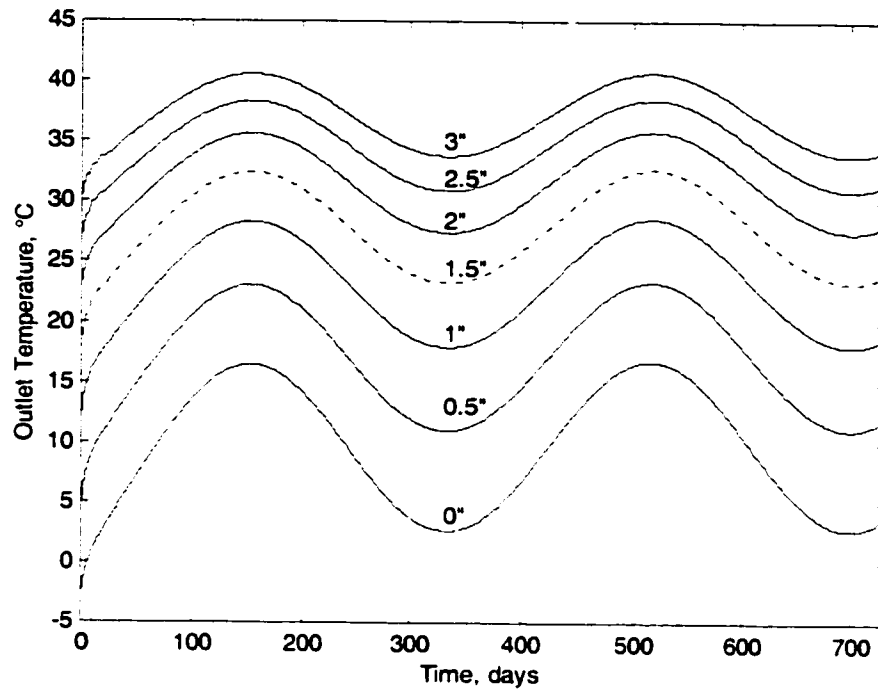


Figure 6.14(b) Temperature with varying insulation thickness

Figure 6.15 shows the pressures of those cases with operating pressures below 10 MPa.

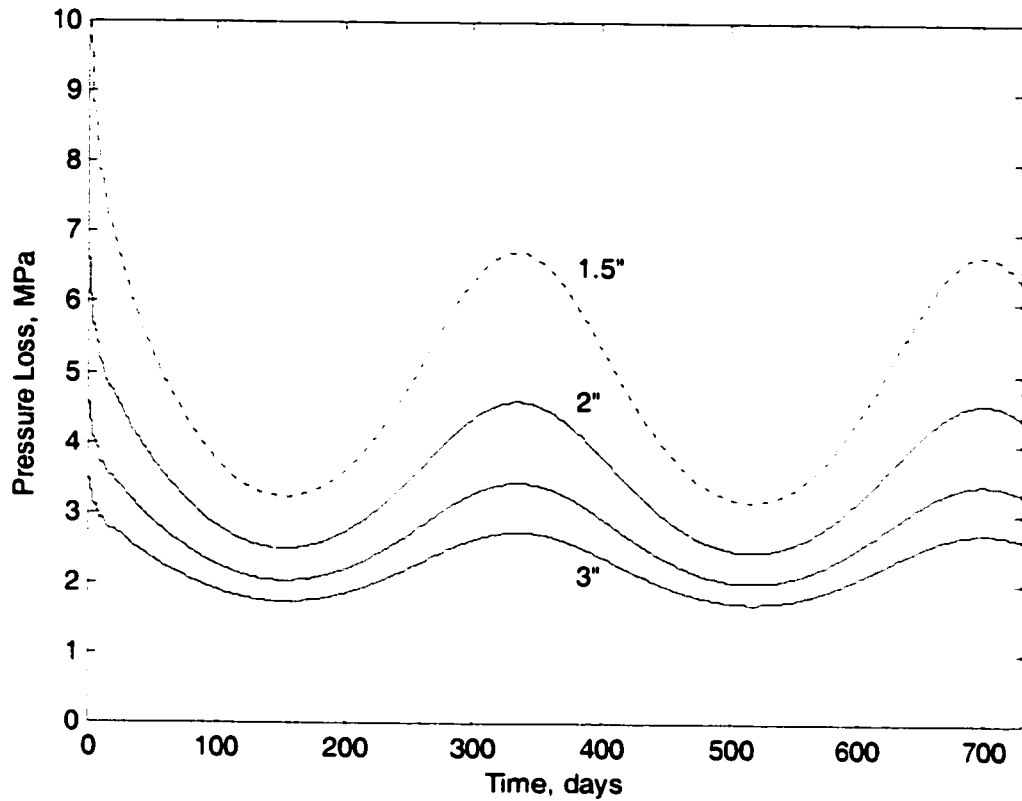


Figure 6.15 Pressure with varying insulation thickness

Insulating a heated viscous oil pipeline is clearly advisable, in that it significantly decreases both the maximum pressure loss during the start-up transient and during regular operation. The principle of diminishing returns applies—adding more and more insulation tends to have less and less further advantage.

6.1.6 Flow Start Date

It is expected that the start date will only affect the pressure over the first few days. It was clearly seen in the above parametric studies that a quasi-steady state is reached quite quickly, at which time only the seasonal temperature variations have any significant effect on the pipeline pressure and temperature. The following examinations of start date will therefore only cover one year of production. The following start dates were used: May 1 (base case), Sept. 30 (when the base case exhibits the lowest pressure drop), March 2 (when the base

case exhibits the highest pressure drop), and July 15 and December 30 (mid way points). Table 6.7 shows the maximum pressure drop for each of these cases.

Table 6.7. Effect of start date on pressure loss

Start Date (Day #)	Maximum Pressure Loss, kPa
May 1 (0)	16,976
July 15 (75)	9354
September 30 (152)	7135
December 30 (243)	10,785
March 30 (333)	18,455

Pressure and Temperature are plotted in Figure 6.16.

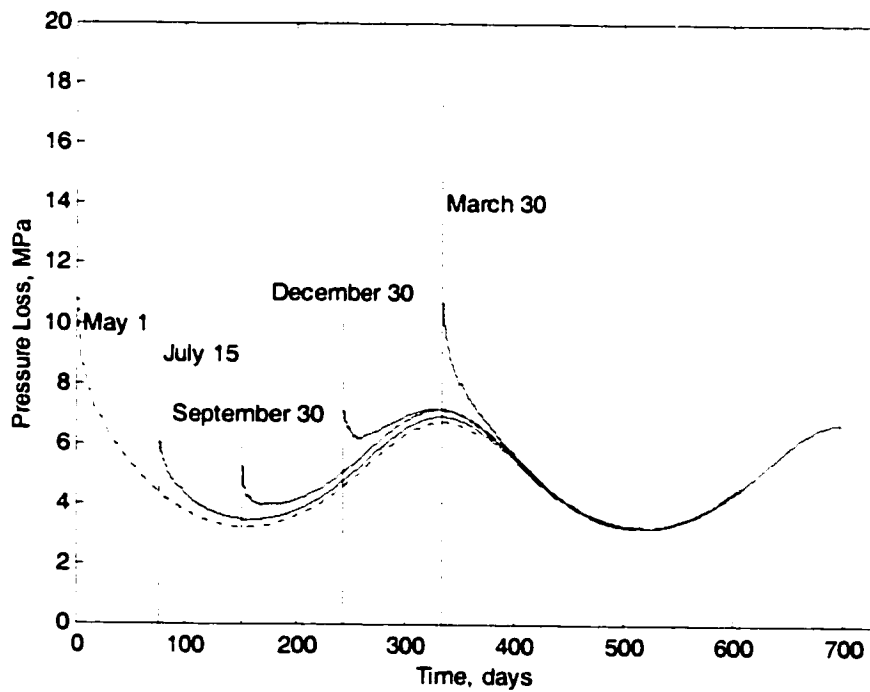


Figure 6.16(a) Effect of start date on pressure loss

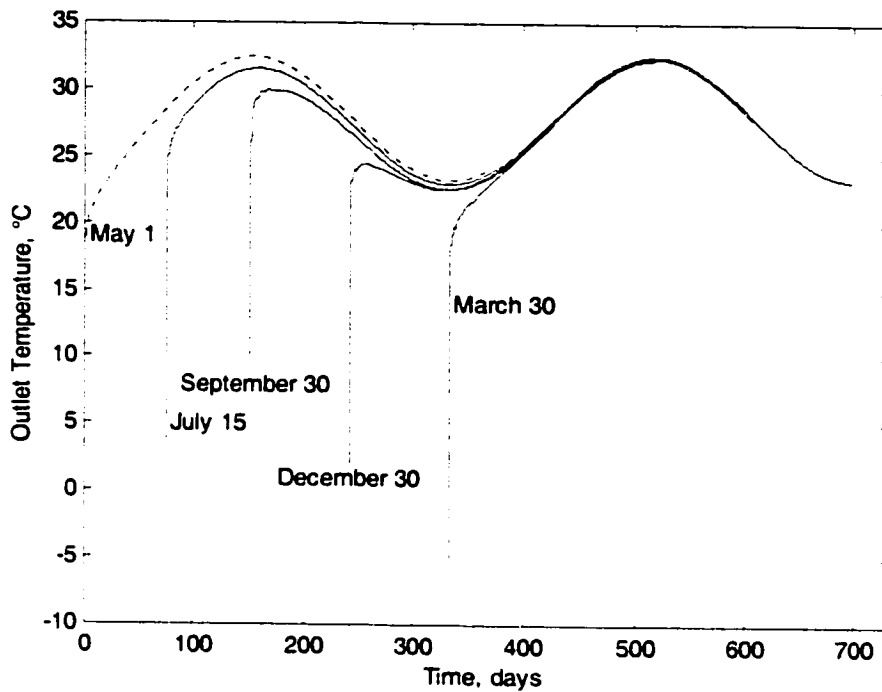


Figure 6.16(b) Effect of start date on temperature

In this case, it is best to start the pipeline in late September, as this is the time when the ground at the pipeline depth is the warmest (because of the phase delay mentioned earlier—note that the warmest time at surface is late July). The maximum pressure during start-up is less than half that of the base case (start-up May 1).

6.1.7 Inlet Temperature

The inlet temperature was varied from 40 to 90°C. The maximum pressure loss (i.e. during the start-up transient) and the maximum pressure loss after 25 days are in Table 6.8.

Table 6.8 Effect of inlet temperature on pressure loss

Inlet Temperature, °C	Maximum Pressure, kPa	Max. Pressure After 25 Days, kPa
40	60,220	35,483
50	38,281	19,636
60	25,153	11,301
70	16,976	6728
80	11,714	4162
90	8238	2682

The maximum pressures are plotted in Figure 6.17.

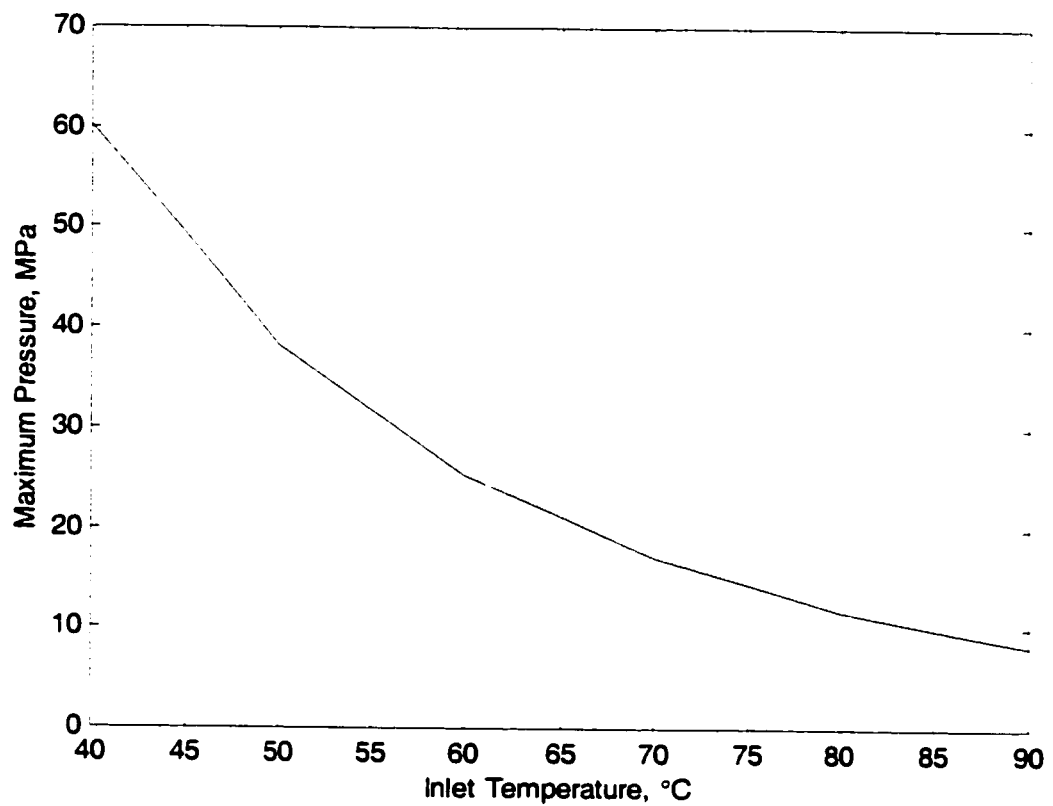


Figure 6.17 Effect of inlet temperature on start-up pressure.

Figure 6.18 shows one year of flow at each of the inlet temperatures in Table 6.8.

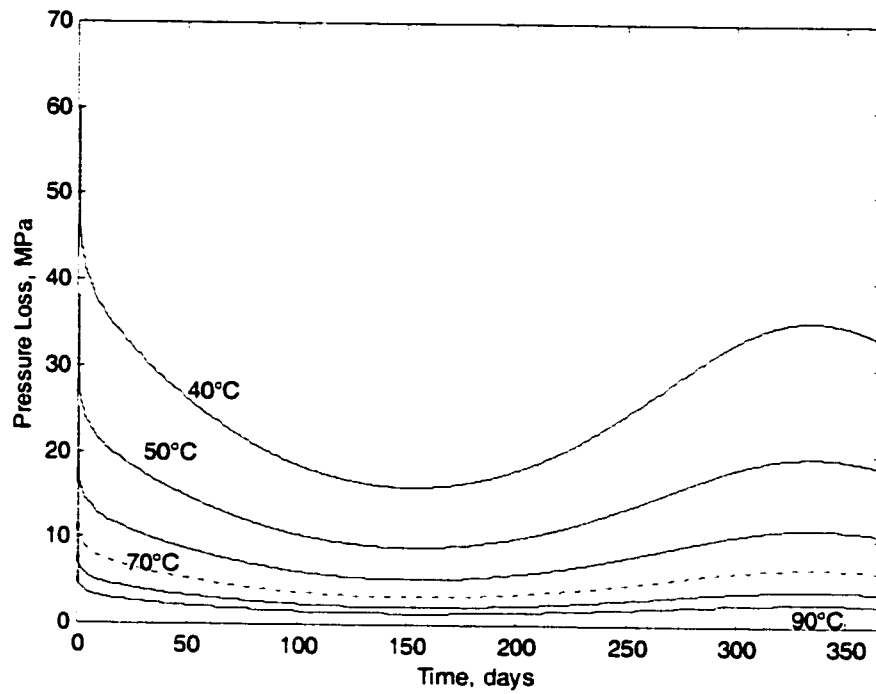


Figure 6.18(a) Effect of inlet temperature on pressure loss

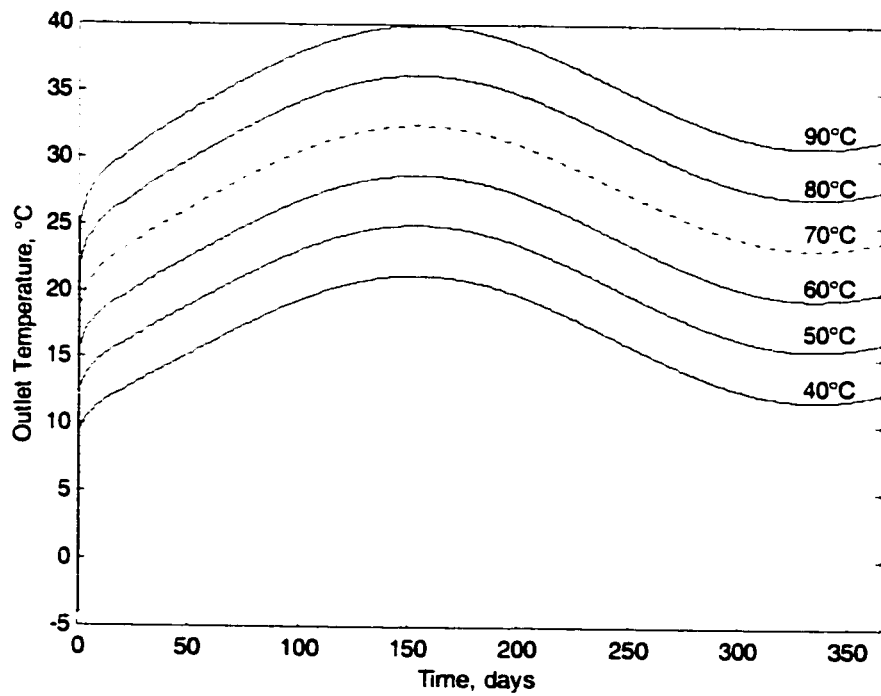


Figure 6.18(b) Effect of inlet temperature on outlet temperature

The outlet temperature essentially has a linear relationship with inlet temperature (except at the start-up transient). This was expected since the heat transfer equations are linear (except for radiation, which is not considered in this work). Note that the Nusselt number is constant so long as the flow is laminar, so the effect of temperature on viscosity does not have an effect on the rate of heat transfer. None of the other important properties (specific heat, thermal conductivity, density) are considered to change with temperature (this is an approximation). Therefore, the heat transfer coefficients are not a function of temperature, so no non-linearities are introduced through them. The pressure loss is not linear with inlet temperature, however, because the pressure loss is dependent upon viscosity, and viscosity is highly non-linear with temperature.

As expected, the higher the inlet temperature, the lower the pressure loss, both during the start-up transient and regular operation. There are obviously economic issues at play here, as it could cost much more to heat up the fluid to a higher temperature than to pump against a higher pressure. This must be compared against the reduced pumping costs.

6.1.8 Fluid Properties

The critical fluid property is viscosity. In Section 2.3.1, a correlation was presented between viscosity, and API gravity and temperature. This was based on Western Canadian heavy crude oils with API gravities ranging from 9-13.3°API. It is generally unwise to use a correlation of this type with heavy oil as heavy oils with the same API gravity can have a wide range of viscosity, even when the oils come from the same field. This correlation will be used here, however, for a parametric study on the effects of fluid properties. Table 6.9 lists the different API gravities tested, with their density (considered to be constant with temperature, although this is a rough approximation) and viscosities at 30°C and 70°C

Table 6.9 Fluid properties

API Gravity	Density, kg/m ³	Viscosity at 30°, cp	Viscosity at 70°C, cp
9	1005	62,465	1407
10	998	24,518	762
11	991	11,267	457
12	984	5838	297
13	977	3322	205

The base case used in the other parametric studies is not used here: all input parameters are the same as in that case, with the exception of oil density and viscosity. The pressures are displayed for each of these cases in Table 6.10.

Table 6.10 Effect of API gravity on pressure

API Gravity	Maximum Pressure, kPa	Max. Pressure After 25 Days, kPa
9	36,204	13,810
10	13,683	5655
11	6105	2714
12	3069	1470
13	1714	865

One year of flow is shown in Figure 6.19.

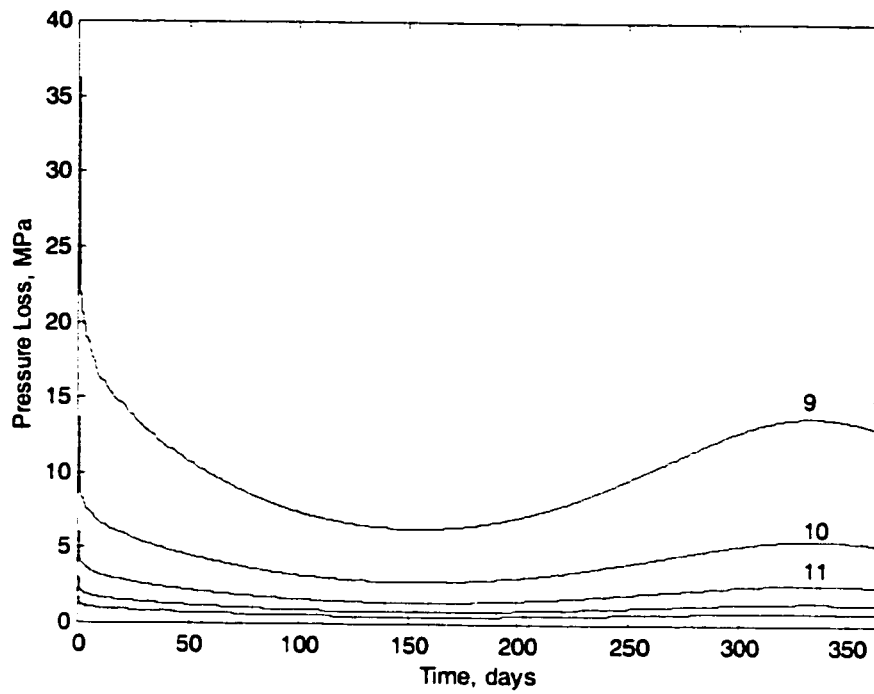


Figure 6.19(a) Effect of API gravity on pressure

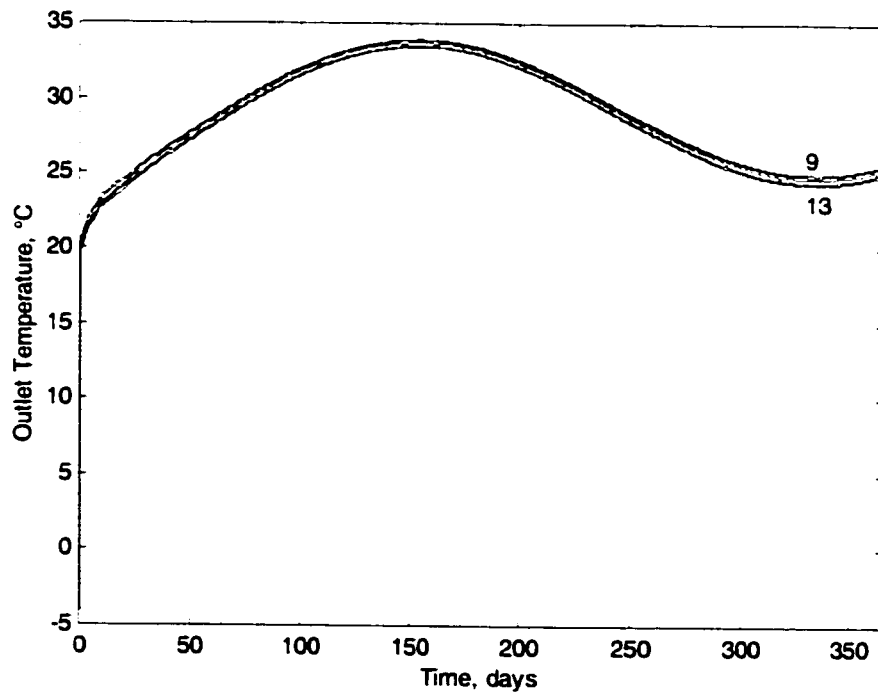


Figure 6.19(b) Effect of API gravity on temperature

Clearly, API gravity can have a significant effect on pressure loss. There is less than 3% difference in density in this range of API gravity, but there is more than an order of magnitude difference in pressure loss. Virtually none of the difference in pressure loss is caused by differences in temperature, though. It is obvious in Figure 6.19(b) that there is very little difference in temperature (and heat transfer) between these different oils.

6.1.9 Preheat Time

One possible means to mitigate the effect of the start-up transient is to preheat the line with hot water. This will heat up the ground surrounding the pipeline without incurring a very high pressure loss. If done for sufficiently long, this could prevent the start-up pressure transient from exceeding the maximum pressure expected after the start-up transient.

This parametric study examines the base case with varying lengths of preheat. The flow rate of water during the preheat is 20 m³/d, and the inlet temperature of the water is 70°C. The oil will still start to flow at time 0 (midnight on May 1) in each case; the preheat occurs before this. Table 6.11 shows the preheat lengths that were tested, and the maximum pressures (both during the start-up transient and regular operation) experienced.

Table 6.11 Effect of preheat length on pressure

Preheat Length, hours	Maximum Pressure, kPa	Max. Pressure After 25 Days, kPa
0	16,976	6728
3	10,499	6728
6	10,242	6728
12	9870	6728
24	9341	6727
36	9007	6726
48	8727	6726

Figure 6.20 shows the first day of operation (from the start of oil flow) for each of these cases.

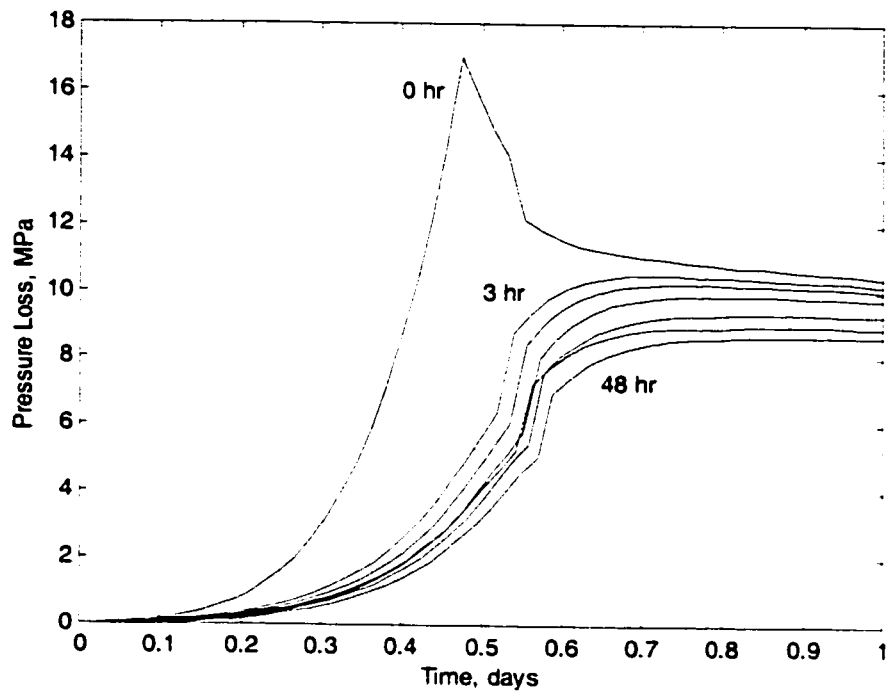


Figure 6.20(a) Effect of preheat length on pressure loss

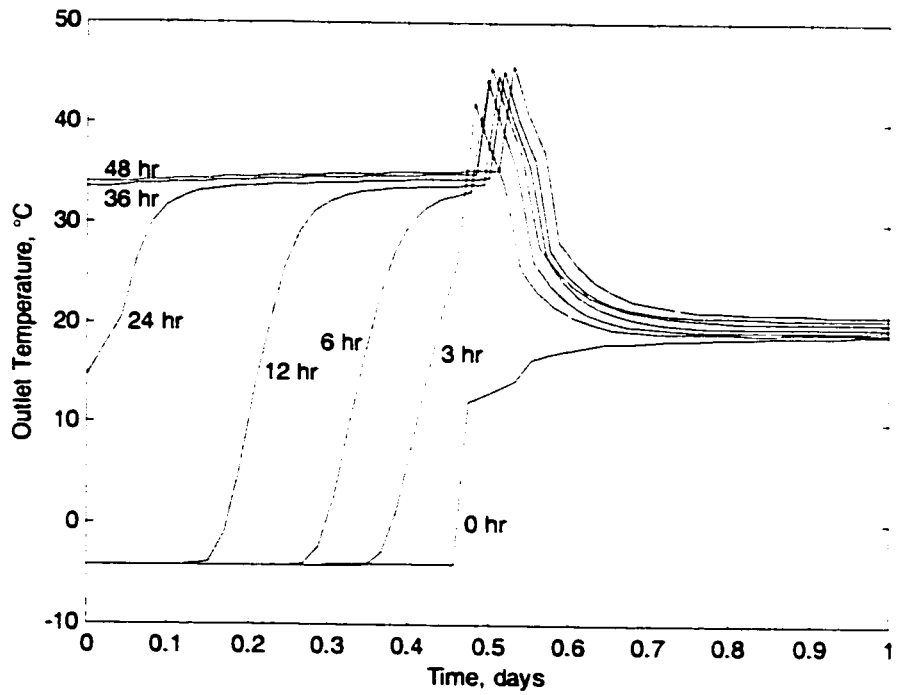


Figure 6.20(b) Effect of preheat length on temperature

It is immediately evident from Table 6.11 that preheat has essentially no effect on the long term operation of the pipeline, but can have a substantial effect on the maximum pressure during the start-up transient. Figure 6.20 shows that the large spike of pressure evident in the no-preheat case is removed even with a very short preheat. The longer the preheat, the less pressure is experienced during the start-up transient. While not tested explicitly here, other factors which could improve the preheat are a higher flow rate or a higher temperature, either (or both) of which would lead to a greater amount of heat transferred to the ground over a given period of time.

6.1.10 Effect of Ground Conductivity

All the calculations presented in this chapter use a value of ground conductivity of $0.5 \text{ W/m}\cdot\text{K}$. This and the density and specific heat are based on the values for “soil” found in tables in an introductory heat transfer text [21]. This value is for dry soil—no water content. Thermal conductivity for sandy soils, silt and clay soils, and peat, can go as high as 3.0, 1.9, and $0.6 \text{ W/m}\cdot\text{K}$, respectively, in unfrozen ground, and as high as 4.0, 2.2, and $1.2 \text{ W/m}\cdot\text{K}$, respectively, in frozen ground, depending on bulk density and water content of the ground [26]. Clearly, the effect of a change in this property must be considered. The current work is concerned with heat transfer in dry ground; the effects of the latent heat of the water-ice phase change will be significant, and are not addressed here. Therefore, any significant water content could cause the results to be erroneous. It should be noted however, that this is only the case if the pipeline being simulated is in a region where the temperature regularly drops below freezing—in tropical regions the current work should be applicable in wet or dry ground.

Table 6.12 shows the maximum pressure experienced in each case.

Table 6.12 Effect of ground thermal conductivity on pressure

Ground Thermal Conductivity, W/m·K	Maximum Pressure, kPa	Max. Pressure After 25 Days, kPa
0.2	14040	4219
0.5	16976	6728
0.7	17470	8818
1.0	17609	11358
1.5	17380	14479
2.0	17045	16749
3.0	20015	20015
4.0	22472	22472

Figure 6.21 shows the pressure loss and temperature over one year of operation for each of the cases shown in Table 6.12.

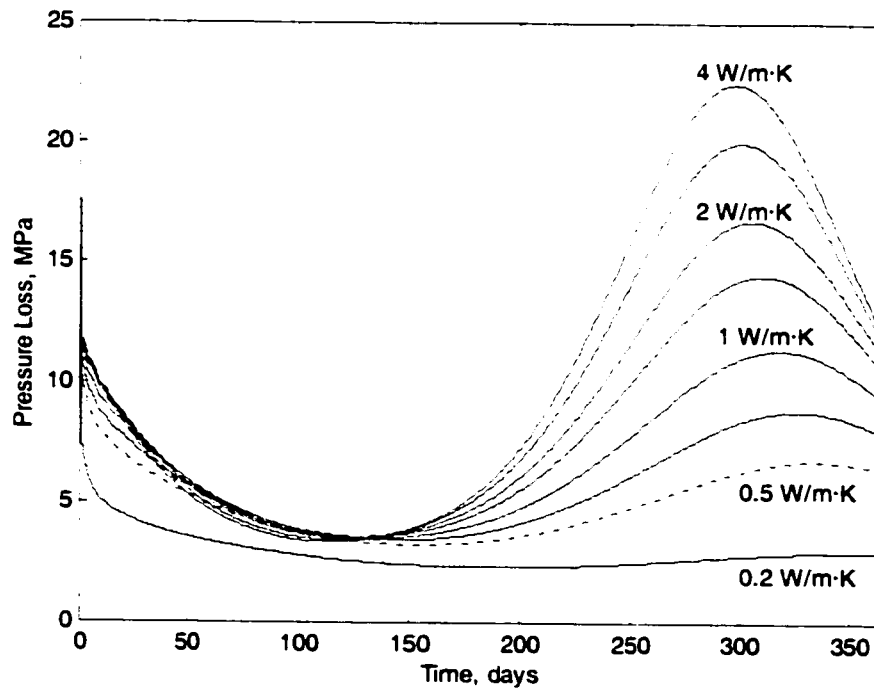


Figure 6.21(a) Effect of ground thermal conductivity on pressure loss

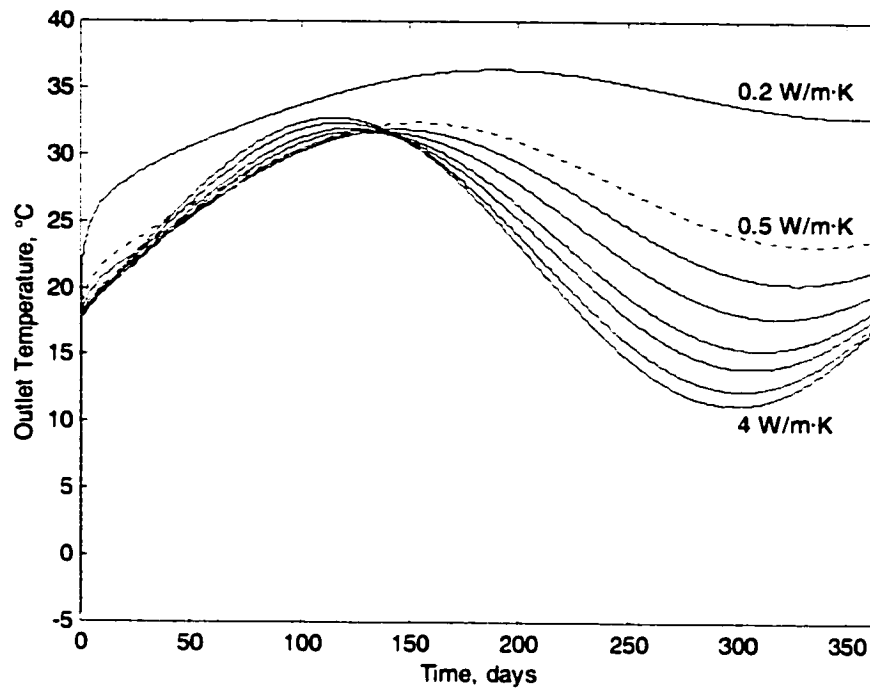


Figure 6.21(b) Effect of ground thermal conductivity on temperature

Clearly, the thermal conductivity of the ground has a significant effect on the temperature and pressure loss in a buried pipeline.

6.2 Parametric Studies in Shutdowns

One of the most important concerns that companies contemplating the use of pipelines to transport heavy oil is the possibility of an unplanned shutdown. Shutdowns could be caused by many factors, including power failure or equipment problems. A pipeline transporting oil that has been heated to reduce its viscosity is very susceptible to problems in the event of a shutdown. When flow stops, the oil in the pipeline will lose heat to the surrounding ground. Viscous oil could increase in viscosity substantially during the flow stoppage, to the point where it may be difficult or impossible to restart the flow when power is restored without an expensive intervention. Pipeline operators would need to know how long they can remain shut down for without causing problems. Procedures would be developed for planned shutdowns as well; these can be simply flushing the oil

out of the pipe with water prior to shutdown. They would also need to establish procedures for dealing with unplanned shutdowns that are longer than acceptable. These procedures would likely be more complicated, and could range from slowly flushing the viscous oil from the line with water, to using a coiled tubing steam injection system to remove oil that is too viscous to flow on its own.

6.2.1 Shutdown Date

In Section 6.1.6, the effect of start-up date was considered. It was shown that starting the pipeline at certain times of the year could result in a smaller pressure transient than at other times in the year. The same thing is true for a shutdown. Here, a one hour shutdown is simulated at each of the five dates used in Section 6.1.6. The flow is run for at least two years prior to the shutdown in each case, to establish that the initial transient has died out. The flow is restarted for two days after the shutdown, at the same flow rate that was used before. All other parameters are as per the base case described in Table 6.1.

The maximum pressure experienced during the restart for each case is plotted in Table 6.13.

Table 6.13 Effect of shutdown date on maximum restart pressure

Shutdown Date	Maximum Pressure Loss During Restart, kPa
May 1	8287
July 15	5216
September 30	3928
December 30	5802
March 30	8832

The pressure and temperature from one day before the shutdown to two days after it are plotted in Figure 6.22.

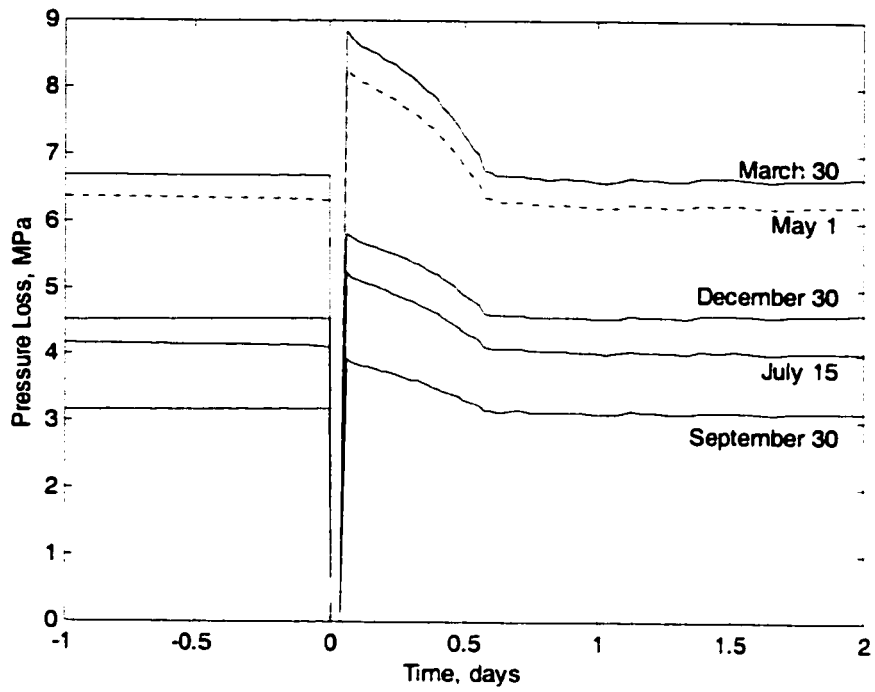


Figure 6.22(a) Effect of shutdown date on pressure

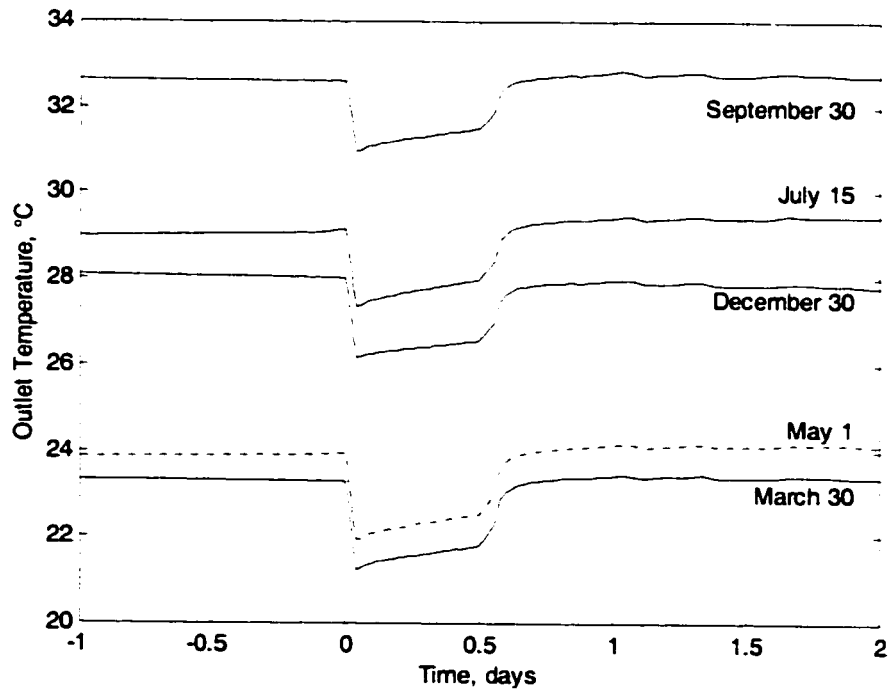


Figure 6.22(b) Effect of shutdown date on temperature

During the shutdown, the pressure loss is clearly zero, as there is no flow. The temperature in the pipeline drops quite quickly (only shown is the temperature at the end of the pipeline—the temperature throughout the pipeline will also drop). The plateau in outlet temperature in each case (and the associated decrease in pressure loss) corresponds to the period in which the hot oil entering the pipeline after the restart is displacing the oil which had cooled off in the pipeline. In each case, there is a spike in pressure after the restart. The increase in restart pressure above the regular operating pressure increases as the regular operating pressure increases (which is due only to the ambient temperature—i.e., related to the time of year). In late September, the restart pressure is only 0.75 MPa above the operating pressure, while in late March, the restart pressure is 2.14 MPa above the operating pressure.

6.2.2 Shutdown Length

As flow is stopped in the pipeline, the oil within it will cool off. If left indefinitely, it will cool to the temperature of undisturbed ground of the same depth. Shutdown lengths from a half hour to 12 hours were modelled. The maximum pressures during restart are shown in Table 6.14.

Table 6.14 Effect of shutdown length on restart pressure

Shutdown Length (hours)	Maximum Restart Pressure, kPa
0.5	7271
1	8287
2	10,598
4	16,417
6	24,210
12	57,812

The pressure and outlet temperature from 12 hours before to two days after the start of the shut down are plotted in Figure 6.23.

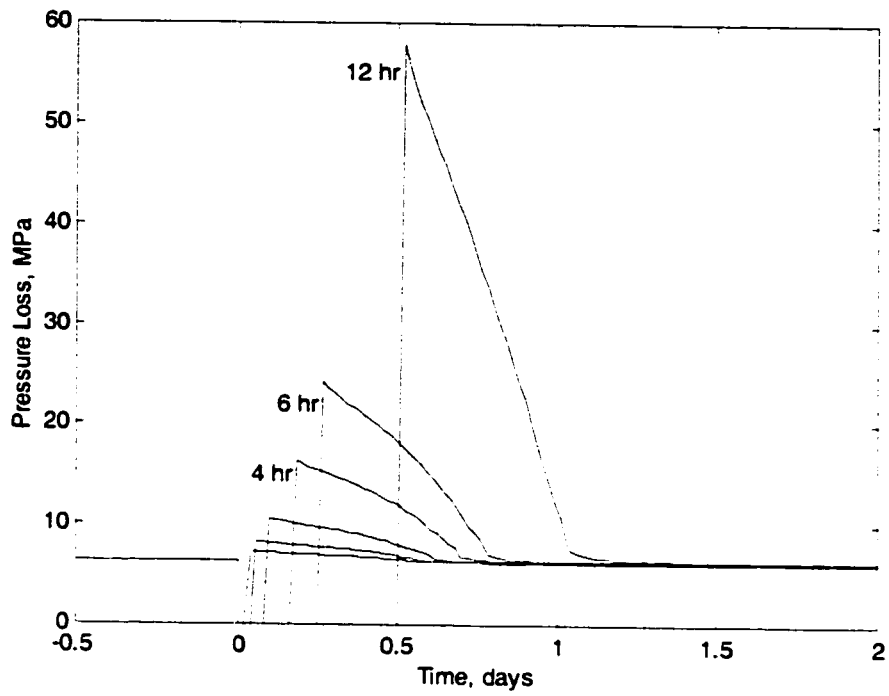


Figure 6.23(a) Effect of shutdown length on pressure

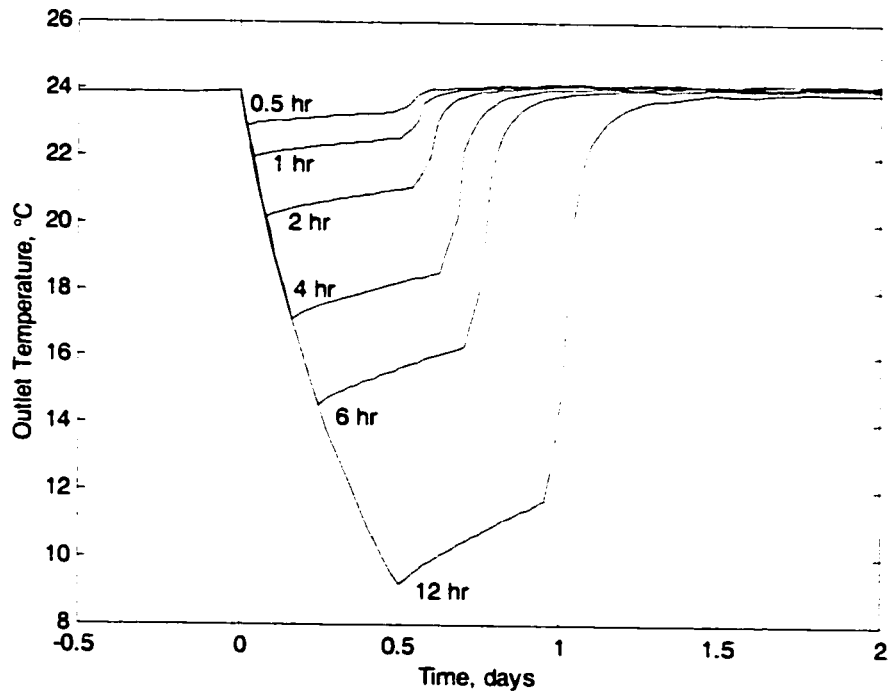


Figure 6.23(b) Effect of shutdown length on outlet temperature

As expected, the longer the shutdown lasts, the colder the oil in the pipeline, and the higher the restart pressure. It can be seen from Figure 6.23(b) that the temperature at the end of the pipeline drops throughout the length of the shutdown. If the shutdown were to last longer, this temperature would asymptotically approach approximately -4°C , the temperature of the ground far from the pipeline, at the pipeline depth, at this time of year. It is unlikely that a pipeline would be designed for a pressure of more than 10-20 MPa, so there would clearly be a problem with this pipeline if a shutdown were to last more than a couple of hours. This is when special restart procedures must be devised.

6.3 Parametric Studies in Varying Flow Rates

In each of the cases examined so far, the flow rate has been constant (with no water). In this section, cases will be examined which have varying flow rates of oil and water. It is assumed that the oil and water mix in an emulsion, as described in Section 2.1.3, with an inversion point of 60% water.

6.3.1 Increasing Oil Flow, No Water

A simulation was performed with the oil rate increasing from $10\text{ m}^3/\text{d}$ to $40\text{ m}^3/\text{d}$ over a two year period, with no water flow. The start date was May 1. The pressure loss, outlet temperature and flow rate are shown in Figure 6.24.

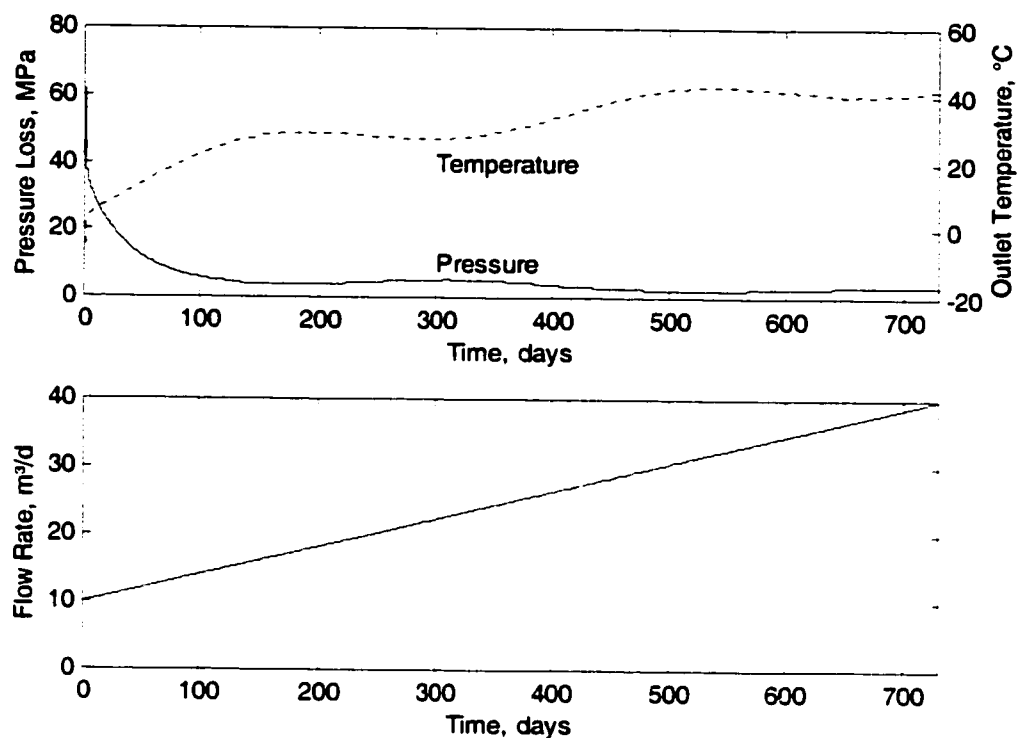


Figure 6.24. Pressure and temperature response to increasing oil rate

The start-up transient is extreme at the low flow rate (over 60 MPa). At low flow rates, even after the transient dies out, the pressure loss is still very high, but comes down as the flow rate increases. In the second year (when the flow rate is over 25 m³/d, the seasonal changes in outlet temperature and pressure loss become less severe.

6.3.2 Decreasing Oil Flow, No Water

The opposite case was also tested, where the oil flow decreased from 40 m³/d to 10 m³/d over two years, with no water flow. The start date was again May 1. The pressure loss, outlet temperature and flow rate are shown in Figure 6.25.

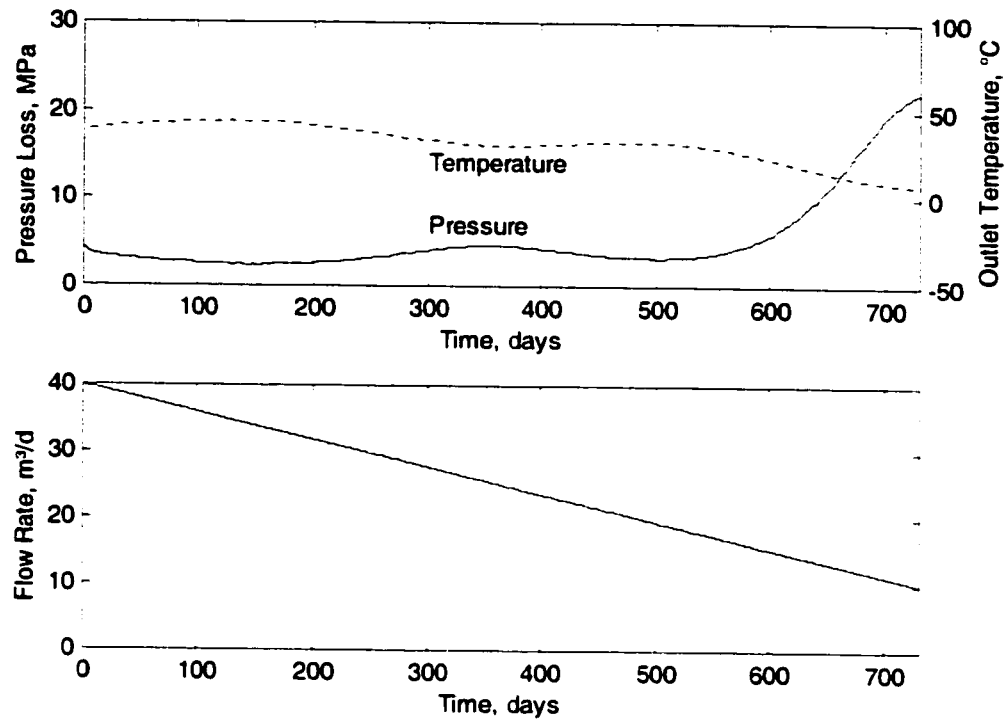


Figure 6.25 Pressure and temperature response to decreasing oil rate

At the higher flow rate, the pressure during the start-up transient is quite small (5800 kPa—compare this to the pressure at the same flow rate and time of year, but after the ground has warmed in the previous case: 3100 kPa), but as the flow rate decreases, the temperature decreases and the pressure increases (although there are still seasonal variations). At the end of the two year cycle, the pressure is 21.9 MPa (as compared to the pressure at the same flow rate and the same time of year in the previous case, but at start-up: 61.6 MPa).

6.3.3 Constant Flow Rate, Increasing Water Fraction

This case also was run for two years starting on May 1. The total flow rate was kept constant at 40 m³/d, but the water fraction was increased from 0 to 100%. Figure 6.26 shows the pressure loss, outlet temperature, and flow rates of water and oil over this period.

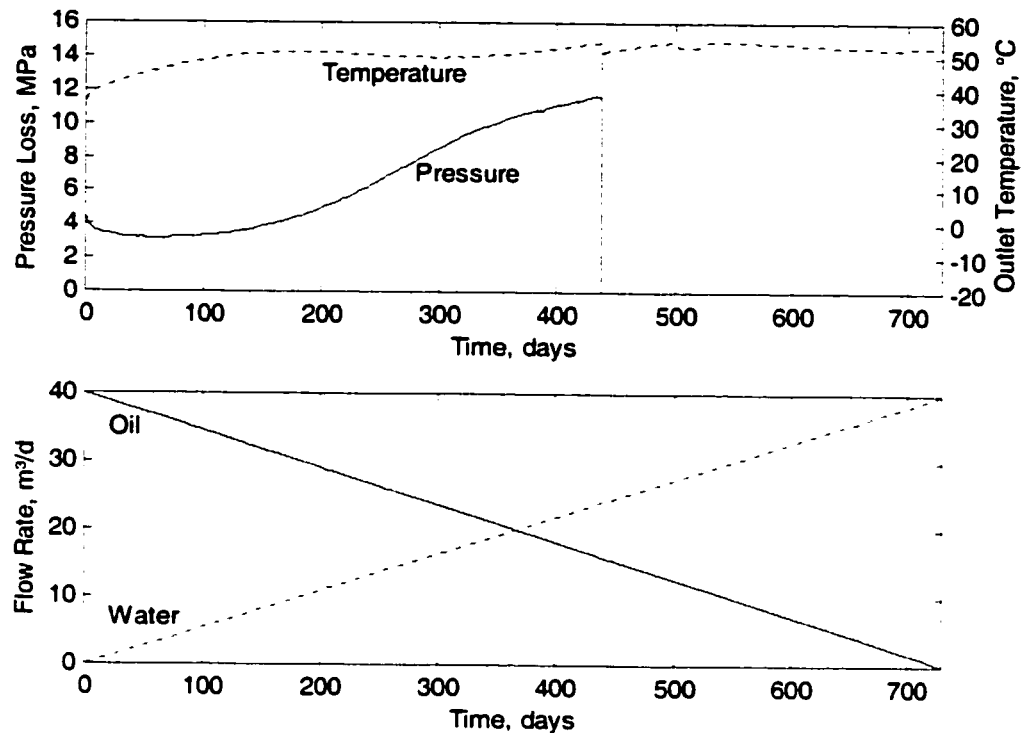


Figure 6.26. Response of pressure loss and temperature to changing water fraction

Due to the high flow rate at the start, the initial pressure transient is quite small (5700 kPa). While the pressure decreases somewhat as the start-up transient dies out and the ground warms up from seasonal effects, the pressure loss starts to increase significantly after about 65 days. This is not due to any temperature effect, but due to the effective viscosity of the emulsion increasing as the water fraction increases. This continues until the water fraction reaches the inversion point of 60%, at which time the emulsion becomes water-continuous, and the pressure loss is insignificant as compared to the oil-continuous emulsion (or even pure oil). There is a change in the thermal conditions at this point as well, since the heat transfer now occurs directly into water instead of into oil, and the flow becomes turbulent. This change causes a small transient in the outlet temperature, but the large thermal mass of the ground damps this out quite quickly.

6.3.4 Constant Flow Rate, Decreasing Water Fraction

This case also was run for two years starting on May 1. The total flow rate was kept constant at 40 m³/d, but the water fraction was decreased from 100% to 0%. Figure 6.27 shows the pressure loss, outlet temperature, and flow rates of water and oil over this period.

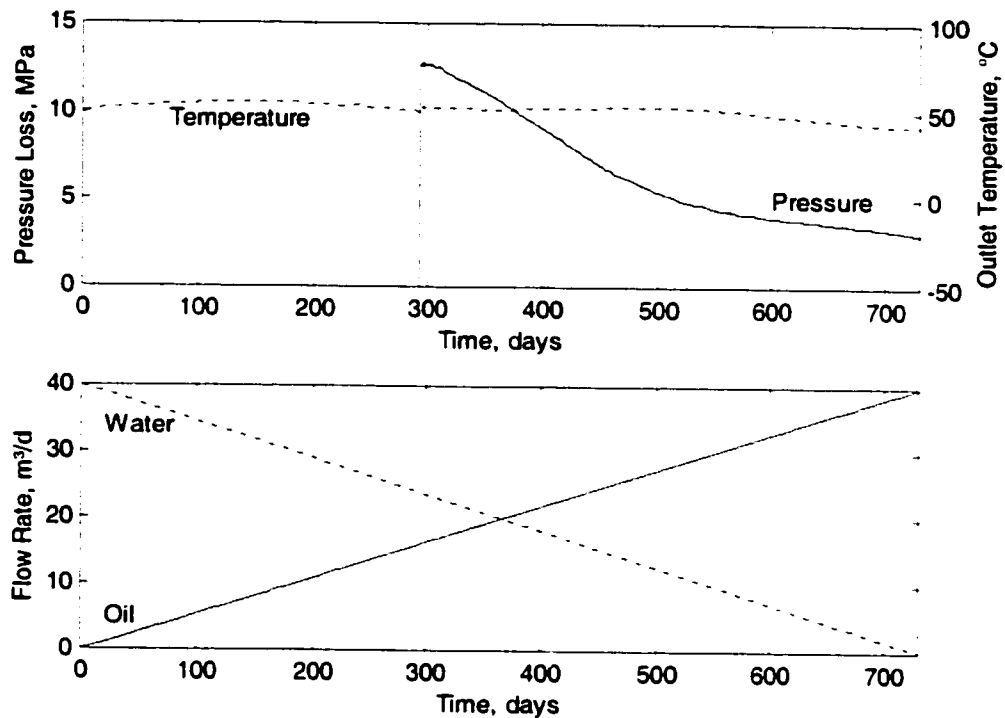


Figure 6.27 Response of pressure loss and temperature to changing water fraction

In this case the temperature very rapidly increases from the initial ground temperature to a near steady state value. There is no change in pressure, however, since the viscosity of the water is not considered to change with temperature in this model. The pressure loss is so low that it is not necessary to consider such small changes in viscosity. The pressure loss does increase slightly in the first period as the discrete phase (oil) increases in concentration. This is not evident in the figure, as the scale is set to show the large pressure losses when the oil is the continuous phase. After the inversion point is reached, the pressure becomes very

large due to the very high viscosity of the water-in-oil emulsion. The temperature changes during the seasons are of less importance to the overall pressure loss than the change in emulsion concentration and viscosity.

It should be recognized that heavy oils will often not tend to form emulsions with water. This is especially true if they are pumped with progressing cavity pumps, which have an inherently low internal shear rate. Therefore the pressure losses shown in Figures 6.26 and 6.27 are likely overly pessimistic. The oil and water would more likely flow in large droplets; the pressure losses for these flows are less well understood.

7. Discretization in Finite Difference Model

The finite difference model described previously contains the following regions, as was shown in Figure 2.1.:

- Pipe
- Insulation
- Ground

Each of these regions is discretized into a group of nodes. The nodes are arranged in layers. Each layer, in each region, must have the same number of nodes. Furthermore, the time domain is also discretized. The discretization of the spatial and time domains are described by the following parameters:

- Nrp The number of layers of nodes in the pipe
- Nri The number of layers of nodes in the insulation
- Nalf The number of layers of nodes in the ground
- Nang The number of nodes in each layer
- Δt The length of the time step

The accuracy of the model is in part determined by these parameters. Increasing the number of nodes and decreasing the size of the time step, is expected to, in general, increase the accuracy of the model at the expense of increasing the amount of storage space required and the amount of time required to perform a simulation.

An analytical model for the full system does not exist, so it is not possible to compare the results obtained with this model to a known correct solution. It is possible, however, to develop a steady state analytical solution. The results obtained below were obtained by running a simulation of five years of pipeline operation. Only one segment of pipeline was used (at the inlet, where the temperature gradients are the most severe). The surface temperature is kept constant—no seasonal variations, as these are not considered in the steady state

solution. For the purposes of this comparison, the fluid is considered not to change in temperature. This assumption is not used in the full model, but is necessary here so that the steady state case is not a function of the size of the time step.

The properties used are listed in Table 7.1.

Table 7.1 Properties used in steady state comparison

Pipe Density	7800 kg/m ³
Pipe Thermal Conductivity	60 W/m·K
Pipe Specific Heat	400 J/kg·K
Insulation Density	190 kg/m ³
Insulation Thermal Conductivity	0.04 W/m·K
Insulation Specific Heat	1000 J/kg·K
Ground Density	2000 kg/m ³
Ground Thermal Conductivity	0.5 W/m·K
Ground Specific Heat	1800 J/kg·K
Fluid Convective Coefficient	4 m
Pipe ID	0.08 m
Pipe OD	0.1 m
Pipe Burial Depth	1.2 m
Insulation OD	0.2 m
Surface Temperature	2 °C
Fluid Inlet Temperature	70 °C

It would be expected that if this type of simulation is run for a sufficiently long time, the temperature profiles in the ground should approach those in a steady state case, which can be calculated analytically. Five years was estimated to represent a sufficient length of time.

Figure 7.1 shows the standard error of the result over a period of time for a case where $N_{rp} = 10$, $N_{ri} = 10$, $N_{alf} = 10$, $N_{ang} = 10$, and $\Delta t = 0.1$ days. The standard error (here and elsewhere in this chapter, and in Chapter 8) was calculated as follows:

$$StdErr = \sqrt{\frac{\sum_{i=1}^n (T_i - T_{st})^2}{n}} \quad (7.1)$$

Where:

T_i is the temperature at each node

T_{st} is the steady state temperature at each node

n is the number of nodes

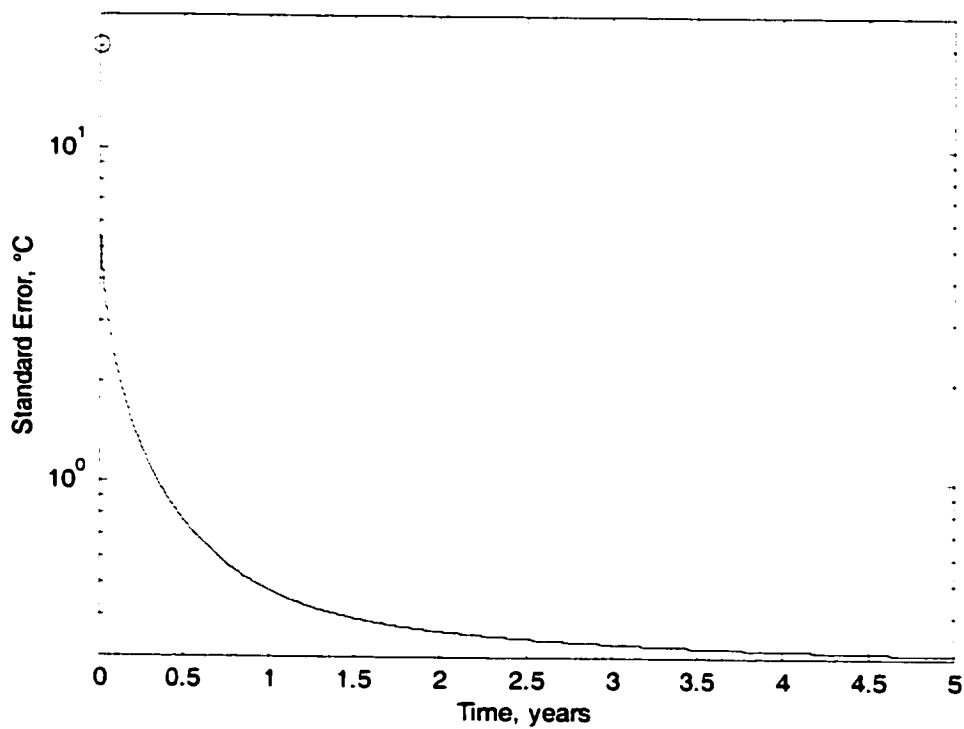


Figure 7.1 Error over time

The figure clearly shows that the changes in temperature have levelled off by about three years of simulation; the use of five years as a comparison time is therefore justified. In this case, the standard error starts at 20.3°C, and is 0.31°C after five years.

7.1 Effects of Varying Spatial Discretization

In each of the calculations represented by the figures in this section, one of the discretization parameters (N_{rp} , N_{ri} , N_{alf} , N_{ang}) was varied. The other parameters were all set to either $N=5$, $N=10$, or $N=15$, depending on the case (as illustrated in the figures). The time step in all cases was 0.1 days.

Figure 7.2 shows the effect of varying the number of layers of nodes in the pipe wall.

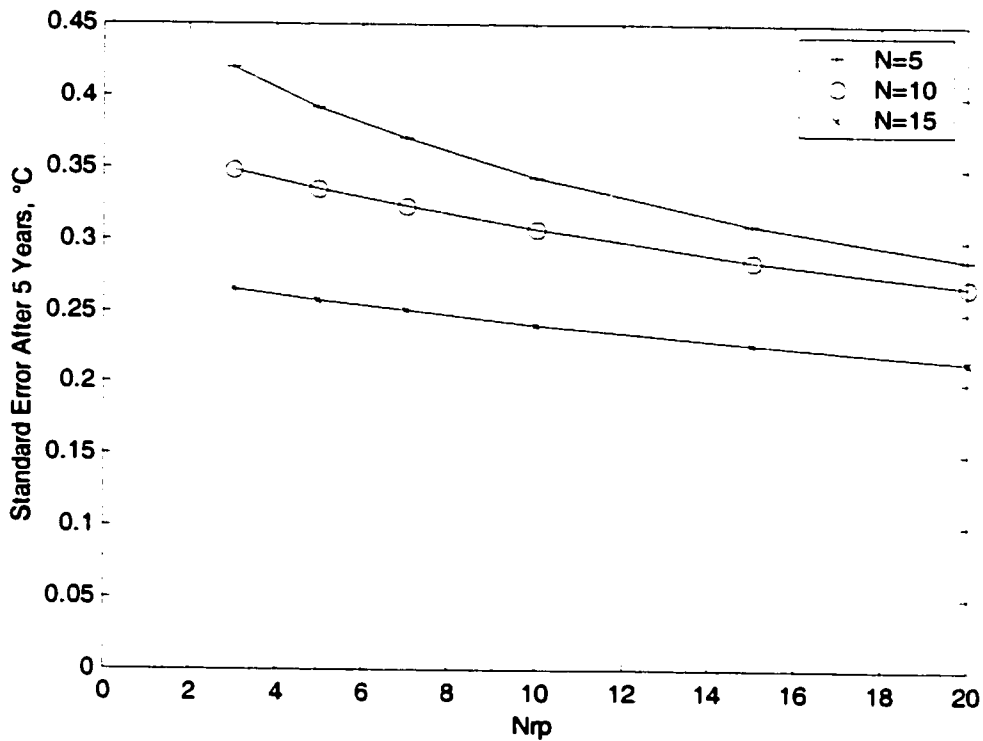


Figure 7.2 Effect of varying the number of layers of nodes in the pipe wall

As the both the overall discretization ($N=5$ to $N=15$) and the number of layers in the pipe increase, the accuracy of the model improves.

Figure 7.3 shows the effect of varying the discretization in the insulation.

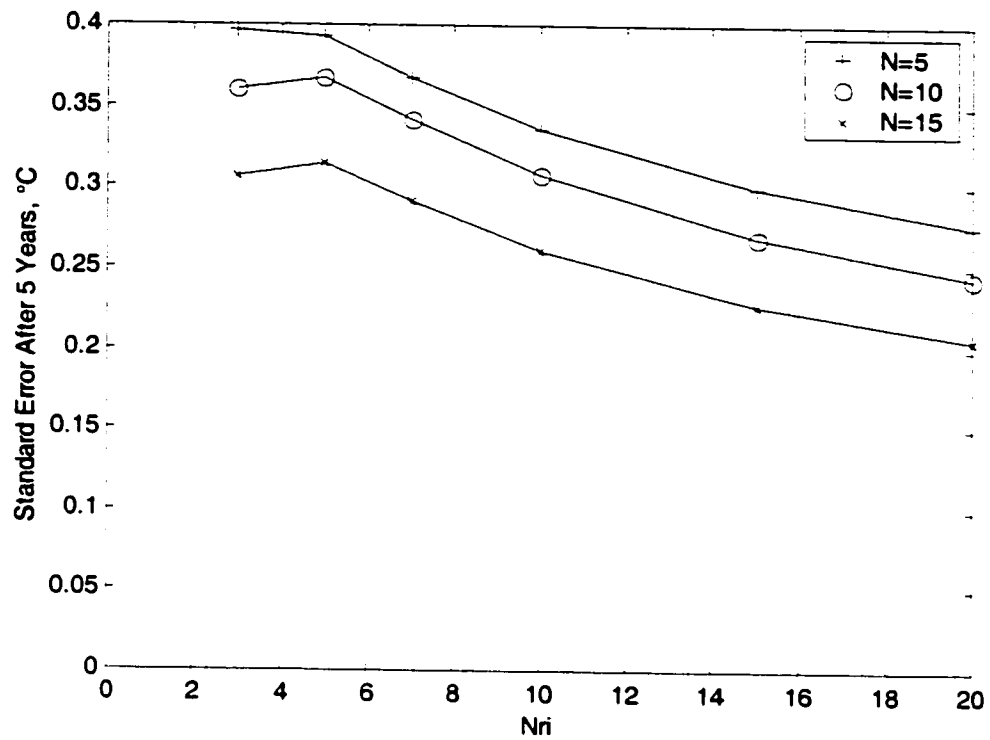


Figure 7.3 Effect of varying the number of layers of nodes in the insulation

A similar behaviour is evident in the insulation: in general, as the number of nodes increases the accuracy increases.

Figure 7.4 shows the effect of varying the discretization in the ground.

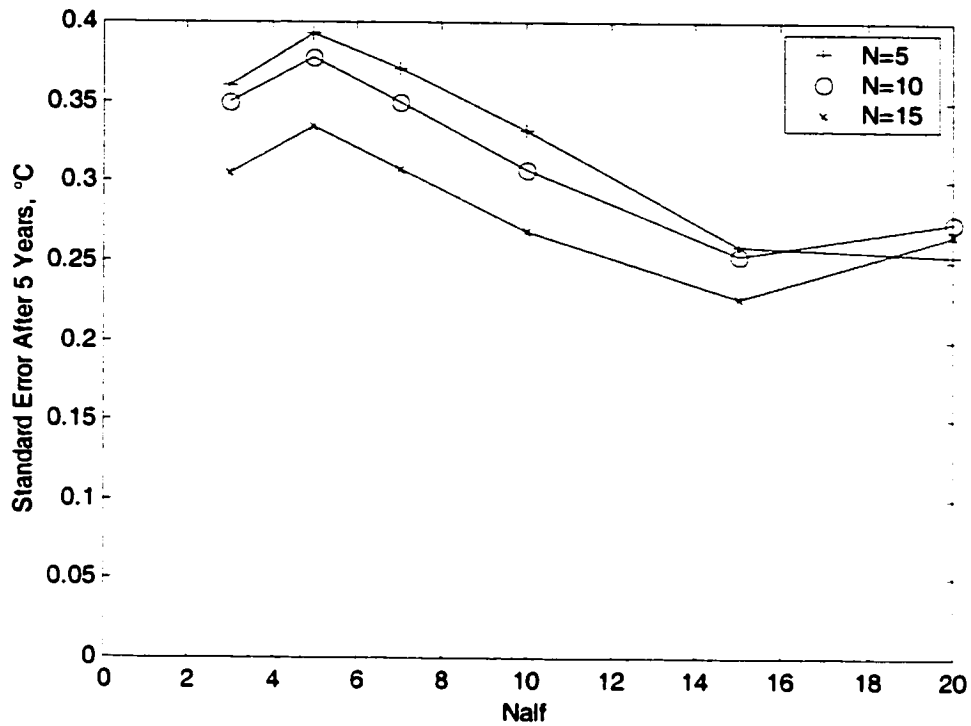


Figure 7.4 Effect of varying the number of layers of nodes in the ground

Again, in general, the accuracy increases with the number of nodes. The variation in this for very low and very high numbers of nodes is due to the way the discretization of the transformed coordinate system works. As α and β tend toward zero, the corresponding node location in the Cartesian plane tends towards infinity. As more discretization is used, the smallest non-zero values of α and β get smaller, and the corresponding node gets further and further from the pipe. The error shown is simply due to the fact that five years of simulation was insufficient to reach a steady state for a node that far from the pipe. (The reduced error for three layers of nodes is because the five years of simulation time allowed the furthest node to get closer to a steady state.)

Figure 7.5 shows the effect of varying the number of nodes in each layer (in the pipe wall, insulation, and ground—all of which must have the same number of nodes in each layer).

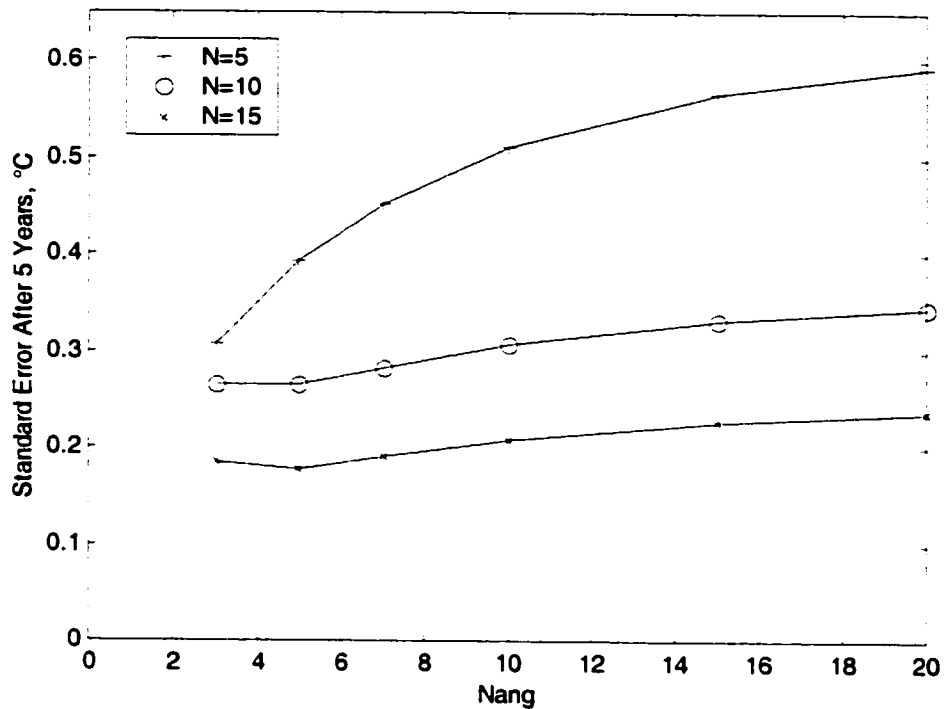


Figure 7.5 Effect of varying the number of nodes in each layer

The evident decrease in accuracy with increased numbers of nodes in each layer is due solely to the effect described above for the discretization in the ground. In a true steady state, there would be no gradients within any of the layers of nodes, and the number of nodes in each layer would therefore be irrelevant. The effect in the figure above is simply due to the fact that a true steady state is not reached; the higher the level of discretization, the less close the solution approaches to a steady state.

The evident inaccuracies with increasing discretization in the ground, as evident in Figures 7.4 and 7.5 should not be construed to imply that a small number of

nodes should be used. These represented steady state or near steady state solutions; the thermal gradients in a transient simulation would be more severe (particularly within each layer of nodes), and increased numbers of nodes would be required to capture these.

7.2 Effects of Varying Time Step

The simulation over five years was performed using a number of different time steps. This was done with all the spatial discretization parameters at either $N=5$, $N=10$, or $N=15$.

Figure 7.6 shows the effect of changing the time step.

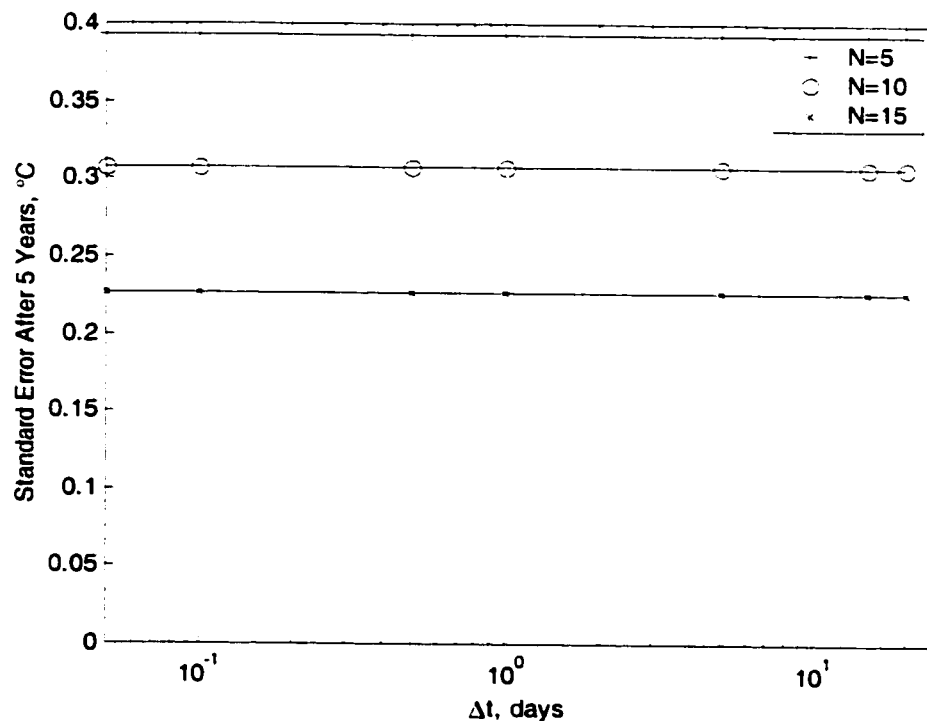


Figure 7.6 Effect of varying the time step.

The size of the time step has essentially no effect on the results after five years. The maximum range in the standard error for any of the three levels of discretization covers 0.00028°C over the range of time steps tested. This is not surprising—it should be expected that the time step will be irrelevant in arriving

at a steady state solution. Like the number of nodes per layer, discussed above, the time step will be significant in affecting the accuracy of a transient solution.

7.3 Effect of Time Step in a Transient Calculation

No analytical solution is available for the complete case. It is assumed that the most accurate solution is the one with the smallest time step. Results with other time steps were compared to it. The system is described by the properties listed in Table 7.1. The spatial discretization were: $N_{rp} = 4$; $N_{ri} = 15$; $N_{alf} = 10$; $N_{ang} = 8$. The time steps used were: 0.005, 0.1, 0.25, 1, 5, 10, 15 days. The simulation will cover the first six months, when the temperatures are making the most significant changes. Figure 7.7a shows the results over six months, while Figure 7.7b shows the results in the first 2 days. The error is plotted for the time steps greater than 0.005 days relative to the results obtained using a time step of 0.005 days.

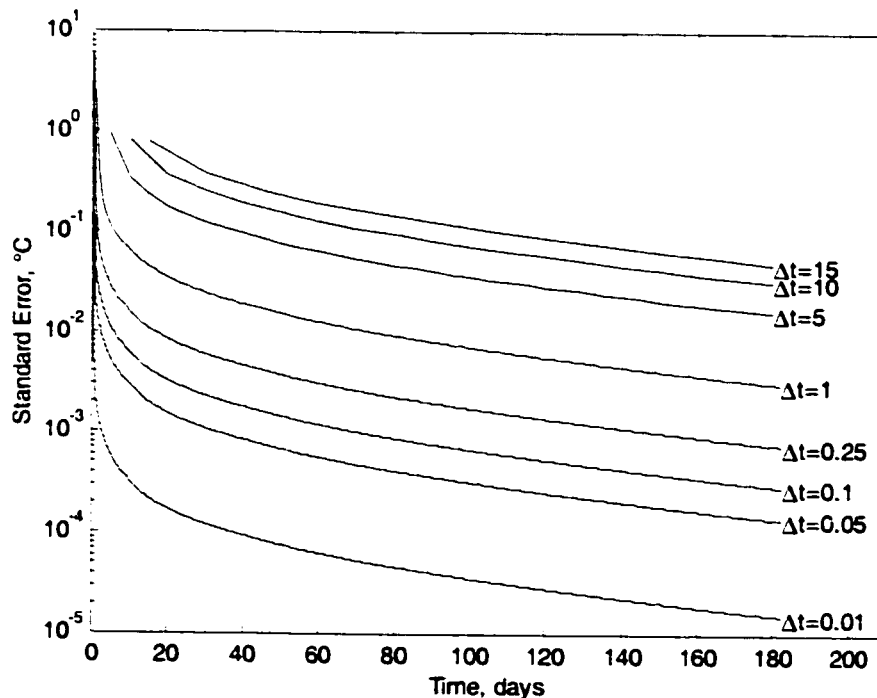


Figure 7.7(a) Effect of time step (in days) in transient calculation

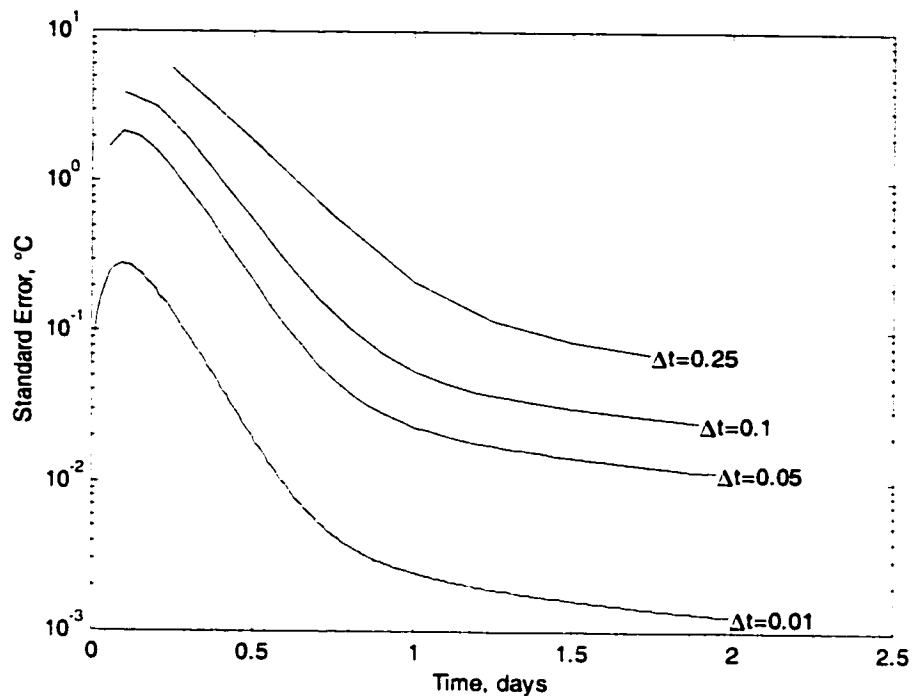


Figure 7.7(b) Effect of time step (in days) in transient calculation

As the time step decreases toward 0.005 days, the results appear to converge. As expected, the error relative to result at a time step of 0.005 day decreases with time (with one exception very early in the 0.01 day time step case). After five years of simulation, the results for all time steps would converge to essentially the same result, as was shown previously. In general, it seems that the error decreases by two orders of magnitude in the first day of simulation for time steps smaller than one day. For larger time steps, the decrease in error is more gradual. For the given case, a time step of five days gives reasonable results except for the first 40-50 days of operation, after which the standard error is less than 0.1°C. Earlier, however, it is important to have a smaller time step to capture the rapidly changing thermal conditions in the ground. This is especially true if it is considered important to know the maximum pressure during start-up if no special procedures (e.g., preheat) are used. A variable time step would be of great value in achieving both the goals of high accuracy and fast computation.

8. Finite Element Modelling of Transient Heat Transfer in Two Dimensions

The prime advantage of a finite element model over a finite difference model is its adaptability to complex geometries and regions with different physical properties. In the buried pipe problem, the pipe and insulation can be represented well using finite differences, as can the ground, but the interface between these two regions cannot be represented as well, as the two coordinate systems do not match up exactly. Also, the node structure used in the finite difference model in the ground cannot represent the frost depth very accurately (if a more advanced model—considering phase change of moisture within the ground—is used). It is also difficult to represent ground of different properties (e.g. backfill around a pipeline), or alternative configurations, such as two pipes in the same trench. One company even tried placing a layer of flat, rigid insulation a short distance above an uninsulated pipe. A finite element model could be used to calculate heat losses in such a geometry. For these reasons, a finite element model is investigated here.

The goal of the work presented here is to establish that the finite element method can be used to calculate the rate of heat transfer from a buried pipe, and to some extent to show that the finite difference solution derived in Chapter 4 gives results that can be verified by a different method. There are certainly more accurate methods of implementing the finite element method (e.g. by using higher order elements) which are not covered here.

8.1 Description of Finite Element Method for Calculating Heat Conduction

All the finite elements used in this model are linear triangular elements (which obviously have three nodes each). Linear triangular elements were chosen for their simplicity. It is recognized, however, that other element types, such as linear quadrilaterals, or quadratic (or even cubic) triangles or quadrilaterals, would provide increased accuracy with the same number of nodes. (The calculation time

at each time step is highly dependent on the number of nodes, not the number of elements, in general.)

All the work in this chapter assumes that the thermal conductivity is isotropic, and that the nodes are arranged in a counter clockwise fashion in each element. The element matrix for this type of element [34, 35] is:

$$K^e = k \begin{bmatrix} K_{11} & K_{12} & K_{13} \\ K_{21} & K_{22} & K_{23} \\ K_{31} & K_{32} & K_{33} \end{bmatrix} \quad (8.1)$$

Where:

$$K_{12} = K_{21} = \frac{1}{4A} [(x_3 - x_2)(x_1 - x_3) + (y_2 - y_3)(y_3 - y_1)] \quad (8.2)$$

$$K_{22} = \frac{1}{4A} [(x_1 - x_3)^2 + (y_3 - y_1)^2] \quad (8.3)$$

$$K_{13} = K_{31} = \frac{1}{4A} [(x_3 - x_2)(x_2 - x_1) + (y_2 - y_3)(y_1 - y_2)] \quad (8.4)$$

$$K_{23} = K_{32} = \frac{1}{4A} [(x_1 - x_3)(x_2 - x_1) + (y_3 - y_1)(y_1 - y_2)] \quad (8.5)$$

$$K_{33} = \frac{1}{4A} [(x_2 - x_1)^2 + (y_1 - y_2)^2] \quad (8.6)$$

The global matrix is assembled from the element matrices for each element. There is one row and column for each node in the system.

To solve a steady-state system, the equation to be solved is:

$$[K]\{T\} = \{F\} \quad (8.7)$$

Where T represents the temperatures at each node, and F represents flux at each node.

In transient analysis, one more matrix is required to represent the heat capacity of the material. For linear triangular elements [34, 35], this is:

$$M = \frac{\rho c A}{12} \begin{bmatrix} 2 & 1 & 1 \\ 1 & 2 & 1 \\ 1 & 1 & 2 \end{bmatrix} \quad (8.8)$$

The system matrix for M is assembled in the same way as for K . The equation to be solved at each time step is now:

$$[M] \{\dot{T}\} + [K] \{T\} = \{F\} \quad (8.9)$$

There are several ways of calculating this, depending on how the time derivative is calculated. Three simple ways of calculating this derivative are forward difference, backward difference, and Crank-Nicholson. If the forward difference is used, the time step must be below a certain value, or the system will be numerically unstable. Both the other methods are unconditionally stable. The backward and forward difference methods have a global truncation error of order $O(\Delta t)$, while the global truncation error of the Crank-Nicholson method is of order $O(\Delta t^2)$. Since the Crank-Nicholson method is of a higher order than the others (and therefore can be expected to result in greater accuracy for the same time step) and is unconditionally stable, its use is preferable. The equation to solve [34] is then:

$$(2[M] + \Delta t [K]) \{T\}^{n+\Delta t} = \Delta t (\{F\} + \{F\}^{n+\Delta t}) + (2[M] - \Delta t [K]) \{T\}^n \quad (8.10)$$

Note that in cases where the boundary conditions are all of the first kind (i.e., specified temperature), the F vector is irrelevant. Its values are 0 away from the boundaries, and while its values are unknown at the boundaries, these rows of the calculation matrix are overridden by the fixed temperature boundary conditions.

8.1.1 Steady State Conduction with only Fixed Temperature or Adiabatic Boundaries

The simplest case is calculating a steady state temperature distribution, where all the boundaries are either adiabatic (no heat transfer at all), or held at a constant temperature. In this case, the solution is:

$$[K]\{T\} = \{F\} \quad (8.11)$$

The F vector is zero for all internal nodes and any nodes on the adiabatic boundaries. It is one for all constant temperature nodes. The K matrix is modified: rows representing nodes with constant temperature boundaries are filled with zeros, except for a one on the diagonal.

8.1.2 Steady State Conduction with Fixed Temperature, Adiabatic or Convective Boundaries

The addition of a convective boundary adds some complications. The basic equation to be solved is very similar:

$$[K']\{T\} = \{F\} \quad (8.12)$$

Where:

$$[K'] = [K] + [K_h] \quad (8.13)$$

The K_h matrix is constructed from elemental matrices [35] of the form:

$$[K_h] = \frac{hl}{6} \begin{bmatrix} 2 & 1 & 0 \\ 1 & 2 & 0 \\ 0 & 0 & 0 \end{bmatrix} \quad \text{or} \quad [K_h] = \frac{hl}{6} \begin{bmatrix} 0 & 0 & 0 \\ 0 & 2 & 1 \\ 0 & 1 & 2 \end{bmatrix} \quad \text{or} \quad [K_h] = \frac{hl}{6} \begin{bmatrix} 2 & 0 & 1 \\ 0 & 0 & 0 \\ 1 & 0 & 2 \end{bmatrix}$$

(8.14a, 8.14b, 8.14c)

Depending on which side of the element is exposed to convection, and where l is the length of that side. Additionally, the F vector is comprised from elemental vectors[35] of the form:

$$\{F\} = \frac{hT_f l}{2} \begin{Bmatrix} 1 \\ 1 \\ 0 \end{Bmatrix} \quad \text{or} \quad \{F\} = \frac{hT_f l}{2} \begin{Bmatrix} 0 \\ 1 \\ 1 \end{Bmatrix} \quad \text{or} \quad \{F\} = \frac{hT_f l}{2} \begin{Bmatrix} 1 \\ 0 \\ 1 \end{Bmatrix}$$

(8.15a, 8.15b, 8.15c)

Once the K matrix and F vector have been built to consider the convective boundaries, as described here, the constant temperature nodes are considered. The rows of the K matrix corresponding to these nodes are filled with zeros, except for a one on the diagonal, and the F vector is set to the specified surface temperature for those nodes.

8.1.3 Transient Conduction with only Fixed Temperature or Adiabatic Boundaries

When there are only adiabatic and constant temperature boundaries, the basic equation to solve is:

$$(2[M] + \Delta t [K])\{T\}^{n+\Delta t} = (2[M] - \Delta t [K])\{T\}^n \quad (8.16)$$

This can be rewritten as:

$$[M']\{T\}^{n+\Delta t} = \{V\} \quad (8.17)$$

Where:

$$[M'] = 2[M] + \Delta t [K] \quad (8.18)$$

$$\{V\} = (2[M] - \Delta t [K])\{T\}^n \quad (8.19)$$

Note that the M' matrix is constant, while the V vector changes at every time step by multiplying the temperature vector by a constant matrix. The constant temperature boundary conditions are set by filling the corresponding rows of the M' matrix with zeros, except for a one on the diagonal. Additionally, after the V vector is constructed at each step, its values corresponding to the constant temperature nodes must be set to the temperature at those nodes. No further action is necessary for adiabatic boundaries.

8.1.4 Transient Conduction with Fixed Temperature, Adiabatic or Convective Boundaries

The basic equation to be solved in this case, assuming the temperature of any convective fluids and the corresponding convective coefficients do not change over the time step, is:

$$(2[M] + \Delta t [K'])\{T\}^{n+\Delta t} = 2\Delta t \{F\} + (2[M] - \Delta t [K'])\{T\}^n \quad (8.20)$$

This can be rewritten as:

$$[M']\{T\}^{n+\Delta t} = \{V'\} \quad (8.21)$$

Where:

$$[M'] = 2[M] + \Delta t [K'] \quad (8.22)$$

$$\{V'\} = 2\Delta t \{F\} + (2[M] - \Delta t [K'])\{T\}^n \quad (8.23)$$

The K' matrix and F vector are constructed as described above in Section 8.1.2. Once again, the M' is constant (if the convective coefficients do not change), and the V vector changes at each time step.

8.2 Verifying Validity of Finite Element Model

In verifying that the finite element method described above gives accurate results, it was necessary to compare results with cases for which the results are known analytically. This was done with two geometries. The first was a rectangular bar, on which two opposite edges were insulated, and the other two were either kept at a fixed temperature or exposed to convection (depending on the case, as described below). The second was a hollow cylinder, on which the two exposed surfaces were either kept at a fixed temperature or exposed to convection. Note that both of these cases are actually one-dimensional, although they were solved in two dimensions using the finite element model. Examples of the grids used each case are shown in Figure 8.1.

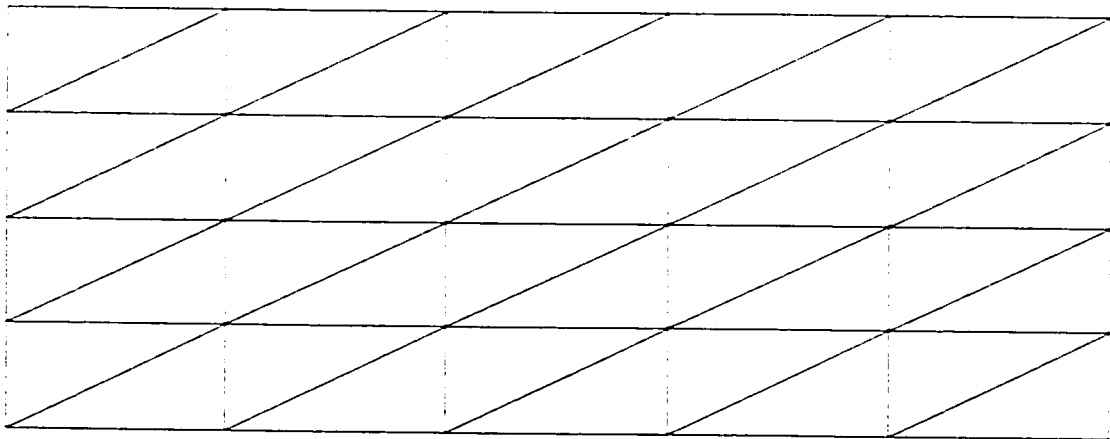


Figure 8.1(a) Sample grid on rectangular bar

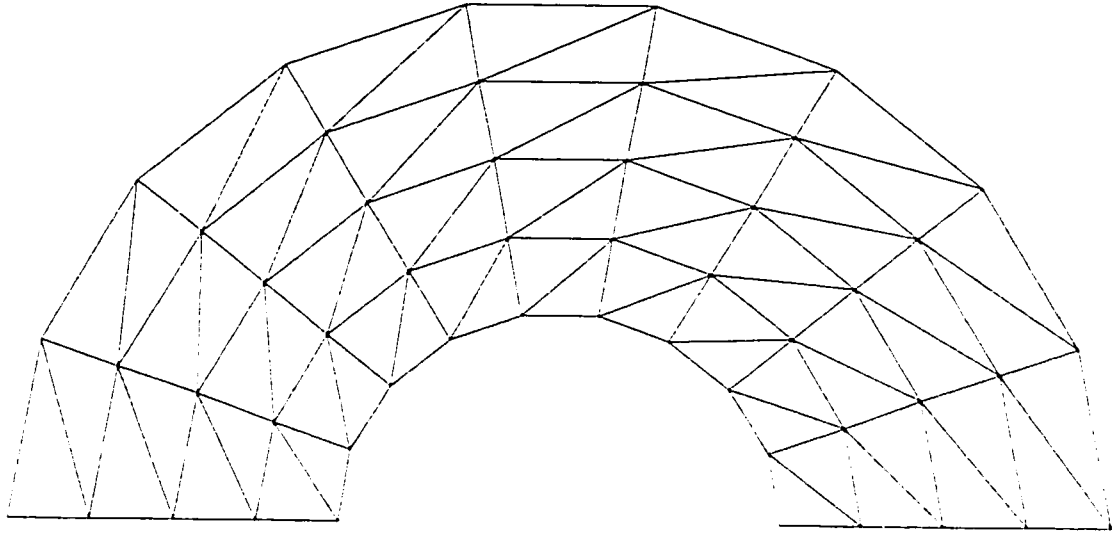


Figure 8.1(b) Sample grid on hollow cylinder

The top and bottom edges of the rectangle are considered to be insulated in all test cases below; the constant temperature or convective boundaries are on the left and right edges. The flat surfaces on the bottom of the half-cylinder are a plane of symmetry, and are therefore considered to be adiabatic. The constant temperature or convective boundary conditions are applied on the inner and outer radial surfaces.

8.2.1 Steady State, Constant Properties, Constant Temperature Boundaries

In this case, the two geometries (bar and hollow cylinder) were given constant temperature boundary conditions, and the steady state problem was solved.

The error in the FEM results for the bar, as compared to analytical results, was zero (within machine precision). This is because the temperature distribution in that case is linear; the linear triangular elements can capture this exactly, even when there are very few elements. The results for a test case are illustrated in Figure 8.2. The test case here was a bar 5 metres long (x direction) and 2 metres wide (y direction), with a thermal conductivity of $5 \text{ W/m}\cdot\text{K}$. At $x = 0$, it is forced

to 5°C and at $x = 5$, it is forced to 20°C. When the number of nodes in one direction was varied, there were 8 nodes in the other direction.

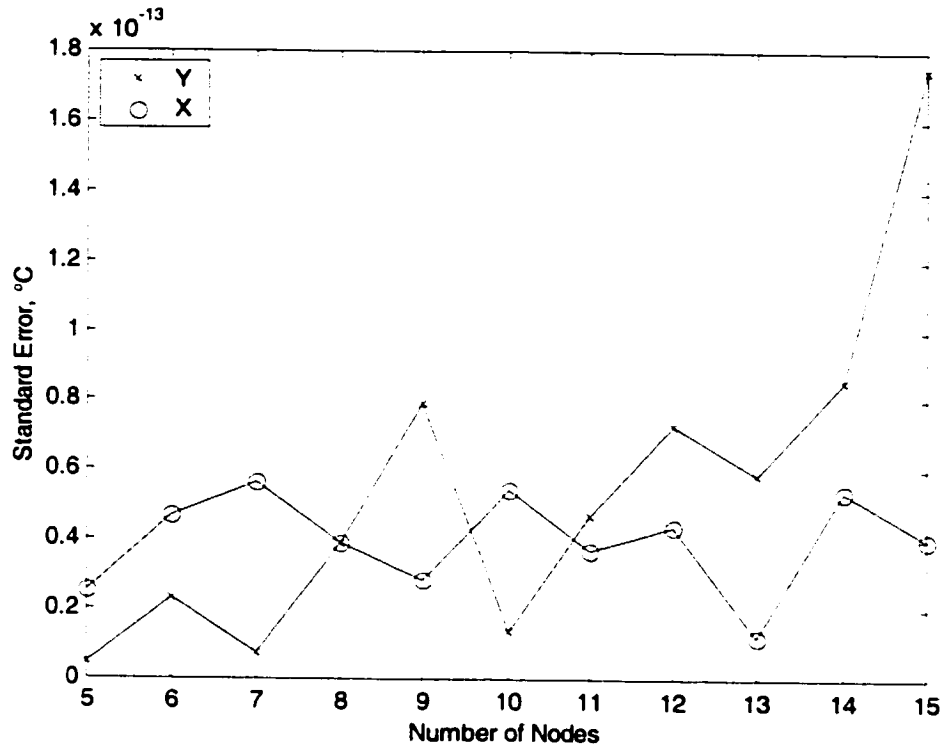


Figure 8.2. Effect of varying number of nodes on steady state calculation of steady state temperature in a bar

The error is not exactly zero, due to the constraints of performing numerical calculations with finite precision. It is, however, fourteen orders of magnitude less than the temperature values in the bar.

The temperature distribution in the cylinder, however, follows a logarithmic distribution with radius [21], so linear elements do not capture it exactly. The more elements in the radial direction, the higher the accuracy. The number of elements in the angular direction, however, has no effect on the accuracy of the results (within the constraints of machine precision). This is shown in Figure 8.3. The test case here is a hollow cylinder with an inner radius of 2 metres, an outer

radius of 5 metres and a thermal conductivity of 5 W/m·K, forced to 5°C on the inner surface and 20°C on the outer surface. When the number of nodes in one direction was varied, there were 8 nodes in the other direction.

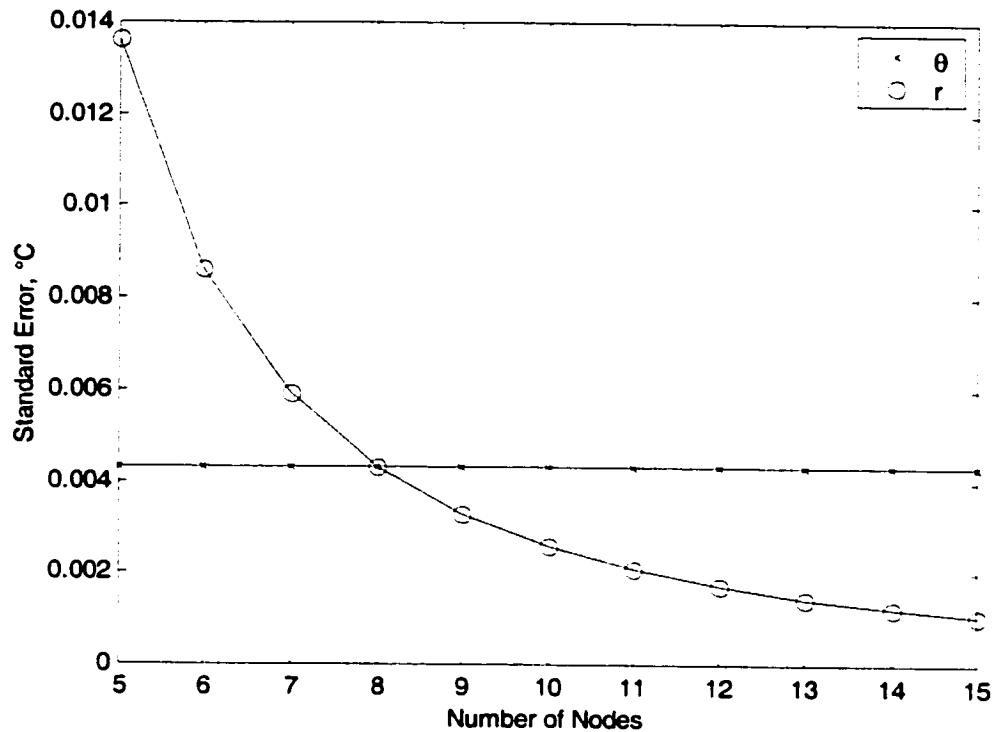


Figure 8.3 Effect of varying number of nodes on steady state calculation of steady state temperature in a hollow cylinder

The effect of element aspect ratio was also investigated. To test this, the solid bar case above was used. A constant number of nodes (eight in each direction) was used, and the length width of the bar were both changed from 0.005 metres to 5000 metres. While one dimension was changed, the other was constant at 5 metres. The results are plotted in Figure 8.4.

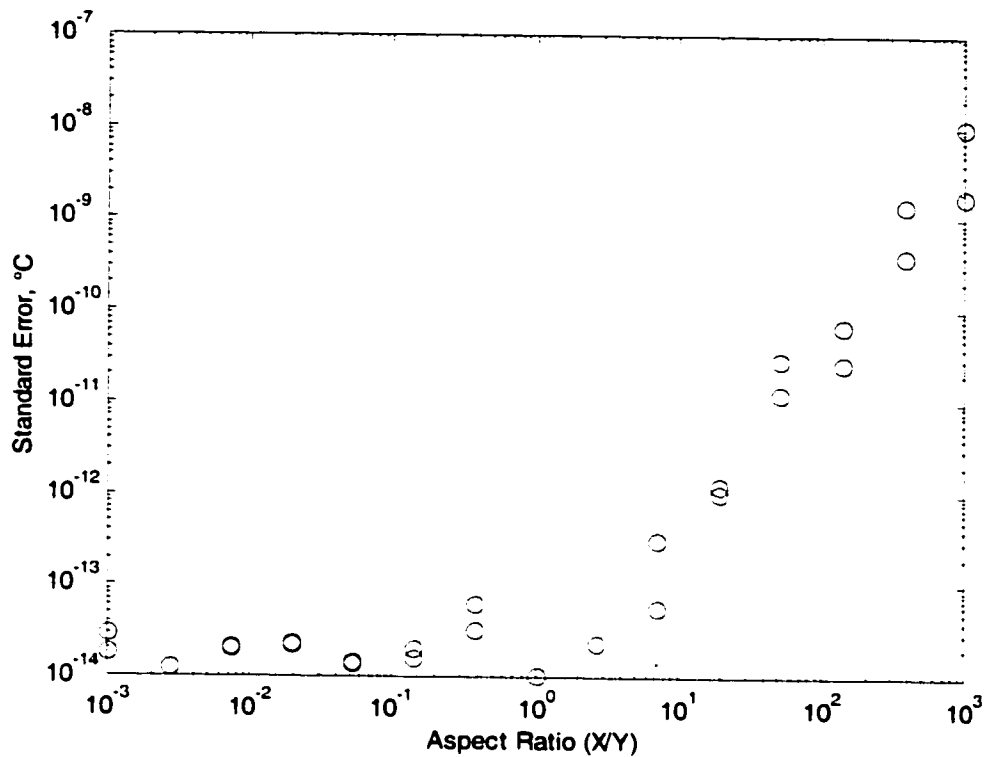


Figure 8.4 Effect of element aspect ratio

There are two points for each aspect ratio because, for example, when the length is 5000 and the width is 5, the aspect ratio is the same as when the length is 5 and the width is 0.005. All the error in these cases is due to numerical precision, but the effect of precision (e.g. truncation error) is dependent on factors such as the size of the elements. The minimum truncation error occurs at an aspect ratio of 1. As the aspect ratio increases in the X direction (the direction in which the temperature changes), the numerical error increases. While this indicates that it is desirable to avoid having elements with skewed shape (especially with the long direction in the direction of the change in temperature), it should be noted that even with an aspect ratio of 1000 to 1, the error is still ten orders of magnitude smaller than the temperature values in the bar. As the aspect ratio increases in a direction in which there is no thermal gradient, there is no effect on the accuracy.

8.2.2 Steady State, Constant Properties, Constant Temperature and Convective Boundaries

In this case, the two geometries are exposed to a constant temperature boundary at one surface and a convective boundary at the other. In the cylinder, it is the inner surface which is exposed to convection.

Once again, the temperature distribution in the bar is linear, so the number of linear elements has no effect on the accuracy beyond the constraints of machine precision. This is illustrated in Figure 8.5. This is the same test case used for the bar in Section 8.2.1, except that the boundary that was forced to 20°C is now exposed to a fluid at that temperature, with a convective coefficient of 3 W/m²·K.

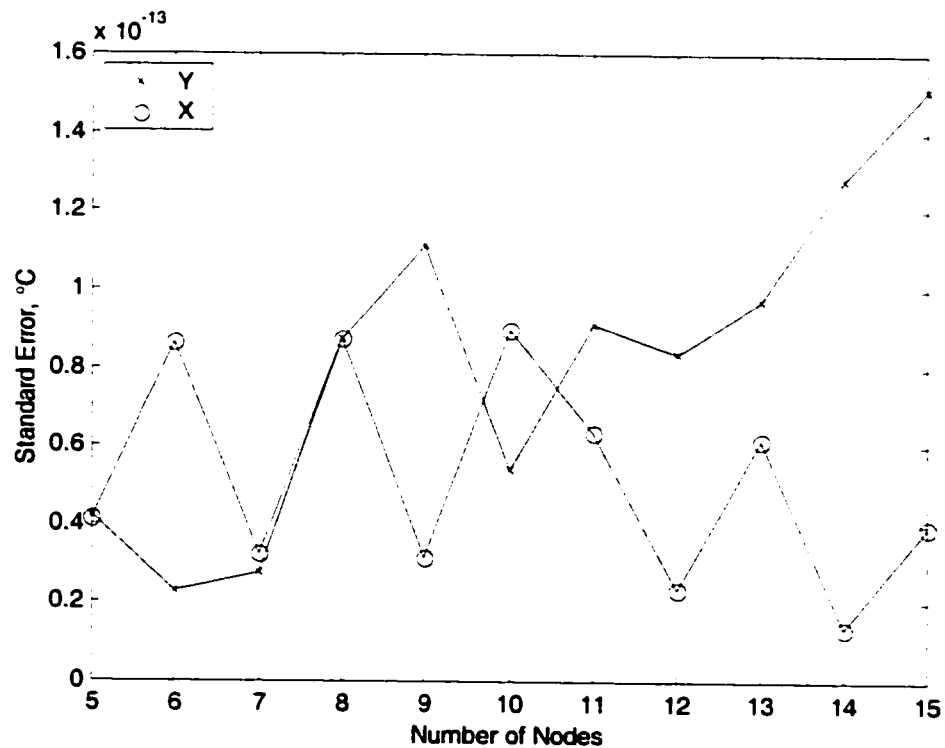


Figure 8.5 Effect of varying number of nodes on steady state calculation of steady state temperature in a bar

In the cylinder in this case, both the radial and angular discretization are important. The test case here was the same as was used for the hollow cylinder in Section 8.2.1, with the boundary that was forced to 20°C now exposed to a fluid

at that temperature, with a convective coefficient of $3 \text{ W/m}^2\text{-K}$. The results are illustrated in Figure 8.6.

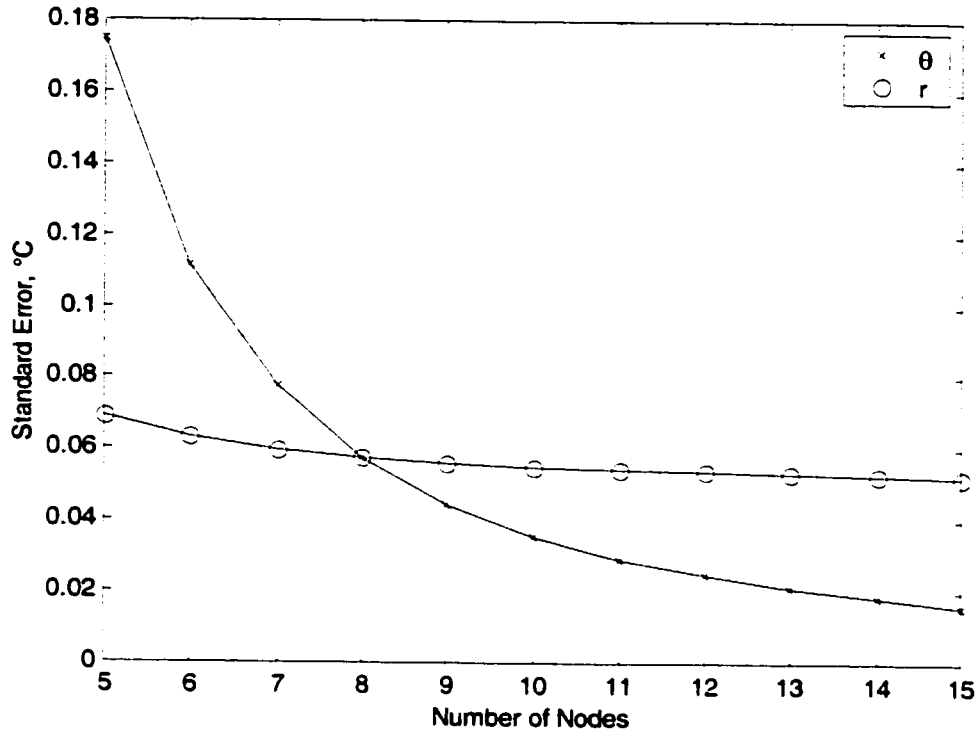


Figure 8.6 Effect of varying number of nodes on steady state calculation of steady state temperature in a hollow cylinder

As in the previous case, the more elements in the radial direction, the closer the linear elements can represent the logarithmic temperature distribution. The change in the error as the number of nodes is increased is about the same as the change exhibited with a constant temperature boundary condition. Unlike the previous case, the number of elements in the angular direction is now important (significantly more so than the number of nodes in the radial direction)—this is because the convection acts over an area, and when there are very few elements, the straight line approximation of the shape gives a poor estimate of the actual area on which the convection acts.

8.2.3 Steady State, Different Properties

Both the cylinder and bar were tested in cases where they were made up of two regions comprised of different materials. Both constant temperature and convective boundary conditions were used. The analytical steady state results were matched exactly in the bar case (within each region the temperature distribution is linear), and were matched as well in the cylindrical case as they were in the constant properties cases above. This implies that the finite element method can be successfully used to calculate the temperature distributions in composite materials. The assumption is that the boundaries between the different materials are modelled by the boundaries between different elements, so that each individual element represents only one material.

8.2.4 Transient, Constant Properties, Constant Temperature Boundaries

Analytical solutions are available for both the bar and hollow cylinder for the transient case. Both of these solutions are comprised of infinite series [28, 36]. Computers have inherent limitations in computing such series beyond a certain level of precision. For this reason, the accuracy of the analytical solution, as calculated by a computer, may not be as high as desired. This is especially true very early in the time scale of each case, when there are very extreme thermal gradients. A finite difference method was also compared to the analytical result in these cases, so that a benchmark would be available to help determine if the accuracy of the finite element model was acceptable. A sample case is illustrated in Figure 8.7.

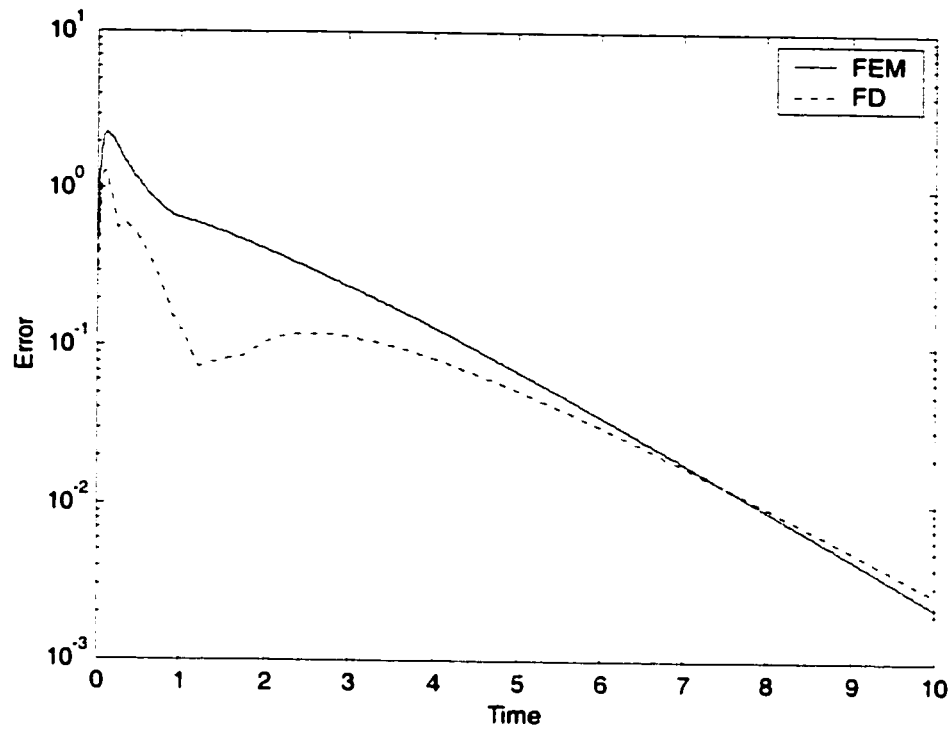


Figure 8.7 Accuracy of transient temperature calculation in bar

Early on, the finite difference model is somewhat closer to the analytical solution. Note that it is possible that the high error in both cases very early in the simulation is due to the computer's inability to calculate enough terms of the infinite series to a high enough level of precision—the analytical solution may actually be a significant source of error. As expected, as the temperature converges toward steady state the error gets smaller.

Figure 8.8 shows the accuracy for a sample case in the hollow cylinder.

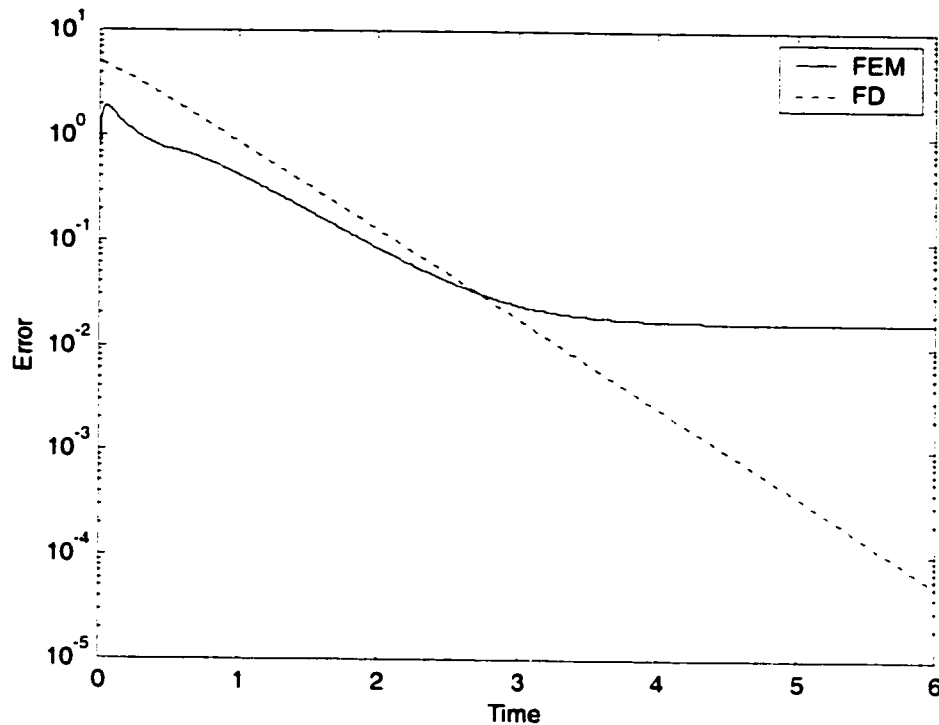


Figure 8.8 Accuracy of transient temperature calculation in hollow cylinder

Again, both solutions are reasonably accurate, and get more accurate as time increases (since the thermal gradients are reduced with time). The finite difference method, when derived without assuming very small discretization (Section 4.2.1.2), is capable of representing the exact steady state solution to this problem, so as time progresses, the error in the finite difference solution will decrease to the magnitude of machine precision (normally in the range 10^{-15} to 10^{-16}). The linear elements in the finite element method, as described above, cannot represent the exact steady state solution, however. In this case, the finite element method is actually more accurate than the finite difference method in the transient solution. This conclusion assumes that the error in these methods is significantly larger than the error in the calculation of the analytical solution. The validity of this assumption is not addressed here.

8.2.5 Transient, Constant Properties, Convective and Constant Temperature Boundaries

This case is done only with the bar, and not with the cylinder. A constant temperature is applied at one end of the bar, and the other is exposed to convection. The accuracy of each of the finite difference and finite element methods are shown for a sample case in Figure 8.9.

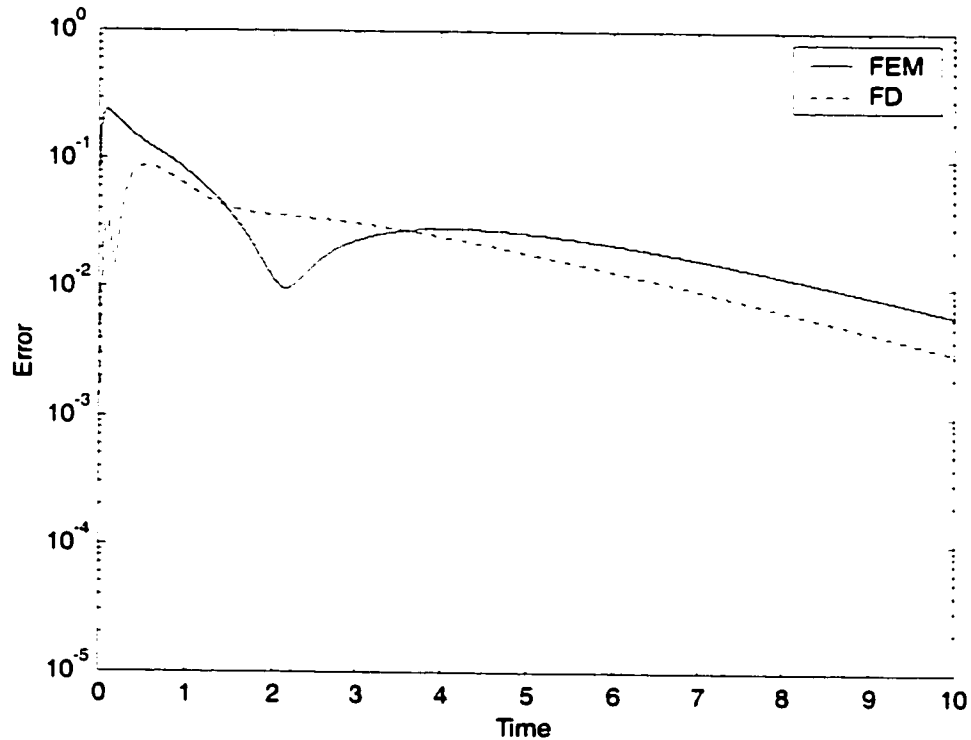


Figure 8.9 Accuracy of transient temperature calculation in bar with convection

Again, both methods give reasonable results. It is worth noting that the maximum error is not as high in this case as it was in the fixed temperature case. This is because the gradients are less severe in this case.

8.2.6 Discussion of Test Cases

The purpose of these test cases was to validate the finite element method for use in transient heat conduction problems with constant temperature and convective boundary conditions. In complicated cases, analytical solutions may not be

available. For this reason, certain cases were performed in steady state only. Other (simpler) cases were performed both steady state and transient. Two different geometries were tested, as well as regions with different properties. In every case, reasonable accuracy was achieved using the finite element method.

The results of these tests, as described above, give sufficient confidence to move on to testing the case of an insulated pipe buried in ground.

8.3 Finite Element Method Applied To Buried, Insulated Pipe

There are two significant problems with the finite difference method of calculating the temperature profile in the ground. First, it is inflexible. It does not allow for variations in geometry (e.g. a second pipe) or in ground properties (e.g. backfill, or freezing of moisture). Secondly, an approximation is applied in connecting the radial and transformed grid systems together. The finite element method can alleviate both these problems.

8.3.1 Grid Construction

Two simple grid structures were investigated. A more advanced method would use complicated grid generation schemes, perhaps even using grid refinement to more accurately capture areas with high thermal gradients, while ensuring that aspect ratios are as close to 1 as possible. This is beyond the scope of the present work.

8.3.1.1 Grid Type #1

The first grid type was based on the same grid used in the finite difference method. The cylindrical pipe and insulation are divided into nodes with equal angular and radial spacing. (The angular spacing is equal for both regions, but each region can have different radial spacing.) The nodes are connected into triangular elements. The nodes in the ground are generated using the transformed (bicylindrical) coordinate system, and are also connected into triangular elements. An example is shown in Figure 8.10. The numbers within the elements refer to

the pipe (1), insulation (2), and ground (3). The geometry in this example is atypical—the ratio of pipe size to depth is larger than would be expected in a gathering system—it was chosen to be able to see the three regions more clearly.

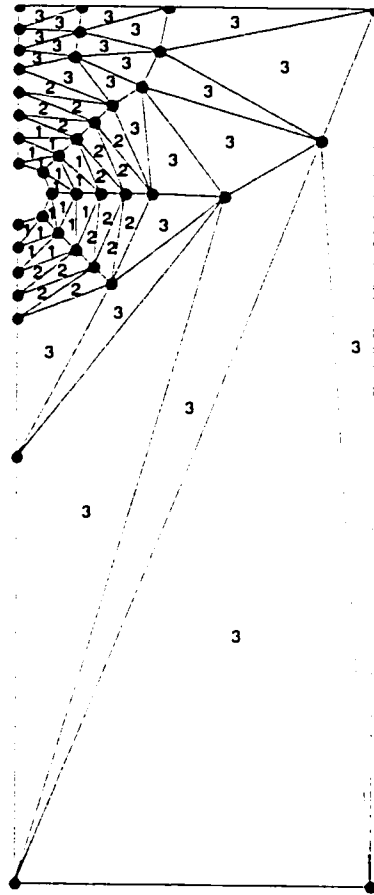


Figure 8.10 First grid type

The main drawback with this type of grid is that the boundaries of the domain in Cartesian space are defined by the calculation algorithm. The advantage of this grid is that the nodes in the ground are selected to lie on isotherms of the steady state case. In this way, they can well capture the thermal gradients. Note that the node at the bottom right corner of the figure above should actually be located at infinity; it is placed instead at a position corresponding the maximum distance in each Cartesian direction from the origin (which is at the top left corner) of any other node.

8.3.1.2 Grid Type #2.

In the second grid type, the cylindrical regions (pipe and insulation) are defined in exactly the same way; it is only the ground which is different. A rectangular domain is specified by the user. The radial lines on which the nodes in the cylindrical regions lie are extended to the boundaries of the domain, and the nodes in the ground are placed equally spaced along these lines. An example is shown in Figure 8.11. This grid uses all the same settings as the previous example, except that a rectangular domain is specified (whereas in the previous case, the grid generation algorithm determined the domain limits).

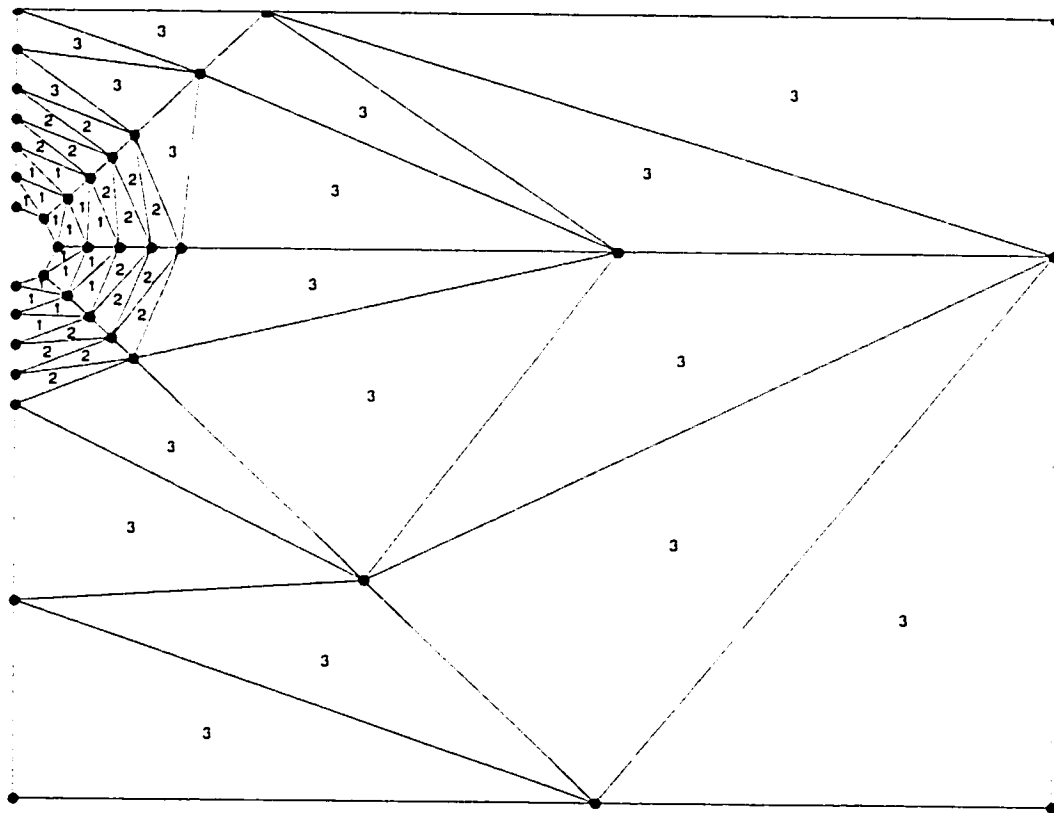


Figure 8.11 Second grid type

The advantage of this grid type is that the user has control over the size of the domain, and it is a simpler grid. The disadvantage is that it does not capture gradients in the ground near the pipe very well, and has more nodes than necessary in the ground far from the pipe. In order to place more nodes in the

ground near the pipe, more nodes are also placed far from the pipe, leading to drastically increased calculation times.

8.3.2 Steady State Case with Constant Temperature Boundaries

Both grids were used to calculate the steady state temperature distribution. The physical problem is described as follows:

Pipe inside radius, 0.03 m
Pipe outside radius, 0.04 m
Insulation outside radius, 0.08 m
Pipe centreline burial depth, 1.5 m
Pipe thermal conductivity, 60 W/m·K
Insulation thermal conductivity, 0.04 W/m·K
Ground thermal conductivity, 0.5 W/m·K
Pipe inside surface temperature, 50°C
Ambient surface temperature, 5°C

In using the two grids defined above, with the same number of nodes in each region, the standard error, as compared to the analytical solution, with the first grid was 0.48°C, and with the second grid was 1.15°C. Clearly, the first grid, defined with consideration of the physics of the situation, is more accurate when used to calculate the steady state temperature distribution in and around a buried, insulated pipe. It is assumed that it will also be more accurate in a transient calculation, and it will therefore be used in the following comparisons

8.3.3 Transient Comparison to Finite Difference Results

No analytical transient solution is available for this problem. (If one were, the present work would be unnecessary.) It is therefore difficult to determine which of the finite element or finite difference methods is more accurate in this application. The following test cases use the data specified in Section 8.3.2, with the addition of the following (needed for transient analysis, but not for steady state):

Pipe Density, 7800 kg/m³
Pipe Specific Heat, 400 J/kg·K
Insulation Density, 190 kg/m³
Insulation Specific Heat, 1000 J/kg·K
Ground Density, 2000 kg/m³
Ground Specific Heat, 1800 J/kg·K

In addition, a convective boundary condition was applied on the inside surface of the pipe, instead of a constant temperature boundary. The convective coefficient was 3 W/m²·K and the fluid temperature was 50°C.

This simulation was run using both the finite difference and finite element methods, with the nodes in the same locations in both methods. Two separate discretizations were used; one with about four times the nodes of the other. The same time step was used in all cases. The results from each were compared to the steady state result. Clearly, the error relative to the steady state would be expected to decrease with time. The results are shown in Figure 8.7.

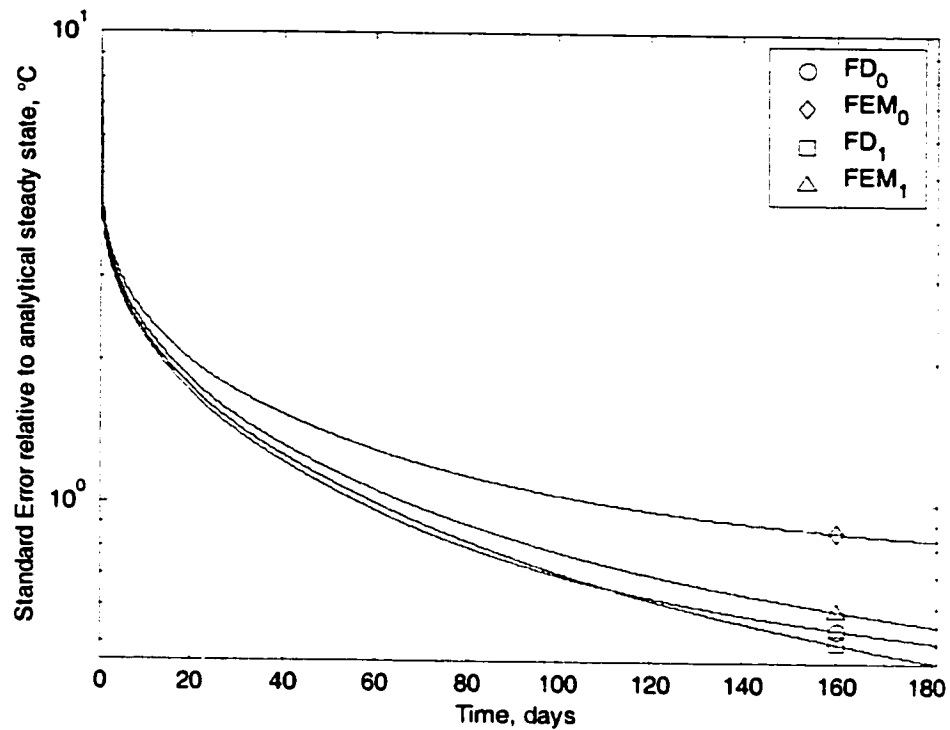


Figure 8.12 Results of transient comparison

In the legend, the subscript 0 refers to the case with fewer (96) nodes, while the subscript 1 refers to the case with more (341) nodes. If it is assumed that more nodes lead to higher accuracy in both the finite element and finite difference methods, then the results of this comparison would imply that the finite difference method is more accurate than the finite element method for this application. The finite difference case with fewer nodes gives very similar results to both cases with more nodes, while there is a large difference between the finite element case with more nodes and all the other cases.

For this straight-forward application, the finite difference method, as developed in Chapter 4, is the best suited for the application. Fewer nodes are needed to achieve a reasonable accuracy. This method may not be appropriate for use in special cases, however, as described in Section 8.3. In these cases, the finite

element method must be used. The above results indicate that more nodes should be used in such an case, to ensure sufficient accuracy.

8.4 Other Issues with FEM

8.4.1 Phase Changes

When there is moisture in the ground, it will act as a buffer to the changes in seasonal temperature in regions where the air temperature goes above and below 0°C on a seasonal basis. This was discussed in Section 3.2.4. There are several methods of incorporating this effect into a finite element method [37]. Unfortunately, these will significantly add to the complication of the model, and can cause calculation times to increase drastically. This is outside the scope of the present work. Care must be used when extrapolating the present work for use in conditions where there is a significant moisture content, and in which there are seasonal freeze-thaw cycles. If the present model is to be improved upon, addressing this limitation should be made a high priority.

8.4.2 Revised Convective Coefficients

The work in this chapter in comparing finite element and finite difference methods and in comparing the finite element method to analytical results, in cases with convective boundaries, used a simple convective coefficient. This assumes that the temperature of the convective fluid does not change as it passes the boundary in question. In Section 4.2.1.6, a finite difference method of considering this was developed. In the calculation procedure described in Chapter 5, one of two methods of calculating the convection effects is used. The basic heat transfer equation for these are:

$$\text{Steady State} \quad \dot{q} = (T_f - T_s) \left(1 - \exp\left(-\frac{L}{\hat{R} \dot{m} c}\right) \right) \dot{m} c \quad (8.24)$$

$$\text{Transient} \quad \dot{q} = (T_f - T_s) \left[1 - \exp\left(\frac{-\Delta t}{R m c}\right) \right] \frac{m c}{\Delta t} \quad (8.25)$$

These are compared to the basic equation for convection inside a pipe if the assumption described above is valid:

$$\dot{q} = \frac{(T_f - T_s)}{R} \quad (8.26)$$

The thermal resistance, R , in the above equations is:

$$R = \frac{1}{hA} = \frac{1}{h2\pi rL} \quad (8.27)$$

Both the basic equation and the modified equations are expressed as a constant times the temperature difference between the fluid and the surface of the pipe. It is therefore possible to rearrange the equations to develop a corrected convective coefficient which considers the change in temperature of the fluid while still being expressed as a simple h value in the finite element model.

9. Summary and Conclusions

Oil companies producing heavy oil would like to be able to use pipelines to transport oil from wells to central gathering or processing facilities. Heavy oil is extremely viscous at lower temperatures, while having a moderate viscosity at higher temperatures; this causes concern about pressure losses in pipelines, especially in winter. Prior to the current work, no design tool existed to assist oil companies in determining the following:

- Will the average pressure loss in a heavy oil pipeline be too high in a given application?
- Will the pressure loss in winter be too high, even if the average pressure loss is acceptable?
- How hot should the oil entering the pipeline be to ensure that the viscosity throughout the pipeline remains sufficiently low?
- Can the pipeline be started up in cold ground without suffering extreme pressure losses?
- If a shutdown in flow occurs, how soon must the flow be restarted before it will become very difficult to restart flow?

A single buried pipe (insulated or not) can be modelled with a finite difference method. The temperature of the ground at various segments along the length of the pipeline is calculated from the time of start-up. The exchange of heat between the ground and the flow in the pipeline is calculated, allowing the temperature profile of the fluid in the pipeline to be known at any given time. The temperature profile allows the viscosity of the fluid to be calculated, from which the pressure loss is calculated in turn. Various situations can be modelled to determine their effect on flow losses. For example, different flow rates, fluid types, pipe sizes, and insulation thicknesses or types can be tested. Start-ups and shutdowns of various lengths can be tested at different times in the year can be

tested. Preheats of the pipeline with water, using different flow rates, preheat times, and water temperatures can be tested. All of this testing can be done on a computer before a pipeline is actually installed. This greatly increases the likelihood of a successful pipeline installation and operation.

Different flow regimes can exist when oil and water flow together in a pipeline. The worst possible case for pressure loss is a water-in-oil emulsion in which the water fraction is just below the emulsion inversion point; the pressure loss in this case can be much higher than for the oil alone. The best cases are high water fraction (although this implies pumping a lot of water along with the oil) and core-annular flow, both of which have pressure losses little higher than for water alone. Other flow regimes lie between these extremes.

The present work showed that in general the following is true for pipelines flowing viscous heavy oil, heated at the source, in a climate such as that in Alberta:

- For a given pipeline, there is a flow rate which will result in a minimum pressure loss (i.e., the relationship between pressure loss and flow rate is not monotonic). This is due to the relationship of viscosity and temperature for heavy oil.
- Pressure loss decreases as pipe size increases. There may be exceptions to this due to the thermal effects.
- As the pipeline length increases, the pressure loss increases substantially.
- As the burial depth increases, up to a point, the pressure loss decreases.
- As insulation increases in thickness, the pressure loss decreases.
- Different times of year are better for starting flow in a new line or restarting flow after a shutdown. This is not necessarily the warmest time of the year at surface; there is a phase delay between temperatures at the surface and at any depth.

- As the inlet temperature increases (or the average annual temperature at surface) increases, the pressure drop decreases.
- As the viscosity of the oil increases, the pressure drop increases.
- A preheat period, in which hot water is circulated prior to the start of oil flow, can significantly decrease the peak pressure experienced when starting a pipeline.

A finite element model can also be used, instead of a finite difference model. More nodes are needed, however, to achieve the same level of accuracy. This leads to longer computation times and higher memory requirements. The advantage of the finite element method is that different geometries can be tested. For example, the effect of backfilling the pipeline trench, where the backfill may have different physical properties from the undisturbed ground, can be considered, as can the effects of running two pipelines in the same trench. While not considered in the present work, the effects of ground moisture freezing and thawing are more easily calculated in a finite element model. The current work assumes a low water content in the soil surrounding the pipeline.

10. Future Work

The following issues have been touched upon in the current work, but not completed in sufficient detail to be included in the calculation model that was built as part of this work:

- Incorporation of multiple pipes in a common trench.
- Variable ground properties (e.g. backfill).
- Phase change in ground (i.e., freezing/thawing of ground moisture).
- Consideration of changes in solid and fluid properties with temperature. The consideration of the change in oil viscosity with temperature is already considered—all other changes with temperature are very small compared to this and were neglected in the current work. The thermal conductivity of moist ground does change significantly between the frozen and unfrozen states; this should be addressed along with the effects of the phase change.
- Investigation into the full effects of the region in which the thermal boundary layer develops on the heat transfer in laminar flow of heavy oil.

A proposal for working on these aspects will be presented to the HOGS project participants to gauge if there is sufficient support for work to proceed.

References

1. *Heavy Oil Gathering Systems—Phase I, Final Report*, C-FER Technologies, Inc., 1999. Confidential to JIP Participants.
2. White, F.M., *Fluid Mechanics (Second Edition)*, McGraw-Hill, New York, 1986.
3. Society of Petroleum Engineers, *Petroleum Engineering Handbook*, Richardson, TX, 1987.
4. Ahmed, N.S., Nassar, A.M., Zaki, N.N., and Gharieb, H.K., "Formation of fluid heavy oil-in-water emulsions for pipeline transportation", *Fuel* 78, 1999.
5. Nunez, G.A., Rivas, H.J., and Joesph, D.D., "Drive to Produce Heavy Crude Prompts Variety of Transportation Methods", *Oil and Gas Journal*, Oct. 26, 1998.
6. Petroleo de Venezuela, S.A., <http://www.pdvsa.com/orimulsion/english/>
7. Nunez, G.A., Rivas, H.J., Rodriguez, D.J., and Layrisse, I.A., "Development of a New Technology: Profiting from Temporary Setbacks During Scale-Up", SPE 30337, 1995.
8. Hasan, A.R. and C.S. Kabir, "A new Model for Two-Phase Oil/Water Flow: Production Log Interpretation and Tubular Calculations," SPE 18216, 1990.
9. Degiorgis, G.L., Maturano, S., Garay, M., Galliano, G.R., and Fomes, A., "Oil Mixture Viscosity Behaviour: Use in Pipeline Design", Society of Petroleum Engineers, 69420, 2001.
10. Al-Besharah, J.M, Akashah, S.A, and Mumford, C.J., "Viscosities of binary crude-oil mixtures correlated", *Oil & Gas Journal*, Feb 20, 1989.
11. *AOSTRA Technical Handbook on Oil Sands, Bitumens and Heavy Oils*, Alberta Oil Sands Technology and Research Authority, 1989.
12. Communication with Darryl Williams, 2001.
13. Arney, M.S., R. Bai, E. Guevera, D.D. Joseph and K. Liu, "Friction Factor and Holdup Studies for Lubricated Pipelining—I," *Int. J. Multiphase Flow* (19) No. 6, pp1016-1076., 1993.
14. Bobok, E., Magyari, D., and Udvari, G., "Heavy Oil Transport Through Lubricated Pipeline", SPE 36841, 1996.

15. Ooms, G., Segal, A., van der Wees, A.J., Meerhoff, R., and Oliemans, R.V.A., "A Theoretical Model for Core-Annular Flow of a Very Viscous Oil Core and a Water Annulus Through a Horizontal Pipe", *International Journal of Multiphase Flow*, 1984.
16. Bannwart, A.C., Rodriguez, O.M.H., de Carvalho, C.H.M, Wang, I.S., and Vara, R.M.O, "Flow Patterns in Heavy Crude Oil-Water Flow", Presented at the Engineering Technology Conference on Energy, 2001, Houston. American Society of Mechanical Engineers.
17. Rivero, M., Guevara, E., Jaua, J., Carabano, N., and Joseph, D., "Preventing Oil Adhesion to Pipe Walls in Heavy Crude Transportation," UNITAR, 1995, Houston.
18. Huang, A., Christodoulou, C., and Joseph, D.D.. "Friction Factor and Holdup Studies for Lubricated Pipelining-II", *International Journal of Multiphase Flow*, 1994.
19. Gillies, R. Confidential communication with C-FER, 1998.
20. Charles, M.E., Govier, G.W, and Hodgson, G.W. "The Horizontal Pipeline Flow of Equal Density Oil-Water Mixtures", *The Canadian Journal of Chemical Engineering*, February, 1961.
21. Incropera, F.P. and D.P. DeWitt, *Introduction to Heat Transfer, Second Edition*, Wiley, 1990.
22. Canadian Standards Association, CSA-Z183-M90, 1990.
23. Cengel, Y.A., and Boles, M.A., *Thermodynamics: An Engineering Approach*, McGraw-Hill, 1989.
24. Government of Canada,
http://www.msc-smc.ec.gc.ca/climate/index_e.cfm.
25. Kazemi, H., and Perkins, T.K.. "A Mathematical Model of Thaw-Freeze Cycles Beneath Drilling Rigs and Production Platforms in Cold Regions", Society of Petroleum Engineers, 3029, 1971.
26. Andersland, O.B., and Anderson, D.M., *Geotechnical Engineering for Cold Regions*, McGraw-Hill, 1978.
27. Communication with David Goodmanson, September, 1999.
28. A.V. Lukov, *Analytical Heat Diffusion Theory*, Academic Press, 1968.
29. R.A. Archer and M.J. O'Sullivan , "Models for Heat Transfer from a Buried Pipe", SPE 36763, 1997.

30. W.W. Martin and S.S. Sadhal, "Bounds on Transient Temperature Distribution due to a Buried Cylindrical Heat Source", *Int. J. Heat and Mass Transfer*, Vol.21, pp. 783-789, 1978.
31. M. Chung, P. Jung, and R. Rangel, "Semi-analytical solution for heat transfer from a buried pipe with convection on the exposed surface", *Int. J. Heat and Mass Transfer*, Vol. 42, pp. 783-789, 1999.
32. Chapra, S.C. and Canale, R.P. *Numerical Methods for Engineers*, Second Edition, McGraw-Hill, 1988.
33. Pozo, R., *Template Numerical Toolkit (TNT)*, <http://math.nist.gov/tnt/>, National Institute of Standards and Technology, 2000.
34. Kwon, Y.W., Bang, H, *The Finite Element Method Using Matlab*, CRC Press, 1996.
35. Moaveni, S., *Finite Element Analysis; Theory and Application with ANSYS*, Prentice-Hall, 1999.
36. Powers, D.L., *Boundary Value Problems*, Third Edition, Harcourt Brace Jovanovich, 1987.
37. Goodrich, L.E., "An Introductory Review of Numerical Methods for Ground Thermal Regime Calculations", National Research Council of Canada, Division of Building Research, Paper No. 1061, 1982.

Appendix A. Transformation of Variables for Bicylindrical Coordinate System

The bicylindrical coordinate transform used to derive positions in the ground is given by[30]:

$$x + iy = c \coth\left(\frac{\alpha + i\beta}{2}\right) \quad (\text{A.1})$$

While obtaining x and y values from this formula is easily done, it is sometimes necessary to express x and y without the use of complex variables. (An example of this is in Appendix B.) This is done as follows.

$$\begin{aligned} \coth(z) &= \frac{\cosh z}{\sinh z} \\ &= \frac{e^z + e^{-z}}{e^z - e^{-z}} \end{aligned} \quad (\text{A.2})$$

Let:

$$a = \frac{\alpha}{2} \quad (\text{A.3})$$

$$b = \frac{\beta}{2} \quad (\text{A.4})$$

$$e^{a+ib} = e^a (\cos b + i \sin b) \quad (\text{A.5})$$

So:

$$\begin{aligned} x + iy &= c \frac{e^{a+ib} + e^{-a-ib}}{e^{a+ib} - e^{-a-ib}} \\ &= c \frac{e^a (\cos b + i \sin b) + e^{-a} [\cos(-b) + i \sin(-b)]}{e^a (\cos b + i \sin b) - e^{-a} [\cos(-b) + i \sin(-b)]} \\ &= c \frac{e^a (\cos b + i \sin b) + e^{-a} (\cos b - i \sin b)}{e^a (\cos b + i \sin b) - e^{-a} (\cos b - i \sin b)} \\ &= c \frac{(e^a + e^{-a}) \cos b + i \sin b (e^a - e^{-a})}{(e^a - e^{-a}) \cos b + i \sin b (e^a + e^{-a})} \end{aligned} \quad (\text{A.6})$$

In a general case:

$$\frac{x_1 + iy_1}{x_2 + iy_2} = \frac{x_1 x_2 + y_1 y_2}{x_2^2 + y_2^2} + i \frac{x_2 y_1 - x_1 y_2}{x_2^2 + y_2^2} \quad (\text{A.7})$$

Now consider:

$$x_1 = (e^a + e^{-a}) \cos b = 2 \cosh a \cos b \quad (\text{A.7})$$

$$x_2 = (e^a - e^{-a}) \cos b = 2 \sinh a \cos b \quad (\text{A.8})$$

$$y_1 = (e^a - e^{-a}) \sin b = 2 \sinh a \sin b \quad (\text{A.9})$$

$$y_2 = (e^a + e^{-a}) \sin b = 2 \cosh a \sin b \quad (\text{A.10})$$

So:

$$x + iy = c \left[\frac{4 \cosh a \sinh a \cos^2 b + 4 \sinh a \cosh a \sin^2 b}{4 \sinh^2 a \cos^2 b + 4 \cosh^2 a \sin^2 b} + i \frac{4 \sinh^2 a \cos b \sin b - 4 \cosh^2 a \cos b \sin b}{4 \sinh^2 a \cos^2 b + 4 \cosh^2 a \sin^2 b} \right] \quad (\text{A.11})$$

$$x + iy = c \left[\frac{\cosh a \sinh a \cos^2 b + \sinh a \cosh a \sin^2 b}{\sinh^2 a \cos^2 b + \cosh^2 a \sin^2 b} + i \frac{\sinh^2 a \cos b \sin b - \cosh^2 a \cos b \sin b}{\sinh^2 a \cos^2 b + \cosh^2 a \sin^2 b} \right] \quad (\text{A.12})$$

$$x + iy = c \left[\frac{\cosh a \sinh a (\cos^2 b + \sin^2 b)}{\left(\frac{1}{2} \cosh 2a - \frac{1}{2}\right) \left(\frac{1}{2} + \frac{1}{2} \cos 2b\right) + \left(\frac{1}{2} + \frac{1}{2} \cosh 2a\right) \left(\frac{1}{2} - \frac{1}{2} \cos 2b\right)} + i \frac{(\sinh^2 a - \cosh^2 a) \cos b \sin b}{\left(\frac{1}{2} \cosh 2a - \frac{1}{2}\right) \left(\frac{1}{2} + \frac{1}{2} \cos 2b\right) + \left(\frac{1}{2} + \frac{1}{2} \cosh 2a\right) \left(\frac{1}{2} - \frac{1}{2} \cos 2b\right)} \right] \quad (\text{A.13})$$

$$x + iy = c \left[\frac{4 \cosh a \sinh a}{(\cosh 2a - 1)(1 + \cos 2b) + (1 + \cosh 2a)(1 - \cos 2b)} + i \frac{4 \cos b \sin b}{(\cosh 2a - 1)(1 + \cos 2b) + (1 + \cosh 2a)(1 - \cos 2b)} \right] \quad (\text{A.14})$$

$$x + iy = c \left[\frac{2 \sinh 2a}{2(\cosh 2a - \cos 2b)} + i \frac{2 \sin 2b}{2(\cosh 2a - \cos 2b)} \right] \quad (\text{A.15})$$

$$x + iy = c \left[\frac{\sinh \alpha}{\cosh \alpha - \cos \beta} + i \frac{\sin \beta}{\cosh \alpha - \cos \beta} \right] \quad (\text{A.16})$$

$$x = c \left[\frac{\sinh \alpha}{\cosh \alpha - \cos \beta} \right] \quad (\text{A.17})$$

$$y = c \left[\frac{\sin \beta}{\cosh \alpha - \cos \beta} \right] \quad (\text{A.18})$$

Appendix B. Derivation of Laplacian for the Bicylindrical Coordinate System

In order to develop a finite difference approximation of heat conduction within the ground around a buried pipe, it is necessary to obtain the Laplacian with respect to temperature for the bicylindrical coordinate system. The Laplacian with respect to temperature in the Cartesian coordinate system is:

$$\frac{\partial^2 T}{\partial x^2} + \frac{\partial^2 T}{\partial y^2} \quad (\text{B.1})$$

The variable transformation (as shown in Appendix A) is:

$$x = c \left[\frac{\sinh \alpha}{\cosh \alpha - \cos \beta} \right] \quad (\text{B.2})$$

$$y = c \left[\frac{\sin \beta}{\cosh \alpha - \cos \beta} \right] \quad (\text{B.3})$$

Generally, the relevant partial derivatives are:

$$\frac{\partial^2 T}{\partial \alpha^2} = \frac{\partial^2 T}{\partial x^2} \left(\frac{\partial x}{\partial \alpha} \right)^2 + 2 \frac{\partial^2 T}{\partial x \partial y} \frac{\partial x}{\partial \alpha} \frac{\partial y}{\partial \alpha} + \frac{\partial^2 T}{\partial y^2} \left(\frac{\partial y}{\partial \alpha} \right)^2 + \frac{\partial T}{\partial x} \frac{\partial^2 x}{\partial \alpha^2} + \frac{\partial T}{\partial y} \frac{\partial^2 y}{\partial \alpha^2} \quad (\text{B.4})$$

$$\frac{\partial^2 T}{\partial \beta^2} = \frac{\partial^2 T}{\partial x^2} \left(\frac{\partial x}{\partial \beta} \right)^2 + 2 \frac{\partial^2 T}{\partial x \partial y} \frac{\partial x}{\partial \beta} \frac{\partial y}{\partial \beta} + \frac{\partial^2 T}{\partial y^2} \left(\frac{\partial y}{\partial \beta} \right)^2 + \frac{\partial T}{\partial x} \frac{\partial^2 x}{\partial \beta^2} + \frac{\partial T}{\partial y} \frac{\partial^2 y}{\partial \beta^2} \quad (\text{B.5})$$

$$\begin{aligned} \frac{\partial^2 T}{\partial \alpha^2} + \frac{\partial^2 T}{\partial \beta^2} &= \frac{\partial^2 T}{\partial x^2} \left[\left(\frac{\partial x}{\partial \alpha} \right)^2 + \left(\frac{\partial x}{\partial \beta} \right)^2 \right] + 2 \frac{\partial^2 T}{\partial x \partial y} \left(\frac{\partial x}{\partial \alpha} \frac{\partial y}{\partial \alpha} + \frac{\partial x}{\partial \beta} \frac{\partial y}{\partial \beta} \right) + \frac{\partial^2 T}{\partial y^2} \left[\left(\frac{\partial y}{\partial \alpha} \right)^2 + \left(\frac{\partial y}{\partial \beta} \right)^2 \right] \\ &+ \frac{\partial T}{\partial x} \left[\frac{\partial^2 x}{\partial \alpha^2} + \frac{\partial^2 x}{\partial \beta^2} \right] + \frac{\partial T}{\partial y} \left[\frac{\partial^2 y}{\partial \alpha^2} + \frac{\partial^2 y}{\partial \beta^2} \right] \end{aligned} \quad (\text{B.6})$$

The partial derivatives of the cartesian coordinates with respect to the transformed coordinates are:

$$\frac{\partial x}{\partial \alpha} = -c \frac{\cosh \alpha \cos \beta - 1}{(\cosh \alpha - \cos \beta)^2} \quad (\text{B.7})$$

$$\frac{\partial x}{\partial \beta} = -c \frac{\sinh \alpha \sin \beta}{(\cosh \alpha - \cos \beta)^2} \quad (\text{B.8})$$

$$\frac{\partial^2 x}{\partial \alpha^2} = c \frac{\sinh \alpha (\cosh \alpha \cos \beta + \cos^2 \beta - 2)}{(\cosh \alpha - \cos \beta)^3} \quad (\text{B.9})$$

$$\frac{\partial^2 x}{\partial \beta^2} = -c \frac{\sinh \alpha (\cosh \alpha \cos \beta + \cos^2 \beta - 2)}{(\cosh \alpha - \cos \beta)^3} \quad (\text{B.10})$$

$$\frac{\partial y}{\partial \alpha} = -c \frac{\sinh \alpha \sin \beta}{(\cosh \alpha - \cos \beta)^2} \quad (\text{B.11})$$

$$\frac{\partial y}{\partial \beta} = c \frac{\cosh \alpha \cos \beta - 1}{(\cosh \alpha - \cos \beta)^2} \quad (\text{B.12})$$

$$\frac{\partial^2 y}{\partial \alpha^2} = c \frac{\sin \beta (\cosh^2 \alpha + \cosh \alpha \cos \beta - 2)}{(\cosh \alpha - \cos \beta)^3} \quad (\text{B.13})$$

$$\frac{\partial^2 y}{\partial \beta^2} = -c \frac{\sin \beta (\cosh^2 \alpha + \cosh \alpha \cos \beta - 2)}{(\cosh \alpha - \cos \beta)^3} \quad (\text{B.14})$$

It can be seen that the following simplifications are true:

$$\frac{\partial x}{\partial \alpha} \frac{\partial y}{\partial \alpha} + \frac{\partial x}{\partial \beta} \frac{\partial y}{\partial \beta} = 0 \quad (\text{B.15})$$

$$\left(\frac{\partial x}{\partial \alpha} \right)^2 + \left(\frac{\partial x}{\partial \beta} \right)^2 = \left(\frac{\partial y}{\partial \alpha} \right)^2 + \left(\frac{\partial y}{\partial \beta} \right)^2 \quad (\text{B.16})$$

$$\frac{\partial^2 x}{\partial \alpha^2} + \frac{\partial^2 x}{\partial \beta^2} = 0 \quad (\text{B.17})$$

$$\frac{\partial^2 y}{\partial \alpha^2} + \frac{\partial^2 y}{\partial \beta^2} = 0 \quad (\text{B.18})$$

These can be used to reduce the Laplacian to:

$$\frac{\partial^2 T}{\partial \alpha^2} + \frac{\partial^2 T}{\partial \beta^2} = \left(\frac{\partial^2 T}{\partial x^2} + \frac{\partial^2 T}{\partial y^2} \right) \left[\left(\frac{\partial x}{\partial \alpha} \right)^2 + \left(\frac{\partial x}{\partial \beta} \right)^2 \right] \quad (\text{B.19})$$

This can be rewritten as:

$$\begin{aligned}
\frac{\partial^2 T}{\partial x^2} + \frac{\partial^2 T}{\partial y^2} &= \frac{\frac{\partial^2 T}{\partial \alpha^2} + \frac{\partial^2 T}{\partial \beta^2}}{\left(\frac{\partial x}{\partial \alpha}\right)^2 + \left(\frac{\partial x}{\partial \beta}\right)^2} \\
&= \left(\frac{\partial^2 T}{\partial \alpha^2} + \frac{\partial^2 T}{\partial \beta^2}\right) \left(\frac{\cosh \alpha - \cos \beta}{c}\right)^2
\end{aligned}
\tag{B.20}$$